

# **UNIVERSITÄTSKLINIKUM HAMBURG-EPPENDORF**

Institut für Immunologie

Direktor Prof. Dr. Bernhard Fleischer

## **UCH-L1 and P2X7 in experimental Glomerulonephritis**

### **Dissertation**

zur Erlangung des Grades eines Doktors der Medizin  
an der Medizinischen Fakultät der Universität Hamburg.

vorgelegt von:

Anna Hammel  
aus Gießen

Hamburg, im August 2013

Datum der mündlichen Prüfung 19.05.2014

Prüfungsausschuss, der/die Vorsitzende: Prof. Dr. Friedrich Koch-Nolte

Prüfungsausschuss, zweite/r Gutachter/in: PD Dr. Catherine Meyer-Schwesinger

Prüfungsausschuss, dritte/r Gutachter/in: PD Dr. Jun Oh

**Table of contents**

---

<b>1. Introduction .....</b>	<b>6</b>
1.1. Nephron and podocyte .....	6
1.2. Glomerulonephritis .....	9
1.2.1. Membranous nephropathy .....	11
1.3. The Anti-Podocyte-Nephritis (APN) model.....	12
1.4. UCH-L1 and the Ubiquitin Proteasome System .....	12
1.4.1. The Ubiquitin Proteasome System (UPS).....	12
1.4.2. UCH-L1 .....	14
1.5. The P2X7 receptor .....	17
1.5.1. P2X7 in the kidney .....	22
1.5.2. Therapeutic targeting of P2X7 - Nanobodies .....	24
<b>2. Working hypothesis .....</b>	<b>26</b>
<b>3. Materials &amp; Methods .....</b>	<b>27</b>
3.1. Materials.....	27
3.1.1. Antibodies .....	27
3.1.2. Chemicals .....	29
3.1.3. Materials .....	30
3.1.4. Animals .....	31
3.1.5. Microscopes.....	31
3.1.6. Software.....	31
3.1.7. Instruments .....	31
3.1.8. Buffers.....	32
3.2. Methods.....	35
3.2.1. General mouse maintenance.....	35
3.2.2. Urine collection .....	35
3.2.3. Urine and serum parameter measurement.....	35
3.2.4. APN induction and monitoring .....	36
3.2.5. Nanobody treatment .....	37
3.2.6. Experimental set-ups, animal sets.....	37
3.2.7. Sacrifice of animals, organ harvesting .....	38
3.2.8. Histology .....	39
3.2.8.1. Preparation of tissue sections .....	39
3.2.8.1.1. Paraffin sections.....	39
3.2.8.1.2. Cryosections.....	39
3.2.8.2. PAS staining .....	40
3.2.8.3. Immunohistochemistry – general principle .....	40
3.2.8.3.1. F4/80 staining.....	41
3.2.8.3.2. Mac2 staining .....	42
3.2.8.3.3. CD3 staining.....	42
3.2.8.3.4. B220 staining.....	43
3.2.8.3.5. WT1 staining .....	43
3.2.8.3.6. P2X7 staining .....	44
3.2.8.3.7. UCH-L1 staining.....	44
3.2.8.4. Immunofluorescence staining (on cryosections) .....	45
3.2.9. Histologic evaluation .....	45

## Table of contents

---

3.2.9.1. Glomerular damage.....	45
3.2.9.2. Podocyte counts .....	46
3.2.9.3. Inflammatory cells.....	46
3.2.10. Western Blot .....	46
3.2.10.1. Procedure .....	46
3.2.10.1.1. Sample preparation.....	47
3.2.10.1.2. Gel electrophoresis .....	47
3.2.10.1.3. Membrane transfer.....	47
3.2.10.1.4. Blocking.....	48
3.2.10.1.5. Detection .....	48
3.2.11. BioRad DC Protein assay (modified from Lowry) .....	48
3.2.12. ELISA.....	49
3.2.12.1. Procedure .....	49
3.2.12.2. Mouse albumin ELISA .....	50
3.2.12.3. Cytokine ELISA .....	51
3.2.13. RNA isolation and real-time PCR analysis.....	52
3.2.13.1. PCR – general principle.....	52
3.2.13.2. RNA isolation from mouse kidney tissue .....	53
3.2.13.3. cDNA Synthesis.....	54
3.2.14. Real-time PCR .....	54
<b>4. Results .....</b>	<b>56</b>
4.1. UCH-L1 KO mice develop a more severe Glomerulonephritis.....	56
4.1.1. Survival past anti-podocyte serum injection.....	55
4.1.2. Evaluation of clinical parameters .....	57
4.1.2.1. Blood Urea Nitrogen (BUN).....	57
4.1.2.2. Albuminuria.....	56
4.1.2.3. Serum Cholesterol.....	58
4.2. P2X7 KO mice are protected against severe kidney damage.....	59
4.2.1. Evaluation of clinical parameters .....	59
4.2.1.1. Body weight.....	59
4.2.1.2. Blood Urea Nitrogen (BUN).....	60
4.2.1.3. Serum Cholesterol.....	61
4.2.1.4. Albuminuria.....	62
4.2.1.5. Histology.....	63
4.2.1.5.1. PAS.....	63
4.2.1.5.2. Podocyte counts.....	65
4.2.1.5.3. Inflammatory cells .....	66
4.2.1.6. Proinflammatory cytokine levels .....	70
4.2.1.6.1. MCP-1 .....	71
4.2.1.6.2. IL-1 $\beta$ .....	73
4.2.1.6.3. IL-6 .....	75
4.3. UCH-L1 and P2X7 are both upregulated in the glomerulonephritic kidney...	77
4.3.1. Immunohistochemistry .....	77
4.3.2. Western Blot Analysis .....	78
4.3.3. Realtime PCR .....	80
4.4. P2X7 activation is altered in UCH-L1 KO mice. ....	82
4.4.1. ADAM17.....	82
4.4.1.1. ADAM17 Western blot.....	82
4.4.1.2. ADAM17 mRNA expression .....	83
4.4.2. EGFR.....	84
4.4.2.1. EGFR Western Blot.....	84

## Table of contents

---

4.4.2.2. EGFR expression/qPCR.....	85
4.4.3. HeyL.....	86
4.5. Therapeutic antagonization of the P2X7 receptor attenuates the development of anti-podocyte nephritis. ....	87
4.5.1. Albuminuria .....	87
4.5.2. IL-6 serum levels.....	88
<b>5. Discussion .....</b>	<b>90</b>
5.1. UCH-L1 KO mice are more vulnerable towards APN.....	90
5.1.1. UCH-L1 KO APN mice exhibit podocytopenia. ....	92
5.1.2. UCH-L1 KO APN mice develop severe proteinuria. ....	94
5.1.3. UCH-L1 KO APN mice show severe glomerular damage and enhanced inflammatory response. ....	95
5.1.4. Systemic, not kidney-limited, UCH-L1 KO might contribute to the aggravated course of glomerulonephritis in UCH-L1 KO mice. ....	98
5.2. P2X7 KO mice are protected against several renal inflammation. ....	98
5.2.1. P2X7 KO animals exhibit attenuated disease.....	99
5.2.2. P2X7 mRNA and protein are upregulated in renal inflammation. ....	100
5.3. P2X7 activation is altered in UCH-L1 KO mice. ....	102
5.3.1. P2X7 protein and mRNA are upregulated in UCH-L1 KO mice.....	102
5.3.2. The “inflammasome axis” seems overactive in UCH-L1 KO APN mice. ....	103
5.3.3. ADAM17 expression is altered in P2X7 KO and UCH-L1 KO mice. ....	104
5.4. Therapeutic antagonization of the P2X7 receptor attenuates the development of anti-podocyte nephritis. ....	107
<b>6. Summary .....</b>	<b>110</b>
<b>7. List of abbreviations .....</b>	<b>111</b>
<b>8. List of references .....</b>	<b>115</b>
<b>9. Appendix .....</b>	<b>130</b>
9.1.1. Acknowledgements.....	130
9.1.2. Affidavit .....	132

## **1. Introduction**

### **1.1.Nephron and podocyte**

The kidneys serve as a systemic blood filter that regulates acid-base balance, electrolyte concentrations, extracellular fluid volume, blood pressure and the detoxification of metabolic waste products. The kidneys' most important operating mechanisms are filtration, reabsorption and secretion, all controlled and exerted inside the nephron (Harrison 2008).

The nephron is the basic functional unit of the kidney. Its chief function is to regulate the systemic concentration of water and soluble substances like sodium salts by filtering the blood, reabsorbing what is needed and excreting the superfluous rest as urine. The nephron eliminates metabolic waste products, such as urea or uric acid. It regulates blood volume and blood pressure, controls levels of electrolytes and metabolites, and regulates blood pH. Its functions are regulated by hormones such as antidiuretic hormone, aldosterone, and parathyroid hormone. A normal human kidney contains more than 1 million nephrons.

Each nephron is composed of the actual filtering component, the renal corpuscle, and a tubular system specialized in reabsorption and secretion. Inside the renal corpuscle, blood is filtered by passing through a tuft of capillaries along the blood-urine-barrier. Water and small solutes are delivered into Bowman's space and the renal tubule as primary urine. Macromolecules and corpuscular components are retained in the bloodstream. A daily volume of approximately 180 liters of primary urine is hence filtered through the entirety of renal corpuscles and enters the renal tubules. The renal tubule is a long epithelial duct arising from Bowman's space. It consists of several segments connected in series, some convoluted, some straight. The epithelia of the renal tubule reabsorb approximately 99% of water and solutes from the primary urine flowing through and in turn secrete other substances from blood into urine, such as urea. The gradual passage of primary urine through the kidneys' tubular system results in the daily production of about 1,5 L final urine (Silbernagl 2007).

The renal corpuscle consists of the glomerulus and the surrounding Bowman's capsule. The glomerulus is a capillary tuft that receives its blood supply from an afferent arteriole of the renal circulation. Each tuft consists of about 30 branching and anastomosing capillaries. Each capillary projects into the urinary space with a major

part of its circumference, building an important part of the blood-urine-barrier. The endothelium of glomerular capillaries is fenestrated (diameter approximately 50-100 nm). The lumen-bound plasmamembrane of the endothelium exhibits a thick, negatively charged glycocalyx covering the fenestrae. The “backbone” of the glomerulus is formed by the mesangium, a conglomerate of branched mesangial cells situated in the center of the tuft. The mesangium serves as adhesion point to the rear side of the capillary loops and stabilizes the tonus of the capillary wall due to the contractility of its cells, which adhere to the glomerular basement membrane via microfibrils.

Bowman's capsule is the glomerular capsule, surrounding the glomerular capillary tuft. During nephrogenesis, this formerly vesicle-shaped blind origin of the metanephron is invaginated by capillaries. It hence is composed of a visceral inner layer, abutting on the capillary tuft, and a parietal outer layer leaving a narrow lumen, Bowman's space, in between them. The visceral leaf of the capsule consists of specialized epithelial cells, called podocytes, and forms, together with the capillary wall, the actual filter between blood and urine compartments. The visceral epithelial cells, or podocytes, are characterized by their long tentacle-like arborescent processes, so-called foot processes. The parietal outer leaflet of Bowman's capsule is composed of a single layer of flat cells lining the inside of the capsule (Lüllmann-Rauch 2006).

The podocytes' cell bodies reach into the urinary space, delegating thick primary foot projections, from which digitiform secondary processes are dispatched. The projections are anchored in the glomerular basement membrane (GBM) via integrins. Primary and secondary foot processes of adjacent podocytes interdigitate and form a densely toothed grid that insulates the capillaries almost completely from the urinary space. Solely small slits with a width of approximately 40 nm, covered by so-called slit diaphragms, are left between the interlocked foot processes. The plasma membrane covering the podocytes towards the urinary space is lined by an anionic glycocalyx. The slit diaphragms resemble cell-to-cell contacts with characteristics of the adhaerens type or a tight junction (Lüllmann-Rauch 2006).

A major component of the diaphragm is the transmembrane protein nephrin (Holzman, St John et al., 1999). The extracellular domains of nephrin molecules on neighbored foot processes bridge the slit with their head domains like a zipper, overlapping in the center of the slit, but leaving small filtration pores on both sides. Several other proteins contribute to the integrity and function of the filter. CD2AP forms the podocyte cytoskeleton, and stabilizes the slit diaphragm (Li, Ruotsalainen et al., 2000). Other podocyte proteins include annexin-4, P-cadherin, ZO-1 or podocin (Saleem, O'Hare et al., 2002). Intact slit diaphragms form the important blood-urine filtration barrier and ensure that large macromolecules, such as serum albumin and gamma globulin, remain in the bloodstream, while water, small solutes and distinct molecules of intermediate size may pass through. The filter exhibits

certain selectivity for these molecules - size and charge are crucial factors for filterability. Size sorting of blood molecules is performed by the molecular fiber grid of the lamina densa and by the filtration pores in the slit diaphragms. Molecules with a radius between 1,8 and 4,4 nm may be filtered through, if not repelled by their charge. Charge selectivity is expressed by the poor filterability of anionic molecules compared to neutral or cationic particles of the same size. This is due to the repulsion of negatively charged molecules by the anionic parts of the glomerular filter (Lüllmann-Rauch, 2006; Adler 1992).

Podocytes are the cellular protagonists in forming the glomerular filter (Figure 1). They provide the crucial barrier to urinary protein loss with hundreds of podocyte foot processes and the interposed slit diaphragms. Structural features of podocytes indicate a high rate of vesicular traffic in these cells. Many coated vesicles and coated pits may be detected along their basolateral domains. In their cell bodies, podocytes possess a well-developed endoplasmic reticulum and a large Golgi apparatus, indicative of a high capacity for protein synthesis and post-translational modifications (Pavenstädt, Kriz et al. 2003). There is also evidence of a large number of lysosomal components seen in podocytes, indicating a high endocytic activity. Podocytes are terminally differentiated cells having lost their capability to divide, rendering the podocyte the only resident glomerular cell type that will not reactively proliferate upon damage, i.e. in the context of inflammatory renal diseases such as glomerulonephritis (Shankland 2006; Pavenstädt, Kriz et al. 2003).

Morphologic characteristics of podocyte injury include foot process effacement and cellular hypertrophy (Figure 1B). According to Kriz et al., „foot process effacement or simplification represents a reduction in the complexity of cell-cell connections, which may range from partial retraction of the foot processes to a total disappearance of the usual interdigitated pattern“ (Kriz, Gretz et al. 1998). Disruption of podocyte morphology in the form of foot process effacement or slit diaphragm reorganization, e.g. altered distribution of nephrin, results in enhanced permeability of the glomerular filter, clinically measurable as proteinuria, and in the expression of a nephrotic syndrome (Somlo and Mundel 2000). Podocytes play a major role in the initiation and progression of glomerular diseases and are a target of both immune-mediated and non-immune-mediated injury (Mundel and Shankland 2002). Little is to date known about the distinct biochemical shiftings occurring inside the podocyte and its protein metabolism under disease conditions. Meyer-Schwesinger et al. (Meyer-Schwesinger, Meyer et al. 2009) found that the diseased podocyte's expression of the regulatory protein ubiquitin and the associated enzyme ubiquitin C-terminal hydrolase L1 (UCH-L1) correlates with an internalization and down-regulation of nephrin. This observation convenes with the findings of Fischer et al. depicting an accumulation of ubiquitin and ubiquitin-dependent internalization of nephrin and podocin Cin85 in CD2AP deficient mice in a model of proteinuric kidney disease (Tossidou, Teng et al. 2010). Ubiquitin metabolism might hence contribute to the emergence of irreversible podocyte injury.

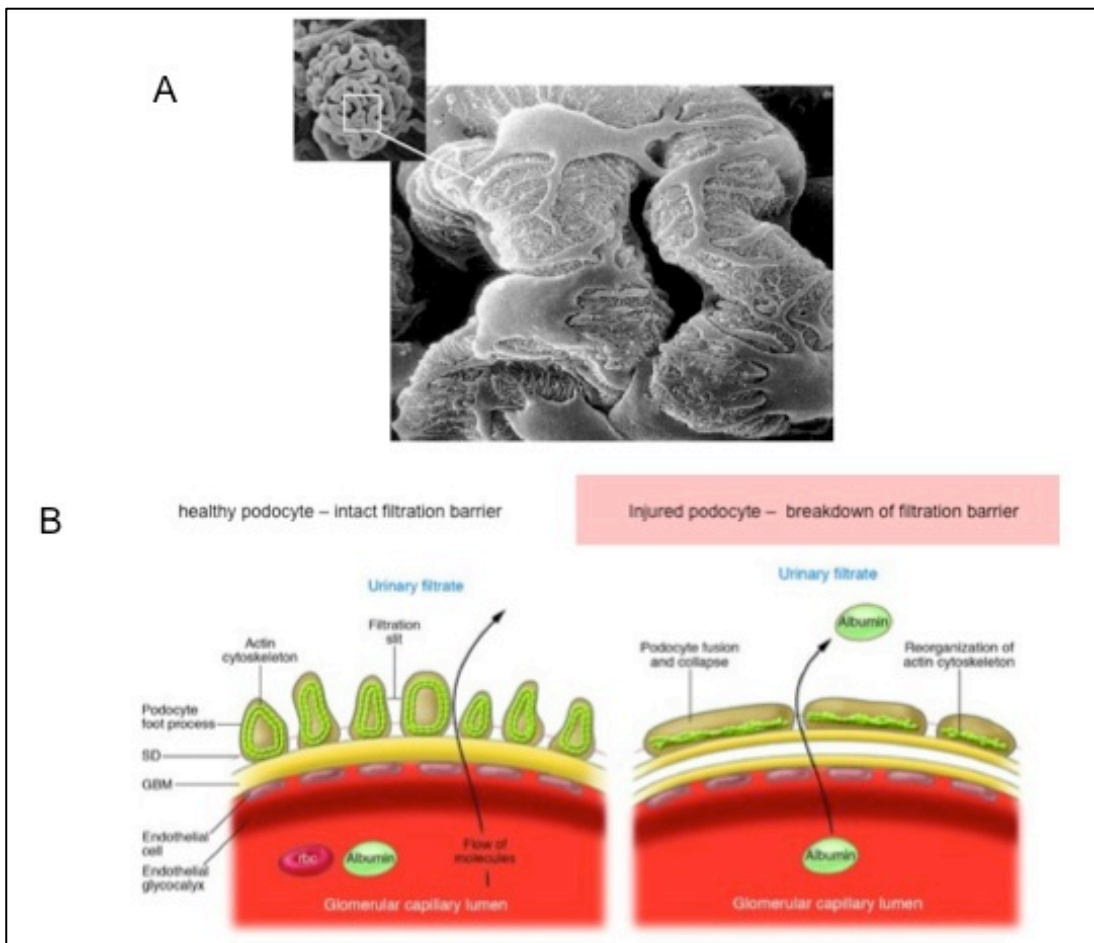


**Figure 1: Podocyte and filtration barrier.** A: electron microscopy of podocytes and capillary tuft, capillaries are covered by a dense grid formed of interdigitating primary and secondary foot processes of adjacent podocytes. (<http://pathology.wustl.edu/~shawlab/podocyte-biology-glomerular-disease.html>)

B The glomerular filtration barrier (Ronco 2007): a healthy filtration barrier, as shown on the left hand side, is maintained by filtration slits in between interdigitating podocyte foot processes, kept in position and formed by an intact actin cytoskeleton. GBM is solely permeable for water and small solutes. Negatively charged glycocalyx repels macromolecules. Albumin is kept inside the capillary lumen. In glomerulonephritic circumstances (right hand side), podocytes fuse and collapse, their actin cytoskeleton is reorganized. GBM is leaky, negatively charged glycocalyx loses its' function. Macromolecules, such as Albumin, will pass into the urine. Breakdown of filtration barrier leads to the formation of nephrotic syndrome.

## 1.2. Glomerulonephritis

The term glomerulonephritis (GN) encompasses a variety of immune-mediated renal diseases, all of them sharing the pathologic traits of causing intraglomerular inflammation and cellular proliferation, which will result in a breakdown of the glomerular filtration barrier and an impaired kidney function.

Humoral as well as cell-mediated immune mechanisms may contribute to the pathogenesis of glomerular inflammation (Figure 2). In anti-GBM-antibody mediated GN, linear IgG depositions against Goodpasture-antigen, a component of type IV collagen, may be found along the glomerular basement membrane. In immune-

complex mediated GN (e.g. membranous GN, Lupus nephritis, post infectious GN), depositions of immune-complexes are distributed along the capillary walls of the glomerulus. In ANCA-associated GN, anti-neutrophil cytoplasmic antibodies (ANCA) initiate glomerular damage via interaction with components of neutrophil granules. Another initiator of glomerular disease may be the activation of cell-mediated immune reactions. T-cells have been identified to promote glomerular inflammation in multiple forms of human glomerulopathies. Following initiation of glomerular damage, a multitude of highly noxious pro-inflammatory mediator systems is mobilized in infiltrating inflammatory cells as well as in glomerular resident cells. Chemotactic cytokines such as MCP-1, expressed and produced by both macrophages and intrinsic renal cells, will recruit peripheral monocytes/macrophages, T-cells and dendritic cells to the inflamed glomerulus as a site of tissue injury. Macrophages are important effectors of injury in GN. Their accumulation is linked closely to the severity of glomerular injury and macrophages are a major source of IL-1 $\beta$ , a proinflammatory cytokine which is known to play an important role in crescent formation and tubulointerstitial injury. IL-1 $\beta$  has also been identified to be constitutively expressed by glomerular endothelium and tubular epithelial cells in normal rat kidney. In a rat model of anti-GBM disease, IL-1 $\beta$  expression was appreciably upregulated by intrinsic glomerular cells, such as podocytes, and tubules, suggesting an important role for these cells in IL-1 $\beta$  dependent crescent formation and tubulointerstitial injury occurring in the context of GN (Tesch, Yang et al. 1997). Infiltrating inflammatory cells will produce further cytokines, such as IL-18, IL-6 or TNF- $\alpha$ , potent inductors of inflammation and immune reaction and fortifiers of oxidant stress. The complement system is activated and infiltration of circulating leucocytes will occur. Cytokines are synthesized and proteolytic enzymes are released. The coagulation cascade is initiated and pro-inflammatory lipid mediators are built (Harrison 2008; Herold 2010; Couser 1999; Chadban and Atkins, 2005).

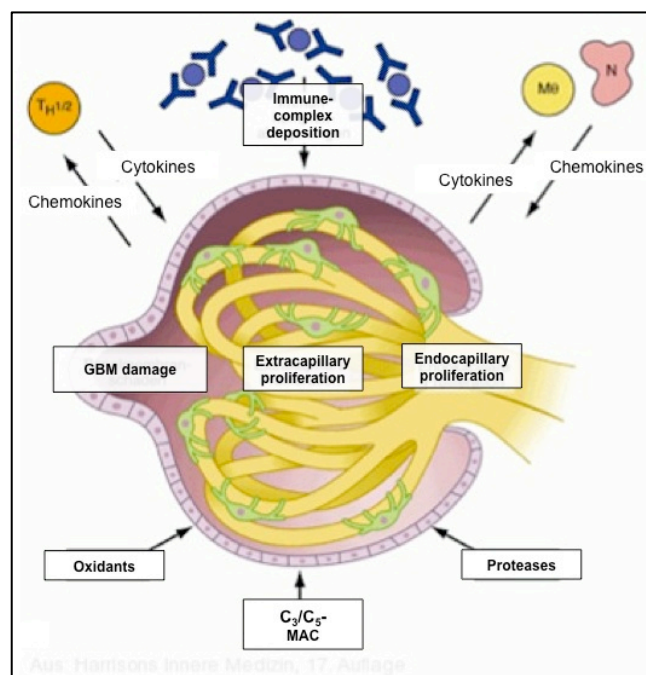


Figure 2:  
**Pathogenesis of GN** (modified from Harrison's Internal Medicine 2008).

### **1.2.1. Membranous nephropathy**

Membranous nephropathy (MN) is, with a quota of 20%, the most common cause of the nephrotic syndrome in adult Caucasian patients. The nephrotic syndrome is a symptom complex comprising proteinuria ( $>3,5\text{g}/24\text{h}$ ), hypoproteinemia, hypalbuminuric edema and hyperlipidemia. While the majority (85%) of cases of MGN are idiopathic, secondary forms can be seen in the setting of autoimmune disease, neoplasia or infection (Harrison 2008).

Membranous nephropathy is an immunologically mediated disease characterized by subepithelial immune complex deposits and a resultant glomerular basement membrane (GBM) thickening. The immune complexes serve as activators that trigger a response from the complement system, which plays a crucial role in the development of MGN (Ronco and Debiec 2006). Deposited immune complexes predominantly consist of unknown antigens, antibodies, mostly IgG4, and the membrane attack complex (MAC), a conglomerate built of complement factors C5b-9. Resulting from the activation of the complement cascade, sublytic C5b-9 complexes will form and insert into the podocyte membrane, where they provoke the production of reactive oxygen species, prostanoids, proteases and cytokines. These noxious processes will cause the GBM and thus the glomerular filtration barrier to lose integrity, resulting in the development of a prominent proteinuria (Nangaku, Shankland et al. 2005).

The formation of immune depots in MGN to date remains unexplained. Various explanations include the subepithelial deposition of systemically circulating complexes due to size and charge characteristics or the deposition of xenoantigen in the subepithelium and resulting immune complex formation in situ. Arguments promoting this hypothesis are the identification of the neutral endopeptidase on glomerular epithelial cells as target antigen in neonatal MGN (Ronco and Debiec, 2010) or the findings of a recent study by Beck et al. that identified antibodies to an M-type phospholipase A<sub>2</sub> receptor in 70% of primary MGN cases evaluated (Beck, Bonegio et al. 2009).

In mice, the anti podocyte nephritis (APN) model of GN to a certain extent resembles the pathognomonic traits found in membranous nephropathy. The anti-podocyte antibody-mediated renal injury maintained by this model leads to heavy proteinuria and is characterized by immune-mediated podocyte loss, foot process effacement and complement activation (Meyer-Schwesinger, Meyer et al. 2007).

### **1.3.The Anti-Podocyte-Nephritis (APN) model**

The Anti-podocyte Nephritis (APN) model (Meyer-Schwesinger et al. 2011; Meyer-Schwesinger et al. 2007), was the first mouse model of polyclonal antibody-induced damage to the podocyte. To establish a mouse model of such injury, wildtype mice were repeatedly immunized with an antiserum that had been obtained from sheep immunized with a suspension of murine podocytes and that hence contained polyclonal sheep anti-mouse podocyte antibodies.

Histologic evaluation of the APN serum treated animals suggested that the podocyte was the main target of the antiserum. Histochemistry revealed diffuse mesangial matrix expansion. Mouse IgG and complement were detected in a linear pattern along the glomerular filter. Numbers of glomerular T cells were increased, whereas podocytes were significantly reduced. Electron microscopy showed flattening of glomerular foot processes in regions with mesangial matrix deposition. Immunohistochemistry detected the injected anti-podocyte antibody solely bound to the glomerular tuft.

The exact mechanisms and targeted effector molecules of podocyte injury accounting for the kidney injury obtained by the model remain to be further characterized and understood. The APN model may serve as a feasible tool in scrutinizing the distinct biochemical shiftings inside the diseased podocyte and its protein metabolism under disease conditions. The role of selected proteins of potential importance in podocyte damage, such as Ubiquitin, may be directedly investigated in affected podocytes in mice of any genotype.

### **1.4.UCH-L1 and the Ubiquitin Proteasome System**

#### **1.4.1.The Ubiquitin Proteasome System (UPS)**

The intracellular degradation of proteins is a strictly regulated process that embodies a crucial actuator in the maintenance of physiologic cell homeostasis. The degradation of most transient proteins in eukaryotic cells is predominantly regulated by the ubiquitin-proteasome-system (UPS).

The UPS is a highly conserved, ATP-dependent system. Proteins are designated to proteasomal degradation by being tagged with the regulatory protein ubiquitin.

Ubiquitin is a small polypeptide with a length of 76 amino acids and was named due to its ubiquitous nature in any known eukaryotic organism.

Ubiquitination of proteins is an important component of multiple central cellular processes such as cell cycle regulation, transcription, signal transduction, localization and activity of receptors, antigen presentation or endocytosis.

The UPS encompasses enzymes that catalyze ubiquitination and deubiquitination of target proteins and contains the 26S-proteasome-complex, responsible for degrading thus labeled proteins.

Ubiquitination is completed via the enzymatic linkage of ubiquitin to the amino acid lysine of the target protein (Figure 3). An isopeptide bond is hence formed between the C-terminal glycine residue of the ubiquitin molecule and the  $\epsilon$ -amino group of the substrate protein's lysine. Three enzyme complexes (E1-E3) are required for the successful catalyzation of this reaction: E1 ATP-dependently activates ubiquitin at its' C-terminal glycine residue. The activated ubiquitin is then transiently linked to E2, a ubiquitin-carrier-protein and is finally bound to the  $\epsilon$ -aminogroup of the target protein's lysine by E3, a ligase.

Target proteins may be modified at one single or at multiple lysine residues by mono- or polyubiquitination, at which length and configuration of the particular ubiquitin chain to be linked determine the protein's fate. Polyubiquitin chains, consisting of at least 4 ubiquitin molecules, are typically attached to the target protein at its' lysine residue on position 48 of the amino acid sequence (K48). K48-polyubiquitination is presumed the objective signal for a protein's degradation via the 26S-proteasome. Polyubiquitinations are also possible on lysine residues K11, K29 or K63, whereby various other functions or destinations of the tagged protein may be triggered.

K63-linked polyubiquitinations play a role in DNA-repair, in the regulation of translational processes and in endocytosis and presumably also exert protein-stabilizing effects, preventing target proteins from proteasomal degradation. K63-polyubiquitination is furthermore considered a signal for a protein's degradation in the lysosome (Hershko and Ciechanover, 1998; Finley, Ciechanover et al. 2004; Hicke 2001).

The cellular monoubiquitin pool requires the maintenance of a stable homeostasis to grant the regular course of proteasomal degradation and to avoid the noxious accumulation of misfolded proteins inside the cytoplasm. This homeostasis is sustained by deubiquitinating enzymes of two types: the Ubiquitin-Isopeptidases (UBPs) and the Ubiquitin-C-terminal-Hydrolases (UCHs), of which UCH-L1 is a prominent member. These enzymes are responsible for the recycling of used ubiquitin molecules by cleaving them from once tagged substrate proteins or by cutting apart polyubiquitin chains to reprocess them to monoubiquitin again. Once cleaved monoubiquitin residues then remain inside the cytoplasm until being reused for posttranslational modifications anew (Wilkinson 2000).

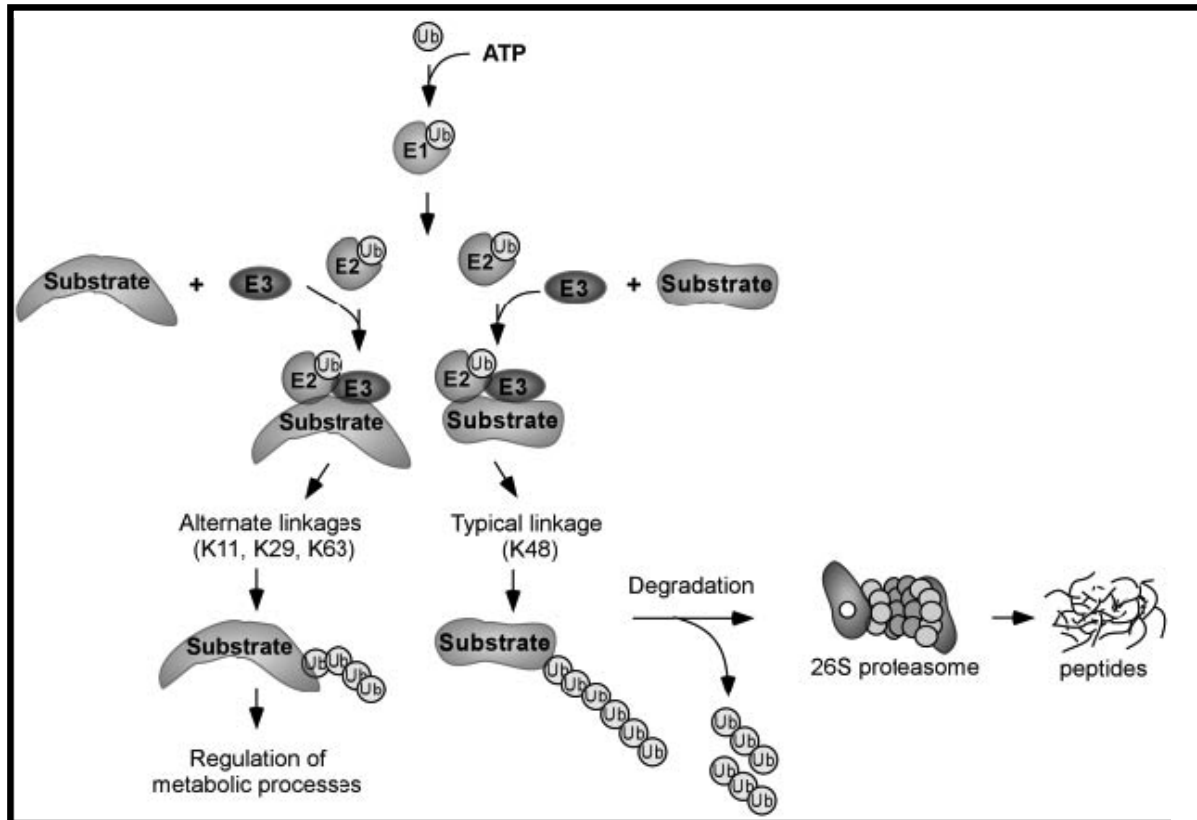


Figure 3: **The Ubiquitin-Proteasome System** (Debigare and Price, 2003). The majority of polyubiquitinations is accomplished via Lysine 48 (K48) and will lead to proteasomal degradation of the polyubiquitinated protein in the 26S proteasome. In contrast, alternative polyubiquitinations on Lysine residues K11, K29 or K63 regulate cell cycle-associated tasks, such as apoptosis or DNA-repair, and other metabolic processes.

### 1.4.2.UCH-L1

The Ubiquitin C-terminal Hydrolase L1 (UCH-L1) is a member of the UCHs (Ubiquitin C-terminal hydrolases), a group of deubiquitinating enzymes that hydrolyze small carboxy-terminal adducts of ubiquitin to generate the ubiquitin monomer. Three human isoforms of the hydrolase have been cloned (Wilkinson 1997), each exhibiting a distinct tissue-specific distribution.

UCH-L1 regulates the intracellular pool of Monoubiquitin (monoUb) via the stabilization of monoUb (Osaka, Wang et al. 2003) and by two further, opposing enzymatic activities (Liu, Fallon et al. 2002): The hydrolase activity enables UCH-L1 to cleave and hydrolyze ubiquitin tags, thus increasing the monoUb pool. On the other hand, its highly controversially discussed ligase activity enables UCH-L1 to mediate

the chain-linking of ubiquitin monomers on lysine residue K63, thus decreasing the cell's monoubiquitin contents.

In addition, UCH isoforms may hydrolyze mono-ubiquitinated substrates (Larsen, Krantz et al. 1998), which will then be protected from being targeted for degradation by the 26S proteasome pathway. This UCH-mediated modification is considered an important regulatory strategy within the Ubiquitin proteasome pathway (Wilkinson, 2000). Furthermore, an involvement of UCH-L1 has been shown in the recycling of free ubiquitin from ubiquitinated peptides originating from proteasomal degradation.

Its diverse capabilities render UCH-L1 an important enzyme within the Ubiquitin proteasome system (UPS) with contrary influence on the cellular monoUb pool. Its hydrolase function increases and stabilizes the pool, while, acting as a ligase, UCH-L1 diminishes monoubiquitin stocks. Resulting from these converse abilities, UCH-L1 may contribute to and influence a vast variety of different intracellular processes.

In most cell types, the distinct role of UCH-L1 to date remains to be further elucidated.

UCH-L1 is a protein of 230 amino acids and exhibits a strict tissue-specific distribution throughout the body (Wilkinson, Lee et al. 1989). It is most notably present in neural tissue throughout all stages of neuronal development, where it holds crucial functions in mediating cell differentiation, synaptic integrity, and process formation (Sakurai, Ayukawa et al. 2006). With a quota of 1-2%, UCH-L1 is one of the most potently expressed soluble proteins in the mammalian brain. It may as well be found in cells of the diffuse neuroendocrine system and their tumors, where it plays a role in both proliferation, and apoptosis (Ermisch, Schwechheimer et al. 1995). UCH-L1 expression has been shown in various other tumor entities, such as pancreatic cancer, colon cancer or small-cell lung cancer (Hibi, Liu et al. 1998). The majority of studies on UCH-L1 in cancer gave evidence of the upregulation of UCH-L1 in disease states. Whether this upregulation is a malign trigger of tumor growth or a benign compensatory response to it currently remains unexplained.

UCH-L1 is also expressed in ovaries and testis, promoting oo- and spermatogenesis (Sekiguchi, Kwon et al. 2006).

In the kidney, UCH-L1 expression has been detected in tubular epithelial cells, in collecting duct cells, and parietal cells (Shirato, Asanuma et al. 2000; Diomedici-Camassei, Rava et al. 2005), where it is thought to contribute to nephrogenesis, cell differentiation in tubulogenesis, and in the regulation of the cell cycle (Debigare, Price et al. 2003; Franch 2002). The enzyme is not expressed in differentiated podocytes of healthy glomeruli (Shirato, Asanuma et al. 2000).

In the central nervous system, it has been shown that modification or downregulation of UCH-L1 is associated with Alzheimer's and Parkinson's disease. A point mutation in the UCH-L1 gene has been implicated as a cause of Parkinson's development (Betarbet, Sherer et al., 2005).

Neuronal loss of UCH-L1 function leads to axonal degeneration in mice. In studies involving UCH-L1 knockout mice, neurodegeneration of the peripheral nervous

system with a lethal outcome has been observed, resulting from the loss of structure and function of the neuromuscular end plate (Wang, Takeda et al., 2004) .

Given that neurons and podocytes largely resemble each other in morphology and in their protein expression pattern (Rastaldi, Armelloni et al. 2006; Kobayashi 2002; Kobayashi and Mundel 1998), one could assume that both cell types share biochemical features as well. Therefore, approaches have been made to investigate the role of UCH-L1 in diseased podocytes.

In a physiological state, there is no UCH-L1 expression in podocytes. However, Meyer-Schwesinger et al. were able to show that UCH-L1 and ubiquitin modification do play a role in podocyte differentiation and injury in the glomerulonephritic kidney (Meyer-Schwesinger, Meyer et al., 2009).

UCH-L1 expression in cultured human podocytes was associated with an undifferentiated status, as it has been observed in neuron cultures before. Contrariwise, differentiation and arborization coincided with decreased UCH-L1 and monoubiquitin expression. Inhibition of UCH-L1 induced time and concentration-dependent process formation with  $\alpha$ -actinin-4 distribution to the cell membrane and processes. An immunohistochemical approach was used in the study to evaluate whether UCH-L1 expression was associated with podocyte injury in 15 different human glomerular diseases. The study's findings show that whereas healthy kidneys expressed no UCH-L1 and little ubiquitin, a subset of human glomerulopathies associated with podocyte foot process effacement (membranous nephropathy, SLE class V, FSGS) exhibited a de novo expression of UCH-L1 in podocyte cell bodies, nuclei, and processes. Furthermore, UCH-L1 expression correlated with podocyte ubiquitin content and internalization of the podocyte-specific proteins nephrin and  $\alpha$ -actinin-4. Glomerular kidney diseases that are typically not attended by foot process effacement (SLE class IV, ANCA+ necrotizing GN, amyloidosis, IgA nephritis) expressed little to no UCH-L1 and ubiquitin.

A study by Manago et al. (Manago et al., 2005) showed that overexpression of UCH-L1 potentiated ATP-induced currents due to the activation of P2X receptors, a family of cation-permeable ligand gated cation channels that open in response to the binding of extracellular ATP. ATP-induced inward currents were measured in mock, wild-type or mutant UCH L1-transfected PC12 cells via whole-cell patch clamp configuration. The amplitude of ATP-induced currents was greatest in UCH-L1-transfected cells. This finding gives the first evidence of a relationship between UCH-L1 and P2X receptors in neuronal cells.

Neurons and podocytes resemble each other in morphology and protein expression pattern, at least in relation to UCH-L1, as well. As mentioned above, UCH-L1 seems to play a role in podocyte injury.

Given the fact that UCH-L1 and P2X receptors interact in neurons, it seems likely to assume that those proteins might also interact in the podocyte.

## 1.5. The P2X7 receptor

Purinoreceptors are cell surface proteins that bind purines with high affinity and trigger intracellular changes which influence the cell's behavior. The best-characterized classes of purinergic receptors in mammals are the P1 receptors, which open in response to Adenosine, and the P2 receptors, which prefer ATP or ADP-ribosylation. Among the P2 receptors, one distinguishes between P2X and P2Y receptor subfamilies. While P1 and P2Y receptors are G-protein coupled, P2X receptors act as ligand-gated cation channels that open upon stimulation via the binding of ATP (or its analog BzATP) or ADP-ribosylation (La Sala, Ferrari et al. 2003). The channels are primarily permeable for Na<sup>+</sup> and K<sup>+</sup> and to a lower degree for Ca<sup>2+</sup>. To date, seven separate genes coding for P2X subunits have been identified, entitled P2X1 through P2X7.

The 7 P2X receptor subunits all share a common topology. They possess two transmembrane domains linked by a large extracellular loop. The carboxyl and amino termini are located in the cytosol. The ectodomain contains 10 cystein residues that contribute to the protein's tertiary structure via the expression of disulfide bonds. Like the majority of ion channels, P2X receptors are oligomer proteins. They assemble as stable homo- or heterotrimeric receptor channels inside the endoplasmic reticulum. Immunoprecipitation experiments have shown that, contrarily to all other P2X subunits, P2X7 receptors solely form homooligomers (Nicke, 2008).

Among the P2X receptor family, P2X7 exhibits several exceptional traits. Its intracellular carboxy terminal domain is much longer (239 amino acids) than those of other P2X receptor subunits (27–129 amino acids), a feature that has been hypothesized to confer the unique functional properties of P2X7. P2X7 may be considered a bifunctional receptor, which, depending on duration and intensity of its stimulation (Chessell et al., 2005), can act either as a non-selective cation channel, or as a large, non-selective pore with permeability to molecules of a molecular mass of up to ~900 Da.

As characterized on T-cells, a short-period (several seconds) stimulation of the receptor via binding of extracellular ATP at micromolar concentrations or via ADP-ribosylation (Seman, Adriouch et al. 2003) leads to opening of the ion channel, that is non-selectively permeable for small cations, i.e. Na<sup>+</sup>, K<sup>+</sup> and Ca<sup>2+</sup>. Channel opening leads to the efflux of K<sup>+</sup> and influx of Ca<sup>2+</sup>, and thus to depolarization of the plasma membrane.

Repeated or prolonged activation at high concentrations of ATP leads to the formation of a P2X7-receptor-mediated cytolytic pore, that is permeable for larger cations (Steinberg, Newman et al. 1987; Hickman, el Khoury et al. 1994; Schilling, Wasylyna et al. 1999; Virginio, MacKenzie et al. 1999). Opening of the pore due to P2X7 stimulation will induce apoptosis of the affected cell.

The various P2X receptors are expressed in a wide variety of tissue and cell types. They have been shown to modulate synaptic transmission on presynaptic and

postsynaptic nerve terminals throughout the central, peripheral and autonomic nervous systems. Furthermore, P2X receptors contribute to initiating contraction in cardiomyocytes (Fleetwood, Gordon et al. 1987; Frolidi, Varani et al. 1997), skeletal muscle (Li, Sinoway et al. 2002), vascular and visceral smooth muscle cells (North 2002) and endothelium (Surprenant, North 2009).

There is some degree of subtype specificity as to which P2X receptor subtypes are expressed on specific cell types.

P2X7 is predominantly present on cells of the immune system and initially was thought to be exclusively expressed on the latter (Collo, Neidhart et al., 1997). It is most prominently expressed and characterized on T-lymphocytes (Baricordi, Ferrari et al. 1996; Labasi, Petrushova et al. 2002; Seman, Adriouch et al. 2003; Kawamura, Aswad et al. 2005), but also on monocytes, macrophages and dendritic cells (Collo, Neidhart et al. 1997; Mutini, Falzoni et al. 1999; Mehta, Hart et al. 2001). P2X7 is involved in the activation and maturation of T-cells (Tsukimoto, Maehata et al. 2006; Aswad, Dennert et al. 2006). Evidence has been given for the participation of P2X7 in the transformation of macrophages to multinucleated giant cells, as seen in granulomatous inflammation (Chiozzi, Sanz et al. 1997; Di Virgilio, Falzoni et al. 1999).

Recent studies have given evidence of a diverse P2X7 distribution (Narcisse, Scemes et al. 2005; Zhang, Han et al. 2005), refuting its exclusiveness to immune-competent cells. For example, P2X7 receptors may appear in neurons, astrocytes (Dubyak et al., 2003) and microglial cells (Di Virgilio, Sanz et al., 1999), where they are thought to be important signaling proteins participating in the information processing of the normal and pathological central nervous system (Sperlagh, Vizi et al. 2006).

Multiple physiological and pathophysiological functions of the P2X7 receptor on the cells types of its expression are being discussed.

Importantly, P2X7 is involved in cytokine metabolism, mediating the processing of inactive pro-IL-1 $\beta$  to active IL-1 $\beta$  and contributing to the release of the mature cytokine (Ferrari, Chiozzi et al. 1997; Mehta, Hart et al. 2001) (Figure 5).

IL-1 $\beta$  is a proinflammatory cytokine and a major mediator of chronic inflammatory and autoimmune diseases, e.g. glomerulonephritis. In contrast to most other cytokines, IL-1 $\beta$ , along with IL-18, is not secreted via the ER-Golgi-pathway. It is synthesized as an inactive cytosolic precursor protein. Its release into the extracellular space requires proteolytic processing and enabling of the passage through the cell membrane.

In inflammatory circumstances, monocytes are stimulated to synthesize the inactive 34 kDa proform pro-IL-1 $\beta$  via bacterial lipopolysaccharide (LPS). Subsequent to the production of the proform, the monocyte's Nucleotide-binding and Leucine-Rich Repeat-, and PYD-Containing Protein 3 (NALP3) inflammasome complex is activated. The inflammasome is a multiprotein oligomer consisting of caspase 1, PYCARD and NALP. It is a component of the innate immune system and promotes the maturation of the inflammatory cytokines interleukin 1- $\beta$  and interleukin 18. The inflammasome activates an inflammatory cascade. Once active, the inflammasome binds to pro-

caspase-1, the precursor molecule of caspase 1 and leads to its mobilization as active caspase 1.

This enzyme, also known as IL-1 $\beta$  Converting Enzyme (ICE), processes pro-IL-1 $\beta$  to the biologically active mature 17 kDa IL-1 $\beta$  cytokine. In direct continuity, the mature cytokine is ATP-dependently discharged into the extracellular space. A brief stimulation of the P2X7 receptor at this juncture mediates the activation of the NALP3 inflammasome and the secretion of the cleaved IL-1 $\beta$  (Verhoef, Estacion et al., 2003, Perregaux, McNiff et al., 2000). It has been shown that macrophages exposed to LPS and ATP, generate 20–35 times more mature IL-1 $\beta$  than if stimulated with LPS alone (Grahames, Michel et al., 1999), which emphasizes the importance of P2X7 in this pathway. Studies involving P2X7 knockout mice have delineated the significance of the receptor in inflammatory conditions, depicting that LPS-activated macrophages of P2X7 KO mice do not secrete IL-1 $\beta$  following ATP-stimulation (Labasi, Petrushova et al. 2002).

Furthermore, P2X7 has pro-apoptotic potential, as prolonged stimulation of the receptor will lead to membrane blebbing or the formation of cytolytic pores and consequentially to apoptosis (Buisman, Steinberg et al., 1988). In HEK-293 cells, membrane blebbing and microvesiculation have been observed within seconds to minutes of P2X7 receptor activation leading to apoptosis (Wilson, Wilson et al., 2002).

Both P2X7 receptor-induced processing and release of IL-1 $\beta$ , and its triggering of the apoptotic pathway can occur simultaneously. However, these events can be dissociated, suggesting that they occur via parallel and independent pathways (Verhoef, Estacion et al., 2003).

Recent data suggests a pivotal role for P2X7 in initiating or maintaining an inflammatory response (Hughes, Hatcher et al. 2007).

Another effect of P2X7-stimulation is the activation of the metalloprotease ADAM17 (Jamieson, Snook et al. 1996; Gu, Bendall et al. 1998; Labasi, Petrushova et al. 2002) (Figure 5). ADAM17 (A Disintegrin And Metalloprotease domain 17), also known as TACE (tumor necrosis factor- $\alpha$ -converting enzyme), is a 70-kDa enzyme that belongs to the ADAM protein family of disintegrins and metalloproteases. Enzymes in this family are transmembrane glycoproteins, characterized by their conserved, multi-domain structure. In an inactive state, membrane-anchored ADAM17 carries a propeptide bound to its actual metalloprotease domain. P2X7-induced intracellular polarization changes result in the cleavage of the ADAM17 propeptide and thus activate the protease.

ADAM17 is involved in the cleavage and release of soluble ectodomains from membrane-bound pro-proteins, a process commonly entitled “shedding”. Being the first so-called 'shedase' to be identified, ADAM17 is understood to play a role in the release of a variety of membrane-anchored cytokines, cell adhesion molecules, receptors, ligands, and enzymes (Black 2002).

Most prominently, it is known to be involved in the processing of tumor necrosis factor alpha (TNF- $\alpha$ ) at the surface of the cell, and from within the intracellular

membranes of the trans-Golgi network. ADAM17 therefore 'sheds' or cuts off the active and soluble TNF- $\alpha$  from its membrane-anchored proform pro-TNF- $\alpha$ .

The protease similarly processes pro-transforming-growth-factor- $\beta$  (TGF- $\beta$ ) to TGF- $\beta$ , a ligand for EGF (epidermal growth factor) receptor, hence activating the receptor (Peschon, Slack et al., 1998). It also sheds Notch-1, inducing the intracellular Notch signaling cascade, which will, among other effects, result in the stimulation of transcription factors such as HeyL and thus stimulate the transcription of the EGF-Receptor protein (Brou, Logeat et al., 2000) (Figure 4). ADAM17 is furthermore involved in the shedding of L-selectin, also known as CD62L, a cell adhesion molecule found on leukocytes. L-selectin acts as a "homing receptor" for leukocytes to enter secondary lymphoid tissues via high endothelial venules (Scheller, Chalaris et al. 2011; Saftig and Reiss 2011; Gooz 2010).

ADAM17 is responsible for leucocyte recruitment in various inflammatory diseases (Garton, Gough et al., 2006) and is associated with tumorigenesis and tumour progression of various tumour entities, such as prostate cancer, where ADAM17 mRNA is increased (Murphy, 2008). ADAM17 is overexpressed in human primary colon carcinoma, and was co-expressed with its putative substrate epidermal growth factor receptor (EGFR) in neoplastic and endothelial cells (Blanchot-Jossic, Jarry et al. 2005). A role for the EGFR system in inflammation-related cell signaling has been suggested in studies on hepatocellular carcinoma (HCC) (Berasain, Perugorria et al., 2009). In chronic kidney disease (CKD), Angiotensin II causes renal lesions through the activation of ADAM17 and the release of TGF- $\alpha$ , which binds to and activates the epidermal growth factor receptor. Renal lesions such as glomerulosclerosis, tubular atrophy, fibrosis, mononuclear cell infiltration and proteinuria following chronic Ang II infusion are substantially reduced in mice treated with a specific ADAM17 inhibitor, and TGF- $\alpha$  KO mice. These findings indicate a disease-promoting role of ADAM17 in CKD (Shah and Catt, 2006).

Melenhorst et al. have reported an upregulation and de novo induction of ADAM17 in human renal diseases, such as membranous nephropathy or FSGS, and showed ADAM17 association with glomerular and interstitial injury, strongly suggesting a role for ADAM17 in the development of renal diseases (Melenhorst, Visser et al., 2009).

Furthermore, ADAM17 is involved in the activation of the Notch1 pathway. Recent studies have shown that this pathway is activated de novo in podocytes in humans with diabetic nephropathy and focal segmental glomerulosclerosis (FSGS) just as in rodent models thereof. Experimental evidence has been provided that Notch1 transcriptional activity in podocytes is responsible for the development of albuminuria and podocyte dysfunction in diabetic nephropathy, and that it leads to podocyte apoptosis (Niranjan, Bielez et al. 2008). It has been found that cleaved Notch1 is expressed on podocytes in proteinuric nephropathies, such as membranous nephropathy, lupus nephritis or IgA nephropathy and that the level of Notch1 expression correlated with the amount of proteinuria. These results raised the possibility that Notch pathway activation is a mechanism contributing to the pathophysiology of acquired renal diseases (Murea, Park et al. 2010).

Altogether, the activation of ADAM17 and consequentially of EGFR and the Notch1 pathway embodies another axis through which P2X7 may exert proinflammatory, disease-promoting effects, especially in the field of renal diseases.

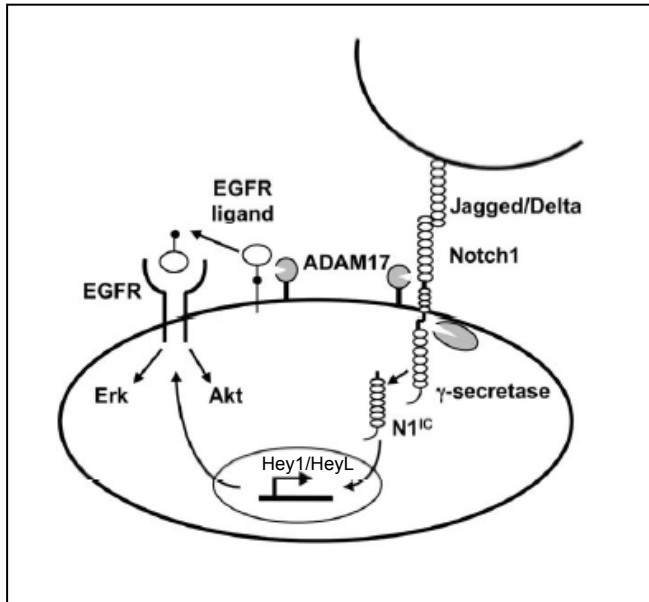


Figure 4: **ADAM17 and EGFR** (Baumgart, Seidl et al. 2010). ADAM17 mediates the shedding of membrane-tethered EGFR ligand precursors from the cell surface. EGFR ligand binding leads to the phosphorylation and activation of EGFR. In addition, ADAM17 regulates the activation of Notch1 signal transduction. Surface-bound Notch ligands, such as Jagged, bind to Notch1, which results in two cleavage steps. ADAM17 mediates proteolysis on the extracellular cleavage site, the  $\gamma$ -secretase complex cleaves on the intracellular cleavage site. The intracellular Notch1 fragment (N1IC) hence gets released and translocates to the nucleus, where transcription factors such as Hey1 or HeyL are targeted. One of the Notch1-regulated genes is the EGFR.

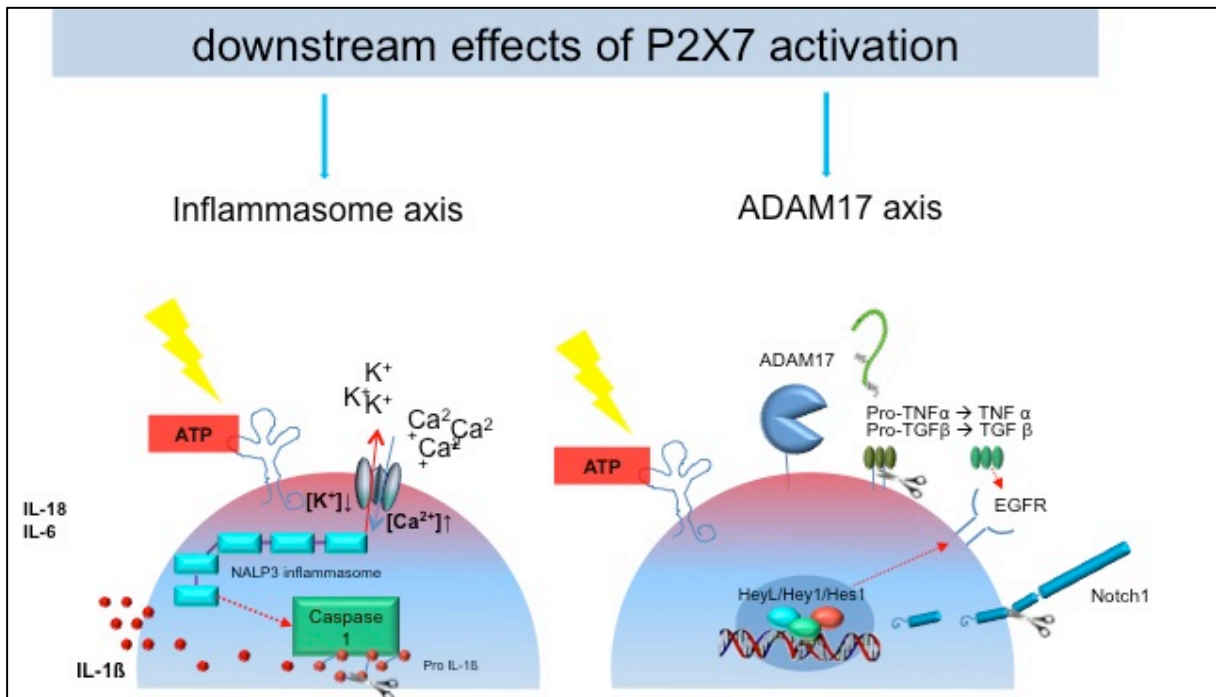


Figure 5: **Downstream effects of P2X7 activation**. Activation of the P2X7 receptor via binding of liberated ATP, e.g. in the context of inflammatory tissue damage, leads to intracellular polarization changes. P2X7 functions as a cation-channel, enabling the efflux of potassium and influx of calcium. Changes in polarization and ion levels lead to activation of Caspase1, an enzyme contained in the NALP3 inflammasome complex. Caspase1 then cleaves the inactive preform of the cytokine IL-1beta, pro-IL-1beta, to mature IL-1beta. P2X7 also is a co-mediator of its consequent release as well as of the processing and release of IL-18. P2X7 furthermore activates the sheddase ADAM17, which will result in e.g. the cleavage and release of mature TNF-alpha or the activation of the EGF receptor by its' ligand TGF-beta.

### **1.5.1.P2X7 in the kidney**

The P2X7 receptor contributes to the processing and release of IL-1 $\beta$ , to apoptosis and necrotic cell death. It activates ADAM17, a sheddase involved in the release of pro-inflammatory cytokines such as IL-6 or TNF- $\alpha$ .

Altered expression of this receptor in the glomeruli of glomerulonephritic kidneys might hence be a possible pathogenetic factor and several studies have been published that investigate the role of P2X7 in rodent and human GN.

Despite the rather low expression of P2X7 detectable in healthy kidneys (Harada, Chan et al. 2000; Turner, Vonend et al. 2004; Hillman, Burnstock et al. 2005), Turner et al. were able to detect upregulated expression of the receptor in the glomeruli of different rodent models of renal disease as well as in human lupus nephritis (Turner, Tam et al. 2007). In streptozotocin-induced diabetic rats, increased P2X7 receptor expression was localized mainly in glomerular podocytes, and to some extent in mesangial and endothelial cells (Vonend, Turner et al. 2004; Solini, Iacobini et al. 2005). Glomerular expression of P2X7 was also reported in transgenic rats with renin-dependent hypertension. Increased expression of P2X7 receptor could be detected in mouse and rat models of anti-glomerular basement antibody-mediated glomerulonephritis in intrinsic glomerular cells and infiltrating macrophages. In rat glomerulonephritis, increased P2X7 mRNA expression coincided with elevated IL-1 $\beta$  mRNA and with the onset of glomerular damage in this model (Turner, Tam et al. 2007).

Investigations in P2X7 knockout mice have provided more evidence for an important role of the receptor in the diseased kidney. Taylor et al. (Taylor, Turner et al. 2009) induced nephrotoxic nephritis in P2X7 knockout mice and found that P2X7 deficiency was significantly renoprotective compared with wildtype control animals. This was evidenced by a better renal function in P2X7 KO mice, a reduction in proteinuria and decreased histological injury. Furthermore, P2X7 KO animals exhibited significantly reduced macrophage infiltration (CD68 staining) and lower levels of urinary monocyte chemoattractant protein 1 (MCP-1). MCP-1 is an important chemokine, recruiting monocytes, memory T cells, and dendritic cells to sites of tissue injury, infection, and inflammation.

A benevolent effect for a selective P2X7-antagonist (A-438079) could be shown in the same study in a rat model of antibody-mediated GN.

Pavenstaedt et al. (Fischer, Saueressig et al. 2001) were able to detect mRNA of P2X7 within murine podocytes. This finding might be a hint of a possible direct function or effect of the receptor on the podocyte under inflammatory conditions.

In summary, current literature has shown that P2X7 seems to play a major proinflammatory role in immune-mediated renal injury. P2X7 deficiency proved to be renoprotective and P2X7 antagonists appear to be able to prevent the development

of disease in rodent models of NTN. P2X7 could therefore embody a target in the therapy of glomerulonephritis.

The P2X7 receptor is able to build both a ligand-gated cation channel and a cytolytic pore leading to membrane blebbing, enabling it to mediate various processes in the context of cell death and inflammation. Its involvement in the processing and release of IL-1 $\beta$  renders it a contributor to many inflammatory and autoimmune diseases. Recent studies using P2X7 receptor knockout mice and specific receptor antagonists have shown that the P2X7 receptor may be a therapeutic target in inflammatory diseases. Selective P2X7 receptor antagonists could be applied as anti-inflammatory agents in common inflammatory diseases. Studies using gene knockout mice and selective P2X7 receptor antagonists suggest that P2X7 is a viable therapeutic target for inflammatory diseases (Taylor et al. 2009; Labasi, Petrushova et al. 2002).

A P2X7 antagonist is currently tested in phase II trials for the treatment of rheumatoid arthritis (Keystone, Wang et al. 2011).

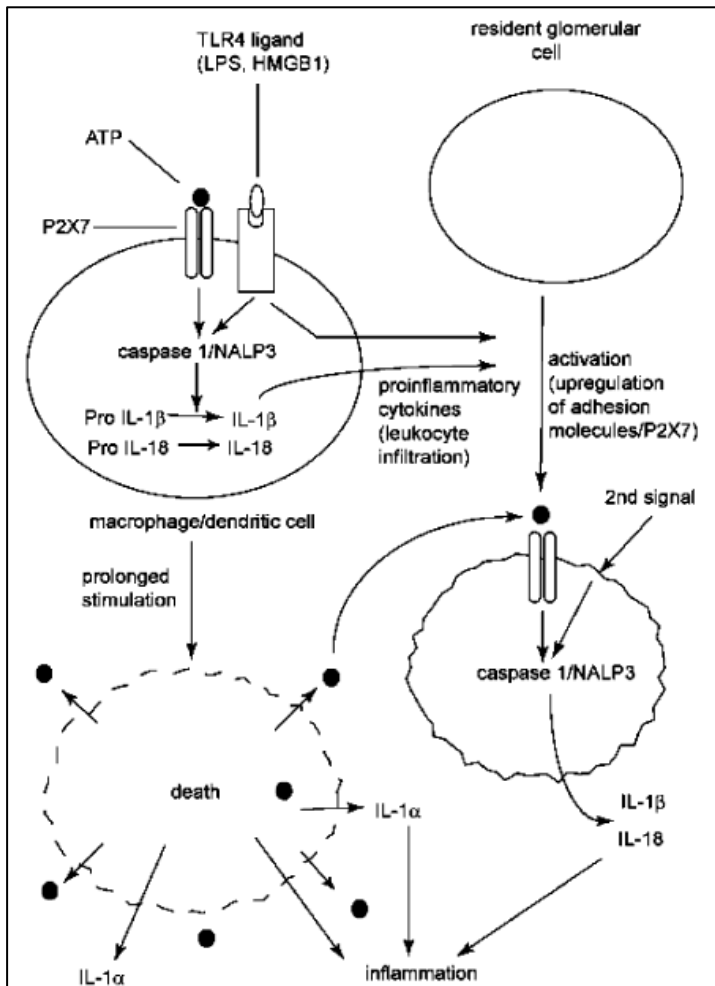


**Figure 6: Hypothetical role for P2X7 in inflammatory glomerular disease**

(Turner, Elliott et al., 2009).

Following incipient kidney injury, ATP is released from damaged cells and activates P2X7. P2X7 activation (probably together with Toll-like receptor (TLR) ligands such as lipopolysaccharide), stimulates the NALP3 inflammasome. Inflammasome activation results in the maturation of caspase 1, which in turn promotes cleavage, maturation and release of IL-1 $\beta$  and IL-18 from resident macrophages. Released cytokines mediate leukocyte influx and stimulate upregulation of P2X7 on resident renal cells, such as podocytes. Prolonged P2X7 stimulation results in cell death with release of intracellular pro-inflammatory mediators such as ATP, resulting in further cycles of P2X7 stimulation, fortifying glomerular injury.

### **1.5.2. Therapeutic targeting of P2X7 – Nanobodies**

One possible approach in specifically antagonizing P2X7 would be the generation of antibodies, or, even more favorable, nanobodies directed against the receptor. Antibodies nowadays embody important tools in experimental research and medical applications. For example, TNF- $\alpha$  neutralizing antibodies have proven to be efficient weapons in the therapy of inflammatory diseases such as rheumatoid arthritis (Feldmann, 2002).

Conventional antibodies are composed of two heavy and two light chains, with both chains contributing to the antigen-binding site. Adding to these common antibodies, camelids, such as llamas, and sharks produce antibodies that are solely composed of heavy chains, lacking the light chains (Hamers-Casterman, Atarhouch et al. 1993; Muyldermans 2001). The antigen-binding site of these so-called heavy chain antibodies (hcAbs) is formed of one single domain, referred to as VHH in camelid hcAbs and VNAR in shark hcAbs. VHH and VNAR may be produced as recombinant proteins. These proteins are then designated single domain antibodies (sdABs) or, due to their small size, nanobodies.

Nanobodies might offer advantageous treatment options compared to conventional antibodies. Favorable features of single domain antibodies, distinguishing them from conventional antibodies, are their small size, a high solubility, their thermal stability and a good in vivo tissue penetration. Various studies have been able to show the therapeutic potential of specific in vivo targeting of systemic disorders by custom-tailored sdABs, for example in models of tumour entities or amyloid diseases (Cortez-Retamozo, Lauwereys et al. 2002; Dumoulin, Last et al. 2003).

Single domain antibodies may be cloned into various formats by fusion to other proteins or peptides. It is thereby possible to individually tailor their utility for selected applications, e.g. for diagnostic or therapeutic purposes. So-called “tandem cloning” of two identical nanobodies connected by a linker peptide provides a bivalent product, that exhibits a higher avidity for the selected antigen. Tandem cloning to a single domain antibody with a distinct specificity, e.g. for serum albumin, can help in targeting the thus created nanobody to a particular compartment, or may help to increase the in vivo half life of the reagent, which would prove especially useful when applied in the context of renal diseases. Nanobodies linked to a sdAB against serum albumin are protected against renal elimination, rendering them suitable devices for therapeutically targeting the kidneys, in spite of their small size (Wesolowski et al., 2009). Single domain antibody reagents directed against cytokines, ecto-enzymes, tumor antigens, toxins or microbes might in the future become viable therapeutic options adding to conventional antibody treatment (Wesolowski et al., 2009).

Antagonizing the P2X7 receptor by the means of anti-albumin VHH coupled nanobodies might embody a promising option in attenuating inflammatory diseases, such as glomerulonephritis

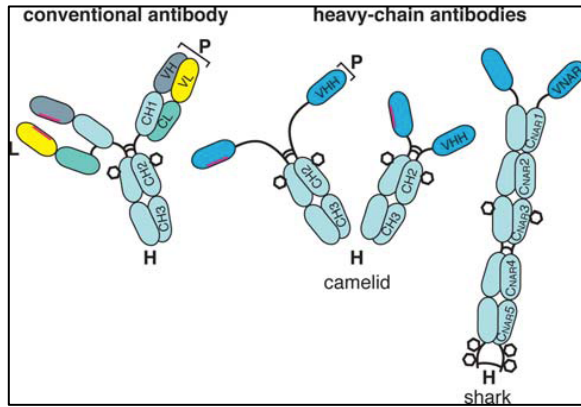


Figure 7:  
**Structural features of conventional and heavy chain antibodies**  
(Wesolowski et al., 2009)

## 2. Working hypothesis

A previous study by Manago et al. suggested a possible relationship between the Ubiquitin C-terminal Hydrolase L1 and P2X receptors in the central nervous system (Manago, Kanahori et al. 2005).

Various other publications respectively provided evidence for a role of UCH-L1 and the pro-inflammatory P2X7 receptor in separate in the context of glomerulonephritis.

It has been shown that a de-novo-expression of UCH-L1 occurs in diseased podocytes in human and rodent GN. However, it remains unexplained whether this cellular process has a renoprotective function or whether it is a noxious co-perpetrator of glomerulonephritic injury. The hypothesis promoted in this thesis is that UCH-L1 expression plays a tutelary role in the diseased podocyte.

An upregulation of the proinflammatory receptor P2X7 in rodent models of GN has been reported by multiple publications. Evidence has also been given that this upregulation does involve the podocyte. P2X7 upregulation is hence considered a deleterious mechanism in the context of GN in this thesis.

An interaction between UCH-L1 and P2X7 could possibly play a role in the pathogenesis and progression of glomerulonephritis. UCH-L1 being considered a protector of the podocyte, this protein might exert attenuating effects on the proinflammatory P2X7 receptor.

The aim of this thesis was to further elucidate the potential protective or noxious functions of UCH-L1 and P2X7 in glomerulonephritis in vivo, using the anti-podocyte nephritis (APN) model, and to scrutinize the hypothesis of a possible interaction between both proteins in this model of GN in podocytes.

In order to investigate this hypothesis, the following questions were addressed:

1. Are UCH-L1 KO mice more vulnerable towards APN induction?
2. How do P2X7 KO mice react towards APN induction? Is there a difference in susceptibility towards podocyte injury in P2X7 KO versus UCH-L1 KO mice?
3. Are there alterations in expression or function of UCH-L1 and P2X7 after the onset of glomerulonephritis in the kidney/podocyte?
4. Is there a relationship between UCH-L1 and P2X7 in the diseased podocyte? What is the nature of this relationship?

### 3. Materials & Methods

#### 3.1. Materials

##### 3.1.1. Antibodies

Table 1: primary/secondary antibodies and nanobodies used

Primary antibody	species	application	dilution	producer
anti-ADAM10	rabbit	Western Blot	1: 1000	Dr.Chalaris/Prof.Rose-John, Biochemical Institute, University of Kiel
anti-ADAM17	rabbit	Western Blot	1: 1000	Dr.Chalaris/Prof.Rose-John, Biochemical Institute, University of Kiel
anti-B220	rat	Immunohistochemistry (IHC)	1:1000	R&D Systems
anti-CD3	rabbit	IHC	1:1000	DAKO
anti-EGFR	goat	Western Blot	1:1000	R&D Systems
anti-F4/80	rat	IHC	1:400	Serotec
anti-IL-1 $\beta$	goat	Western Blot	1: 1000	R&D Systems
anti-Mac2	rat	IHC	1:1000	Cedarlanes
anti-P2X7 (C-terminal)	rabbit	Western Blot	1: 1000	Alomone
anti-P2X7 (N-terminal)	rabbit	Western Blot	1:500	Alomone
anti-P2X7 #230	rat	IF/IHC	1:100	Koch-Nolte Lab, Institute for Immunonology, UKE
anti-P2X7 #229	rat	IF/IHC	1:100	Koch-Nolte Lab, Institute for Immunonology, UKE

Materials & Methods

anti-P2X7 #241	rat	IF/IHC	1:100	Koch-Nolte Lab, Institute for Immunonology, UKE
anti-P2X7 K1G	rabbit	IF/IHC	1:400	Koch-Nolte Lab, Institute for Immunonology, UKE
anti- $\beta$ -Actin	mouse	Western Blot	1: 3000	Sigma
anti-UCH-L1 U104	rat	Western Blot/IHC	1:1000/ 1:20	Prof. Grötzinger, Biochemical Institute, University of Kiel
anti-WT1	rabbit	IHC	1:600	Santa Cruz

secondary antibody	species	conjugate	dilution	producer
anti-mouse	donkey	HRP	1: 40 000	Jackson Immunoresearch Laboratories (IL)
anti-rabbit	donkey	HRP	1: 10 000	Jackson IL
anti-rat	donkey	HRP	1: 15 000	Jackson IL
biotinylated anti-rabbit	mouse	Biotin	1:400	Vector Labs
biotinylated anti-rat	donkey	Biotin	1:400	Jackson IL

Nanobody	function
Anti-P2X7 14D5	antagonistic
Anti-P2X7 13A7	agonistic
Dummy	non-binding control

Table 2: primers used

Primer/target	producer	sequence
18s	Invitrogen	F: CAC GGC CGG TAC AGT GAA AC R: AGA GGA GCG AGC GAC CAA A
ADAM17	Invitrogen	F: GCA CAG GTA ATA GCA GTG AGT GC R: CAC ACA ATG GAC AAG AAT GCT C
Hey1	Invitrogen	F: CGG GCG CAG ATG ACC GCC R: ATG CAC TCG CTG AAG CCG GC
HeyL	Invitrogen	F: GGA GAG GCT GCC AAG GTT TT R: GCA AAT TGG CCG TCA GGA
IL-1 $\beta$	Invitrogen	F: GCTCAGGGTCACAAGAAACC R: CATCAAAGCAATGTGCTGGT
MCP-1	Invitrogen	F: AGC CAA CTC TCA CTG AAG CC R: CAT TCA AAG GTG CTG AAG ACC
P2X7 Balb/c	Invitrogen	F: TGC ACA TGA AGA ACA CCT TCC R: CCT GCA AAG GGA AGG TGT AG
P2X7 C57/Bl6	Invitrogen	F: GAC GCT GAA GAA CAC CTT CC R: CCC ACC CTC TGT GAC ATT
UCH-L1	Invitrogen	F: AGC TGG AAT TTG AGG ATG GA R: GGC CTC GTT CTT CTC GAA A

F=Forward primer sequence (5'-3'); R= Reverse primer sequence (5'-3')

### 3.1.2. Chemicals

ABC AP Kit	Vector
Albumin, from bovine serum (BSA)	Sigma
Aqua ad iniectabilia	Braun
Avidin- Biotin- Blocking Kit	Vector Labs
BM Blue POD Substrate	Roche
Calyculin A	Merck
Complete 25x	Merck
DAKO pH9 target retrieval solution	DAKO
DAPI Vectashield Hard Set Mount	Vector Labs
ECL chemiluminescence developer	Pierce
Ethanol 100%	J.T. Baker
First Strand Buffer	Invitrogen
FITC- Avidin	Vector
Fluoromount	SouthernBiotech
Formalin	Merck
Glycin	Roth
Goatserum	Vector
Haematoxylin	Serva
HCl 1N	Merck
H <sub>2</sub> SO <sub>4</sub> 1N	Roth
Horse serum	Vector Labs
Hydrogen peroxide (H <sub>2</sub> O <sub>2</sub> ) 30%	Sigma
Isofluran	Abbot
Isopropanol	Fluka
M-MLV Reverse Transcriptase	Fermentas
Milk powder (Blocking Solution WB)	Spinnrad
Methanol	Roth
Morpholinopropansulfonacid (MOPS)	Serva
Na <sub>2</sub> HPO <sub>4</sub> x 2 H <sub>2</sub> O	Merck
Naphtol- AS- Bisphosphat	Fluka
Neufuchsin	Serva
Paraformaldehyd (16%)	EM Sciences
Periodic acid	Merck
Phenolchloroforme	Fluka
Random Hexamer Primers	Invitrogen
Reagent A+B, Protein Assay	BioRad
RNAse Out	Invitrogen
Schiff reagent	Sigma
Sodium acetate 3M	Merck

Sodium azide	Serva
Sodium chloride	Serva
Sodium citrate x 2 H <sub>2</sub> O	Merck
Sodium dodecyl sulfate (SDS)	Merck
Sodium fluoride	Merck
Sodium iodate	Merck
Sodium vanadate	Merck
Superblock blocking reagent	Pierce
TissueTec freezing medium	Jung
T- Per Tissue Protein Extraction Reagent	Pierce
Tris	Sigma
Triton X 100	Sigma
Trizol	Invitrogen
Tungsten carbide beads	Invitrogen
Tween 20	Sigma
Xylol	Th. Geyer GmbH
ZytoChem-Plus AP Polymer-Kit	Zytomed

### 3.1.3. Materials

Blot Chamber (Novex Mini Cell)	Invitrogen
Gel Chamber	Peqlab Biotechnology
NuPage 4-12% Bis- Tris- Gel	Invitrogen
Petri dishes	Sarstedt
96 well plates	Sarstedt
PVDF- Membrane (Immobilon)	Millipore
Albumin ELISA Kit (Mouse urine)	Bethyl
X-ray film (Super RX)	Fuji
High Performance Chemoluminescence film	GE Healthcare
sponges	Invitrogen
scalpels	Braun
Urine Stix (Multistix 10SG)	Siemens
Whatman Filter paper	Schleicher & Schuell
Mouse-Interleukin 1 $\beta$ ELISA Kit (DuoSet)	R&D Systems
Mouse-Interleukin 6 ELISA Kit (Quantikine)	R&D Systems
Mouse-MCP-1 ELISA Kit	BioLegend
SYBRGreen reagent	Biozym

### 3.1.4. Animals

UCH-L1 KO C57/Bl6 mice  
WT C57/Bl6 mice  
WT Balb/c mice  
P2X7 KO C57/Bl6 mice  
P2X7 KO Balb/c mice

Animal facilities UKE Hamburg

### 3.1.5. Microscopes

Light microscope (Axioskop 40)  
Inverse microscope (Axiovert 25)  
Inverse microscope (IM 35)  
Confocal microscope (LSM 510  $\beta$ )

Zeiss  
Zeiss  
Zeiss  
Zeiss

### 3.1.6. Software

Adobe Illustrator  
Adobe Photoshop  
GraphPad Prism 5  
ImageJ  
StepOne Software (qPCR)  
Excel  
Windows XP

Adobe  
Adobe  
GraphPad  
Leica  
AB Applied Biosystems  
Microsoft  
Microsoft

### 3.1.7. Instruments

Autoclave (KSG 114)  
Blot device (Novex Mini Cell)  
ELISA Reader  
Gel electrophoresis chamber  
Heat block (Thermomixer)  
fridge 4°C  
freezer -20°C  
freezer -80°C  
magnetic stirrer (Variomag Maxi)  
power supply  
Personal Computer  
pH- Meter (Inolab)  
PlateReader EI 808

KSG Sterilisators GmbH  
Invitrogen  
Dynatech Laboratories  
Peqlab Biotechnology  
Eppendorf  
Liebherr  
Privileg  
Privileg  
Komet  
Pharmacia Biotech  
LG Systems  
WTW  
Dynatech Laboratories

Pipets	Sarstedt
Automatic pipet device (Accujet)	Brand
x-ray film developer (CP 1000)	Agfa
shaker (Rocky)	Fröbel Labortechnik
Thermocycler	Biometra
Desk centrifuge (Type 5415 R)	Eppendorf
Desk centrifuge (Mini Spin)	Eppendorf
Vortex	Janke & Kunkel
scale (SBA 41)	Scaltec
centrifuge (Biofuge primo R)	Heraeus
centrifuge (Megafuge 1.0 R)	Heraeus
realtime PCR System (StepOne Plus)	AB Applied Biosystems
Photometer	Eppendorf
Vacuum drier	Eppendorf

### 3.1.8. Buffers

#### Binding Buffer pH 9,6 (Mouse Albumin ELISA)

0.05 M carbonate-bicarbonate  
ad 1 L H<sub>2</sub>O

#### Blocking Buffer pH 8,0 (Mouse Albumin ELISA)

50 mM Tris  
0.14 M NaCl,  
1% bovine serum albumin  
ad 1 L H<sub>2</sub>O

#### Blocking Solution (Western Blot)

3-5% milk powder  
in TBST

#### Blotting Buffer (Western Blot)

192 mM Glycin  
50 mM Tris  
ad 1 l H<sub>2</sub>O

#### Boehmer's Haemalum solution

200 ml	H <sub>2</sub> O
10 g	Aluminium potassium sulfate x 12 H <sub>2</sub> O
0,1 g	Sodium iodate
0,5- 1 g	Haematoxylin
10 g	NN- Dimethylformamide

Citrate Buffer pH 6,0-6,1 (10mM)

2,35 g	Sodium citrate x 2 H <sub>2</sub> O
0,31 g	citric acid monohydrate
1 l	H <sub>2</sub> O

Loading Buffer (Western Blot (LDS 4x))

Nu Page Loading buffer 4x LDS
0,4 M DTT

Lysis Buffer (Western Blot)

1x	Complete Protease Inhibitor Cocktail (25x)
1mM	Natriumvanadate
1mM	Natriumfluoride
1mM	Calyculin A
Ad	TPER

Morpholinopropansulfonic acid buffer (MOPS) 20x

50 mM	MOPS
50mM	Tris Base
0,1 %	SDS
1 mM	EDTA
ad 1 l	H <sub>2</sub> O

Neufuchsin solution

0,3 g	sodium nitrite
7,5 ml	H <sub>2</sub> O
300 ul	Neufuchsin stock solution
800 ul	Naphtol- AS- Bisphosphate- solution
150 ml	TNT- Puffer

Neufuchsin stock solution

2,5 g	Neufuchsin
50 ml	2 N HCl

PFA – tissue fixative

4%	Paraformaldehyde (16%)
in PBS	

Phosphate-buffered saline (PBS)

137 mM	NaCl
2,7 mM	KCl
1,4 mM	KH <sub>2</sub> PO <sub>4</sub>
4,3 mM	Na <sub>2</sub> HPO <sub>4</sub> x 2H <sub>2</sub> O
ad 1 l H <sub>2</sub> O	

TBS Buffer

10 mM Tris (pH 7,4)  
100 mM NaCl  
ad 1 l H<sub>2</sub>O

TBST Buffer

0,05 % Tween 20  
in TBS

Washing Buffer (ELISA)

50 mM Tris  
0.14 M NaCl  
0,05% Tween-20  
pH 8,0  
ad 1 L H<sub>2</sub>O

## **3.2.Methods**

### **3.2.1.General mouse maintenance**

All C57/Bl6 (wildtype, UCH-L1 KO and P2X7 KO mice) and Balb/C (wildtype and P2X7 KO) mice were bred and maintained in the animal facilities of the UKE Hamburg under special pathogen free conditions.

Animals were housed in individually ventilated cages and provided weekly with fresh water and food. Mice between 8 and 10 weeks of age were used for experiments in accordance with local animal experimentation guidelines.

### **3.2.2.Urine collection**

Urine was collected from mice for a 6-hour time period using metabolic cages, providing the mice with fresh drinking water.

### **3.2.3.Urine and serum parameter measurement**

The measurement of all clinical parameters (urine urea nitrogen, blood urea nitrogen, cholesterol, triglycerides, creatinine) was kindly performed by the central laboratory, Clinical Chemistry Department at the UKE Hamburg. Urine and serum creatinine were measured using routine diagnostic methods according to Jaffé.

BUN and creatinine are rather error-prone kidney retention parameters and may be influenced by extrarenal factors like nutrition and general health condition (e.g. reduction in muscle mass in poor health status). Levels of Creatinine and BUN hence had to be considered as approximately indicative of changed kidney function and should be regarded in context with all other clinical parameters measured (indicators of nephrotic syndrome, proteinuria, weight changes).

Creatinine is produced in the muscle as a degradation product in creatinine phosphate metabolism. In the healthy kidney, creatinine is almost completely filtered out from the blood flow by the intact glomerulus.

Serum Creatinine levels roughly correlate with the glomerular filtration rate (GFR) and hence give evidence of normal or impaired kidney function. Urea is the final product of protein metabolism. Its blood levels depend on the volume of glomerular filtrate operated by the kidney and on urea reabsorption in the renal tubule, which may vary between 40% in diuresis and 70% in antidiuresis.

### 3.2.4. APN induction and monitoring

Anti-podocyte Nephritis (APN) was similarly induced in wildtype, UCH-L1 KO and P2X7 KO mice of C57/Bl6 and Balb/C strains. Glomerulonephritis induction was performed via injection of sheep anti-mouse podocyte serum pursuant to the protocol published by Meyer and Schwesinger in 2007 (Meyer, Schwesinger et al. 2007). The serum was concentrated twofold by high-pressure membrane filtration technique.

On day 0 of the experimental course, a group of mice representing each of the three genotypes to be investigated were injected intravenously with 150 $\mu$ l (Balb/c mice) or 300 $\mu$ l (C57/Bl6 mice) of AP (anti podocyte) serum via the tail vein. This serum was obtained from sheep immunized with a suspension of murine podocytes and hence contained polyclonal sheep anti-mouse podocyte antibodies (Meyer, Schwesinger et al. 2007). Another group of mice of each genotype was treated with an equal dose of preimmune (PI) serum, which had been drawn from sheep before immunization. PI serum treated mice served as healthy control animals.

A total of 6 mouse groups was investigated throughout the experimental course – two wildtype mouse groups, one AP- and one PI-serum treated, P2X7 KO AP and PI and UCH-L1 KO AP and PI mouse groups respectively. Glomerulonephritis development was monitored for 20 days in animal set 1 and 14 days in sets 2 and 3. In animal set 1, 3 UCH-L1 KO animals treated with AP-serum died prematurely due to a severely impaired constitution following anti-podocyte nephritis induction.

Weighing and urine collection were performed every 3 days and albumin ELISA from each urine sample was used to assess the course and levels of proteinuria.

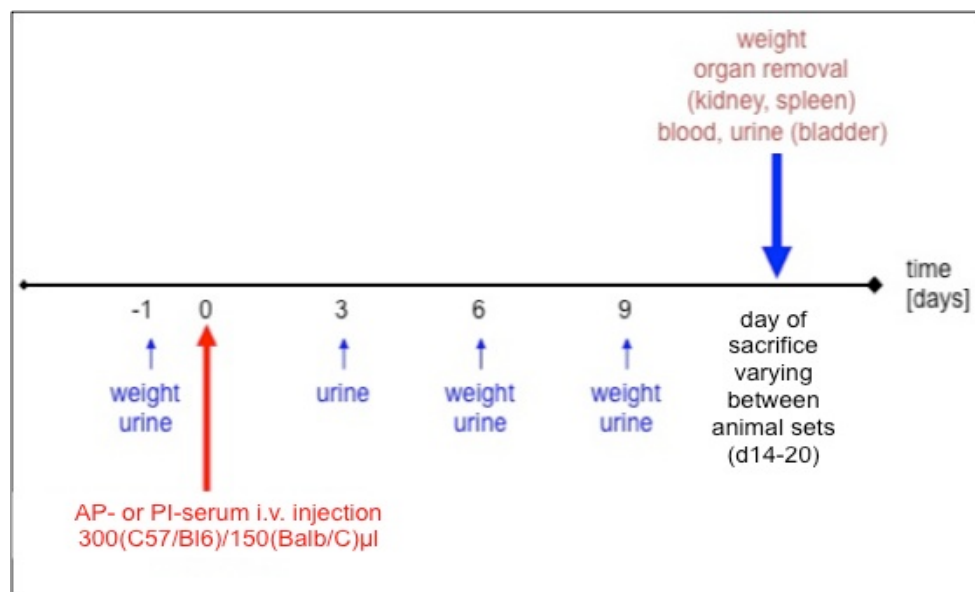


Figure 8: APN induction and monitoring plan

### 3.2.5. Nanobody treatment

Three different nanobody (NB) constructs were used in this study (Danquah 2012; EP2370465 Laeremanns, Stortelers et al. 2011). The constructs consisted of a tandem chain of three genetically fused nanobodies connected by a flexible linker peptide of 25 amino acids (G4S)<sub>5</sub>. Two of these nanobodies were directed against P2X7, the bivalency increasing the avidity for P2X7. Nanobody 14D5 was used as P2X7-agonist, 13A7 as antagonist of the receptor. The third nanobody used was directed against mouse albumin (so-called “dummy” NB). All three nanobodies were anti-albumin VHH coupled. This tagging protected the NBs against renal elimination and granted a longer half-life, which were crucial traits considering the kidney being the designated therapeutic target of the nanobodies. All nanobodies were diluted to the desired concentration (first dosage 50 µg, following doses 25 µg) in sterile water and injected intraperitoneally according to the treatment plan showed below (Figure 9).

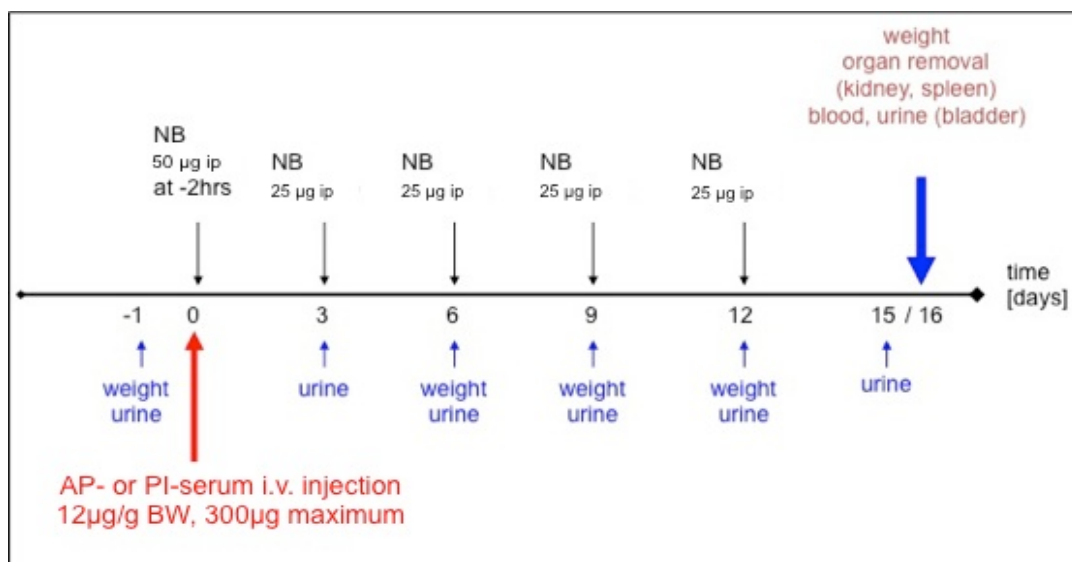


Figure 9: **Nanobody treatment plan**

### 3.2.6. Experimental set-ups, sets of animals

Anti-podocyte nephritis was induced as described above in a total of 3 animals sets. The first 2 sets were intended to monitor and compare the development and peculiarity of renal disease in wildtype versus P2X7 or UCH-L1 KO animals and P2X7 KO versus UCH-L1 KO respectively. The experimental set-up was mainly similar in these 2 sets with APN induction and without any further treatment post APN induction.

Set 1 comprised Balb/c P2X7 KO, Balb/c wildtype mice, C57/BL6 UCH-L1 KO mice and C57/BL6 mice heterozygous for UCH-L1 (as control). A total of 6 mice per

genotype were treated and split equally – 4 mice were administered AP serum while 2 control animals received PI agent.

In set 2, involving only C57/Bl6 mice of all 3 genotypes (wildtype, P2X7 KO, UCH-L1 KO), a higher quantity of animals was analyzed. A total of 10 wildtype mice were treated, among which 6 animals were injected with AP serum and 4 animals served as PI control. P2X7 KO and UCH-L1 KO groups were split and treated equally, both comprising 10 animals respectively.

Animals set 3 comprised exclusively C57/BL6 wildtype animals and involved anti P2X7 nanobody treatment (see above). A total of 24 mice were analyzed. 4 animals were injected with PI serum and did not receive any nanobody treatment, serving as healthy and untreated control. 3 more mice were treated with PI serum and received the “dummy” nanobody in addition as control for possible effects mediated by recombinant Nanobodies purified from yeast cells. 6 more wildtype mice received the dummy nanobody while being treated with anti-podocyte serum, thus embodying the diseased control, free of directed nanobody treatment. 6 mice were treated with the P2X7 agonistic nanobody in addition to AP serum. 5 more animals received the P2X7 antagonist after being injected with AP serum as well.

In all 3 sets, clinical parameters, comprising the course of proteinuria and weight change as well as all urine and serum parameters mentioned above were analyzed to gain information about the vulnerability of the different genotypes towards glomerulonephritis progression. Inflammatory response and expression patterns of selected proteins (UCH-L1, P2X7, ADAM17) and cytokines (IL-1 $\beta$ , MCP-1, IL-6) were compared using biomolecular techniques and immunohistochemistry staining.

### **3.2.7. Sacrifice of animals, organ harvesting**

On days 11 to 20 (see above) past APN induction, mice were sacrificed via terminal bleeding and organs were harvested. First, animals were anesthetized by isoflurane/O<sub>2</sub> inhalation. The abdominal and retroperitoneal cavity of the narcotized mice was opened longitudinally and the aorta was punctured for blood withdrawal. Blood was pipetted into eppendorf tubes and later centrifuged at 13200 rpm, resulting in the sedimentation of corpuscular blood components at the tube bottom with separation of serum as supernatant. Serum was then pipetted into separate tubes and stored at -20°C for further analysis of serum parameters (see above). Kidneys and spleen were extracted, weighed and processed for further analysis. A half of one kidney was transferred to a 4% formaldehyde solution for 24 hours and then retransferred to PBS for subsequent paraffin embedding and histological evaluation. About one sixth of a kidney was embedded in TissueTec and deep frozen for cryosectioning and immunohistochemistry. The remaining kidney tissue was cut into pieces of approximately 30-50  $\mu$ g and snap-frozen in liquid nitrogen. The tissue

pieces were then stored at -80°C for further analysis. Mouse spleens were processed similarly.

### **3.2.8. Histology**

#### **3.2.8.1. Preparation of tissue sections**

##### **3.2.8.1.1. Paraffin sections**

Before 1-3 µm thin tissue sections could be prepared for staining procedures and histologic evaluation, mouse organs had to be processed to an appropriate matter for cutting and long-term storage. The aim of processing was to remove water from tissues and replace it with a medium that solidifies to allow thin sections to be cut. For light microscopy, paraffin wax is most frequently used as tissue matrix. Since it is immiscible with water, samples first had to be dehydrated by being transferred through baths of progressively concentrated ethanol of 60%, 70% and finally 100% concentration for 1,5 hours of incubation in each bath. This was followed by two baths in the hydrophobic clearing agent xylene at a concentration of 100%, to remove the alcohol. Finally, specimens were incubated in 2 paraffin baths for 1 hour before being embedded in paraffin wax in molds. The hardened blocks containing tissue samples were then ready to be sectioned using a microtome. To grant adherence of kidney and spleen sections on object slides, fixation was obtained by incubating the section slides in an oven at 40°C overnight.

Preliminary to each staining procedure, sections were deparaffinized in xylene baths for 3 x 5 minutes. Subsequently, rehydration was performed by transferring sections through ethanol baths of decreasing concentration (100%, 95%, 75%, twice for 5 minutes in each bath). Finally, sections were rinsed in water.

##### **3.2.8.1.2. Cryosections**

About one sixth of a kidney from each mouse was embedded in TissueTek and deep frozen for cryosectioning and immunofluorescence staining after harvesting. TissueTek is a gel like formulation of water-soluble glycols and resins and provides a specimen matrix for cryostat sectioning at temperatures of -10°C and below. When frozen, Tissue Tek has the same density as frozen tissue

The key instrument for cryosectioning is the cryostat, which is essentially a microtome inside a freezer. The specimen is placed on a metal tissue disc inside the cryostat which is then secured in a chuck. Subsequently, it is cut frozen with the microtome portion of the cryostat. The section is then picked up on a glass slide and may afterwards be deep frozen again until staining is performed.

### **3.2.8.2. PAS staining**

PAS-stain (Periodic Acid Schiff-stain) is a staining method used to detect glycogen in tissues (Gomori 1952). The reaction of periodic acid selectively oxidizes glucose residues, creates aldehydes that react with Schiff reagent and finally results in a purple-magenta coloring of carbohydrate structures. It is mainly used for staining structures that contain high amounts of carbohydrate macromolecules, like connective tissue or basal laminae. A suitable nuclear stain like Boehmer's haemalum is often used as counterstain.

Deparaffinized tissue sections were primarily incubated in 1% periodic acid for 1 minute. Hydroxyl groups of saccharides were thus oxidized to aldehyde groups. After rinsing 2-3 minutes in warm tap water, sections were incubated in Schiff's reagent for 40 minutes. The contained sulfuric acid Fuchsin thereby built purple-magenta coloured complexes with the aldehyde groups. This was followed by another 5 minute washing step in water. For a better display of nuclei, a subsequent haemalum nuclear stain was accomplished. Sections were therefore incubated in haemalum solution for 3 minutes and dipped in a mixture of hydrochloric acid and alcohol for differentiation. Finally, dehydrated sections were covered with glas cover slips using Eukitt agent.

### **3.2.8.3. Immunohistochemistry – general principle**

Immunohistochemistry (IHC) refers to the detection of an antigen (e.g. a protein) in cells of a tissue section by exploiting the principle of specific antibodies binding their antigen in biological tissues. IHC is used in research to understand the distribution and localization of biomarkers and differentially expressed proteins in different compartments of a tissue (Ramos-Vara 2005). Visualization of an antibody-antigen interaction can be accomplished by different techniques. Commonly, the last of the antibodies used throughout a staining procedure is conjugated to an enzyme, e.g. a peroxidase, that can catalyze a color-producing reaction once its substrate is added. The substrate has to be bound to a chromogen for visualization of the enzymatic reaction. After developing the stain by adding this substrate, the distribution of the stain can be examined by microscopy. Alternatively, the antibody can also be tagged to a fluorophore like FITC or AlexaFluor (immunofluorescence staining).

In staining procedures where antibodies are visualized via an enzyme-catalyzed reaction, the first step is binding of the specific primary antibody to the cell or tissue sample. The detection of the primary antibody may then be accomplished directly or indirectly. In direct detection, the primary antibody is directly tagged with an enzyme, which is then used to catalyze a chemical reaction to generate a coloured product. In indirect detection, primary antibodies can be tagged with a small molecule that may be recognized by another enzyme-conjugated binding molecule with high affinity. The most common example of this principle is a biotin linked primary antibody that binds

to an enzyme-bound streptavidin. This method can be used to amplify the signal. Alternatively, an untagged primary antibody is detected using a general secondary antibody that recognizes all antibodies originating from same animal species. The secondary antibody is then tagged with the enzyme.

There are two enzymes commonly used in this sub-class of immunohistochemistry – peroxidase (HRP) and alkaline phosphatase (Miller et al., 1973).

Hydrogen peroxide serves as substrate for the peroxidase. Release of protons causes oxidization of the colourless chromogen to a coloured end product. Possible chromogens are DAB (3,3'-Diaminobenzidin), Luminol (as described in Western Blotting) or TMB (Tetramethylbenzidin).

Organic phosphate compounds serve as substrate for the alkaline phosphatase (AP). AP cleaves the phosphate residues and the liberated product reacts with the chromogen to a coloured end product. The most prominent chromogen is Neufuchsin, resulting in a purple-magenta reaction product.

*All staining procedures described below were performed on formalin-fixated paraffin mouse kidney sections.*

#### **3.2.8.3.1. F4/80 staining**

F4/80 is a glycoprotein of 160 kDa, an antigen expressed on murine macrophages, monocytes and dendritic cells (Leenen et al., 1994). The antibody used (rat anti-mouse F4/80, Serotec) binds to macrophages of variable origin (e.g. peritoneal cavity, lungs, spleen). To perform F4/80 staining on mouse kidney sections, sections were first deparaffinized as described above. Deparaffinization was followed by a washing step in PBS (3 x 5 minutes) and antigen retrieval. Antigen retrieval was obtained by incubation of the sections in 0,05% Trypsin-EDTA for 15 minutes at 37°C. Subsequently, sections were dipped shortly in 100% Ethanol and again washed in PBS. Afterwards, blocking of non-specific binding was obtained by incubating the sections in a mixture of 2% horse serum, 1% BSA, 0,1% “kalte Fischhautgelatine”, 0,1% Triton X 100, 0,05% Tween 20 in PBS (pH 7,2) for 30 minutes at room temperature. Following the blocking step, the primary anti-F4/80 antibody was added, prediluted 1:400 in a mélange of 1% BSA and 0,1% “kalte Fischhautgelatine” in PBS (pH 7,2). The sections were incubated with the antibody for 1 hour at RT. Afterwards, non-bound antibody was rinsed off using PBS (3 x 5 minutes). Subsequently, the prediluted secondary antibody (1:500 in PBS) was pipetted on the sections and incubated for 30 minutes at room temperature. A washing procedure using PBS and TBS followed antibody incubation. Subsequently, Streptavidin-AP was applied on the slides and incubated for 30 minutes at room temperature. After rinsing off any reagents using TBS, color development was achieved by incubating the sections in Neufuchsin for about 30 minutes in the dark. Dipping the sections in tap water

stopped the color reaction. Subsequently, a 1,5 minute incubation in Boehmer's haemalum was performed for the depiction of nuclei. Sections were then expurgated in tap water and finally covered using glass cover slips and Arabic gum.

### **3.2.8.3.2. Mac2 staining**

Mac2 staining is used for the depiction of intraglomerular macrophages in mouse kidney sections (Flotte et al., 1983). The Mac2 antibody used specifically binds to mouse Mac2, a membrane-bound antigen of 32 kDa expressed by a subpopulation of macrophages (e.g. interdigitating dendritic cells, Langerhans cells, peritoneal macrophages) and on epithelial cells.

To perform Mac2-staining on mouse kidney sections, sections were first deparaffinized and rehydrated as described above. This was followed by antigen retrieval through boiling in citrate buffer (pH 6,1) for 25 minutes. The container containing buffer and sections were cooled on ice 15 minutes. Subsequently, sections were washed twice in distilled water and twice in PBS for 5 minutes. Blocking of non-specific binding was obtained by pipetting 5% horse serum in PBS on the sections for 30 minutes at room temperature. The primary anti-Mac2 antibody (rat anti-mouse Mac2, Cedarlanes) was diluted 1:1000 in 5% horse serum and incubated overnight at 4°C. On the next day, sections were washed in PBS and a biotinylated secondary antibody (biotinylated donkey anti-rat IgG, Jackson Labs), diluted 1:400 in 5% horse serum, was added and incubated for 30 minutes at RT. Following another washing step in PBS, 1:100 diluted Streptavidin-AP in PBS was pipetted on the sections and incubated for 30 minutes at RT. Another washing step was followed by neufuchsin-development in the dark for approximately 10-20 minutes. Sections were then incubated in a mixture of HCl and distilled water for 20 minutes and then rinsed in tap water. A 1-minute incubation in Boehmer's Haemalum stain was performed for the depiction of nuclei. After a final washing procedure, slides were covered using glass cover slip and liquid arabic gum.

### **3.2.8.3.3. CD3 staining**

CD3 staining was performed to depict T-cells on mouse kidney sections. CD3 Antigen (CD3-receptor) is a cell surface antigen on T-cells (Kanellopoulos et al., 1983). It is a protein-complex, consisting of 4 different polypeptide chains ( $\gamma$ ,  $\delta$ ,  $\epsilon$ ,  $\epsilon$ ). In association with the T-cell receptor (TCR) and the  $\zeta$ -chain (CD247), they form the TCR-CD3-complex, which generates an activation signal in T lymphocytes.

This staining was accomplished following the same protocol as described for Mac2 staining. Primary rabbit polyclonal anti-mouse CD3 $\epsilon$  antibody (DAKO) was used in a 1:1000 dilution in prediluted goat serum. A biotinylated goat anti-rabbit IgG antibody (Vetor Labs) in a 1:400 dilution in prediluted goat serum served as secondary antibody.

#### **3.2.8.3.4. B220 staining**

B220 designates a mouse B-cell marker (Coffman 1982). This name refers to the molar mass (220 kDa) of the molecule CD45R. CD45 is a tyrosin phosphatase present on cells of the hematopoietic system. Depending on the particular cell type, different splice or glycosylation variants of CD45 are expressed. Mouse B-cells express the variant CD45R. B220 staining was performed to depict B-cells on mouse kidney sections. This staining was accomplished following the same protocol as described for Mac2 staining. Primary rat anti-mouse B220 antibody (R&D Systems) was used in a 1:1000 dilution in 5% horse serum.

#### **3.2.8.3.5. WT1 staining**

It has been recognized that measurement of podocyte number by light microscopy is difficult while using stainings that emphasize glomerular morphology, like PAS, because of the complexity of both podocyte and glomerular structure and the difficulty to discriminate between podocytes and other resident cells (Basgen and Nicholas, 2010). WT1 (Wilms-Tumor Protein) is a stable podocyte marker (Rauscher et al., 1998). WT1 is involved in the induction of the renal Wilms-tumor in pediatric patients. WT1 is a zinc finger transcription factor that recognizes the early growth response (EGR-1) sequence in promoters of growth factors. Staining kidney sections against WT1 enables to clearly identify podocytes in a glomerulus and count them properly. The podocyte counts of a glomerulus are indicator of glomerular health and filtration barrier integrity.

To perform WT1-staining on mouse kidney sections, 3  $\mu$ m thin sections were first deparaffinized as described above. Deparaffinization was followed by 3 washing steps in distilled water for 5 minutes each. This was followed by boiling in citrate buffer (pH 6,1) for 25 minutes in a microwave at 680W. The container containing buffer and sections was then put on ice for cooling for 15 minutes. Subsequently, sections were washed three times in PBS for 5 minutes. Blocking of non-specific binding was obtained by pipetting 5% goat serum in PBS on the sections and incubating for 30 minutes at room temperature. The primary rabbit anti WT1 antibody (Santa Cruz) was diluted 1:500 in 5% goat serum in PBS and incubated with the slides for 2 hours at room temperature. Afterwards, sections were washed three times 5 minutes in PBS and a biotinylated secondary antibody (Vector Labs), diluted 1:200 in 5% goat serum in PBS, was added and incubated for 30 minutes at RT. Following another washing step in PBS (3 x 5 minutes), 1:100 diluted Streptavidin-AP in PBS was pipetted on the sections and incubated for 30 minutes at RT. Another washing step (3 x 5 minutes in PBS) was followed by neufuchsin-development in the dark for approximately 10-20 minutes. Sections were then incubated in a mixture of HCl and distilled water for 20 minutes and then rinsed in tap water. A 1-minute incubation in Boehmer's Haemalum stain was optionally performed for the depiction of nuclei. After a final washing procedure, slides were covered using glas cover slip

and liquid arabic gum and dried at room temperature. As a result of the IHC staining, WT-1 as a nuclear antigen appeared red.

#### **3.2.8.3.6. P2X7 staining**

Following deparaffinization and rehydration, sections were incubated at 98°C with DAKO pH 9 target retrieval solution, a Tris/EDTA buffer intended for heat-induced antigen retrieval prior to immunohistochemical staining procedures, for 15 minutes and then cooled down at room temperature for further 15 minutes.

To avoid background staining due to nonspecific binding of the primary or secondary antibody to occur, sections were subsequently incubated with a protein blocking solution contained in the AP polymer staining kit used (Zytomed ZytoChem-Plus AP Polymer Kit) for 5 minutes at room temperature. Following two 2-minute washing steps with PBS, the primary polyclonal rabbit anti-P2X7 antibody (K1G, Institute for Immunology UKE Hamburg) (Adriouch et al. 2005) was added in a 1:400 dilution in 5% horse serum and sections were incubated with the antibody overnight at 4°C.

The antibody of then washed off with PBS (3x5 minutes) and sections were incubated with the AP polymer contained in the staining kit for 30 minutes at room temperature. The enzyme polymer used consists of covalently bound molecules of secondary antibody (anti-rabbit Ig) and alkaline phosphatase (AP). The visualization is obtained via enzyme-substrate-reaction in the presence of a coloring component, which finally enables microscopic evaluation of the stained sections. Color development was achieved by incubating the sections in Neufuchsin for about 30 minutes in the dark. Dipping the sections in tap water stopped the color reaction. Subsequently, a 1,5 minute incubation in Boehmer's haemalum was performed for the depiction of nuclei. Sections were then expurgated in tap water and finally covered using glass cover slips and Arabic gum.

#### **3.2.8.3.7. UCH-L1 staining**

UCH-L1 staining was accomplished following the same protocol as described for P2X7, using the Zytomed PolAP Kit.

Primary UCH-L1 antibody (U104, Biochemical Institute, University of Kiel) was used in a 1:20 dilution in 5% horse serum.

#### **3.2.8.4. Immunofluorescence staining (on cryosections)**

Prior to each staining procedure, deep frozen sections were thawed and dried at room temperature for 30 minutes. Subsequently, tissue sections were fixated by incubating in 4% PFA for 10 minutes. Different protocols for P2X7 immunofluorescence staining were tested.

Fixation was usually followed by blocking, for example in 5% horse serum and 0,05 % Triton X 100 in PBS for 30 minutes at room temperature. After washing off the blocking solution with PBS (3x5 minutes), a primary P2X7 antibody was added in the desired concentration (e.g. anti-P2X7 K1G 1:100) and incubated for 1 hour at room temperature or overnight at 4°C, depending on the respective protocol. The primary antibody was then washed off (PBS 3x5 minutes) and a secondary antibody was added (e.g. a biotinylated anti-rabbit antibody) and incubated for 1 hour at room temperature. In staining procedures involving Avidin-Biotin-binding, Streptavidin-FITC was added after washing off the secondary AB (e.g. 1:200 SA-FITC for 30 minutes at room temperature). For desired depiction of the cytoskeleton, actin filaments were stained using FITC-conjugated Phalloidin (e.g. 1:200 in PBS, incubated together with SA-FITC for 30 minutes at RT). Finally, sections were covered using Fluoromount. If a display of nuclei was favored, a mounting medium containing DAPI (4',6-Diamidino-2-phenylindol, DNA-binding dye) was used.

#### **3.2.9. Histologic evaluation**

##### **3.2.9.1. Glomerular damage**

To assess and compare the severity of kidney damage in the six mouse groups investigated, kidney sections from 4 animals per group were examined and 20 glomeruli per section were evaluated via light microscopy under blind trial conditions. 3 consecutive PAS-stained paraffin kidney cross-sections from each mouse were used, giving the best morphologic resolution. The scoring system ranged between 3 grades of glomerular disease: grade 0 represented a healthy glomerulus free of any signs of damage and scored 0 points. Disease grade 1 stood for a mild glomerular damage, scoring 0,5 points per glomerulus. Disease grade 2 represented severe glomerular damage and scored 1 point per glomerulus. The signs of glomerular disease that were screened comprised deposition of PAS-positive material (e.g. fibrin as a sign of glomerular thrombosis), swelling of podocytes, GBM-thickening and glomerular capillary occlusion or capillary patency respectively. All animals being examined, glomerular disease scores were summed up and the obtained results for a total of 80 glomeruli per group were compared.

### **3.2.9.2. Podocyte counts**

The reduction of podocyte number and density per glomerulus is linked to the development of proteinuria and the progression of disease (Mundel and Shankland 2002). For assessment of glomerular health and filtration barrier integrity, podocytes were counted and tuft area in  $\mu\text{m}^2$  was measured using Zeiss AxioVision software in 40 glomeruli per animal and 4 animals per group under blinded trial conditions. Display of podocytes was obtained via WT-1 staining of the selected sections. Results were presented as podocytes per tuft area in  $\mu\text{m}^2$  and compared between all the PI and APN treated groups.

### **3.2.9.3. Inflammatory cells**

Infiltration with macrophages, T- and B-cells was quantified to assess and compare the severity of inflammation among the different PI and APN mouse groups. Cells were counted in 20 glomeruli per animal and 4 animals per group under blinded trial conditions. Display of interstitial macrophages was obtained via F4/80 staining of the selected sections, sections were Mac2-stained for visualization of glomerular macrophages. T-cells were displayed by CD3 staining and B-lymphocytes were made visible via B220 dyeing. Results were compared between all PI and APN treated groups.

### **3.2.10. Western Blot**

#### **3.2.10.1. Procedure**

Western Blotting is an analytical technique used to detect specific proteins in a given sample of cell suspension or tissue homogenate (Burnette 1981). The technique comprises separation of sample proteins on a gel, their electrophoretic transfer from the gel to a nitrocellulose sheet and finally their detection based on antigen-antibody-binding and luminescence signaling.

First, gel electrophoresis is performed to separate denatured proteins by their size, creating size-sorted protein bands. These protein bands are then transferred to a PVDF (Polyvinylidene fluoride)-membrane by the means of an electric field, which is applied perpendicularly to the polyacrylamide gel. Proteins are moved from within the gel onto the membrane, they are immobilized by filtering and adhere to the membrane on the basis of hydrophobic interactions and hydrogen bonds. Target proteins may subsequently be detected on the membrane's surface using specific antibodies.

### **3.2.10.1.1. Sample preparation**

Protein lysates were prepared from snap-frozen mouse kidney tissue. After being cut to an accurate size (i.e. one quarter to one sixth of a kidney), tissue pieces were first weighed and an adapted amount of lysis buffer containing detergent (10 fold amount of sample weight in liquid, e.g. 300 µl of buffer for a kidney piece of 30 µg) was added to each sample in an Eppendorf tube. To gain a tissue homogenate, kidney pieces were triturated using a mortar and then incubated in lysis buffer for 30 minutes on ice. Subsequently, the suspension was centrifuged at 4°C and maximum speed (13200 rpm) for 20 minutes. The centrifugation step bestows phase separation, leaving a sediment of washed-out tissue fragments on the bottom of the tube and the desired lysate of protein as supernatant. The supernatant was transferred to precooled Eppendorf tubes and was then ready to be processed for further analysis (e.g. denaturation for subsequent gel electrophoresis) or to readily be used as test specimen (e.g. in ELISA). Remaining protein lysate was stored at -80°C for future analysis.

### **3.2.10.1.2. Gel electrophoresis**

First, proteins were denatured by adding 4x LDS (Lithium dodecyl sulfate) to the protein lysate in a 3:1 ratio (e.g. 10 µl of LDS to 30 µl of lysate). LDS is a compound that unravels proteins by disrupting their non-covalent bonds, denaturing them, and causing the molecules to lose their native conformation. The mixture was then incubated for 10 minutes in a heat block at 72°C. 4-12% NuPage gradient gels were used for electrophoretic separation. Before sample application, gels were washed twice using MOPS running buffer. Depending on the detectability of the particular protein of interest, 18-30 µl of denatured protein were loaded on the gel wells. Electrophoretic separation of the proteins was performed at an amperage of 60 mA per gel at room temperature for 1h in a Peqlab gel chamber.

### **3.2.10.1.3. Membrane transfer**

Having been electrophoretically separated in size on the NuPage gel, proteins were subsequently blotted onto a PVDF-membrane in a blot chamber (Novex Mini Cell). An electric field was used to pull the proteins from the gel onto the membrane with the proteins maintaining the organization they had within the gel while moving. As a result of the blotting process, proteins were exposed on the membrane surface layer for antibody detection. Preceding the blotting procedure, PVDF membranes were activated by incubation in Methanol at room temperature for 2 minutes before being put onto the gel in anodic direction, avoiding air bubbles to occur in between the two interfaces. Both gel and membrane were fixated inside the blot chamber using a

stack of filter paper and fiber pads drenched in blotting buffer. The protein transfer was performed at a voltage of 30V for 1 hour, the blot chamber being placed on ice.

#### **3.2.10.1.4. Blocking**

Blocking of non-specific binding was achieved by placing the membrane in a dilute solution of 3-5% non-fat dry milk in Tris-buffered saline with Tween 20 as detergent (TBST) for 1 hour at room temperature. The milk solution protein attached to the membrane in all places where the proteins had not been transferred to.

#### **3.2.10.1.5. Detection**

After blocking, a dilute solution of the desired primary antibody directed against the respective protein of interest was incubated with the membrane overnight at 4°C. Primary antibodies were diluted 1:500-1:1000, depending on their binding potential, in SuperBlock blocking buffer. After rinsing the membrane 4 times for 5 minutes in TBST to remove unbound primary antibody, the membrane was exposed to the secondary antibody, which was directed at the species-specific antigen (e.g. anti rabbit IgG) bound to the primary antibody. Secondary antibodies were derived from animal sera and were linked to horseradish peroxidase as reporter enzyme. Membranes were incubated with secondary antibody diluted in dry milk TBST for 1 hour at room temperature. Afterwards, secondary antibody was rinsed off as described previously. Subsequently, membranes were incubated in ECL development solution, a chemiluminescent serving as substrate to HRP, for 5 minutes. The horseradish peroxidase-link was used to cleave this chemiluminescent agent, and the reaction product produced luminescence in proportion to the amount of protein. As a final development step, a sensitive sheet of photographic film was placed against the membrane, and exposure to the light produced by the enzymatic reaction created an image of the antibodies bound to the blot. Density of protein bands was measured using ImageJ software.

#### **3.2.11. BioRad DC Protein assay (modified from Lowry)**

The Bio-Rad DC Protein Assay is a colorimetric assay for protein concentration following detergent solubilization. The reaction is similar to the method described by Lowry in 1951 (Lowry, Rosebrough et al. 1951). Lowry's protein assay is a biochemical assay in which the total protein concentration is exhibited by a color change of the sample solution in proportion to its protein concentration. This may then be measured using colorimetric techniques.

The assay is based on the reaction of protein with an alkaline copper tartrate solution and Folin reagent. As described in the Lowry assay, there are two steps which lead to color development: The reaction between protein and copper in an alkaline medium,

and the subsequent reduction of Folin reagent by the copper-treated protein. Color development is primarily due to the amino acids tyrosine and tryptophan (to a lesser extent cystine, cysteine and histidine). Proteins effect a reduction of the Folin reagent by loss of oxygen atoms, thereby producing one or more of several possible reduced species which have a characteristic blue color with maximum absorbance at 750 nm and minimum absorbance at 405 nm.

The Assay was performed following the manufacturer's protocol. Starting the procedure, serial dilutions of a protein standard (BSA) of known concentration were prepared. 10 mg of BSA were diluted in 1mL of buffer, serving as the highest concentrated standard solution (10 mg/mL). 5 subsequent dilutions were prepared, resulting in a minimal concentration of 0,3125 mg/mL BSA in standard number 6. The standards were prepared in the same buffer as the selected sample (e.g. lysis buffer for measurement of protein content in western blot lysates). Afterwards, the samples to be measured were diluted, depending on their expected protein content. Kidney lysates were diluted 1:5 in lysis buffer. Subsequently, 5 µl of standard or sample were pipetted on a 96-well plate in duplicates in row. Following this step, 25 µl of reagent A, an alkaline copper tartrate solution contained in the assay kit, were added to each sample. Directly afterwards, 200 µl of reagent B, a dilute Folin Reagent also supplied in the kit, was pipetted into each well. Tapping gently against the plate led to mixture of the preparation. Shortly after adding reagent B, a color change became visible - formerly colorless samples turned blue. After an incubation period of 15 minutes, absorbance was read in a plate reader at 650 nm.

### **3.2.12. ELISA**

#### **3.2.12.1. Procedure**

Enzyme-linked immunosorbent assay (ELISA) is a biochemical technique used to quantify the presence of an antigen in a sample (Engvall et al. 1971).

An unknown amount of antigen is affixed to a surface and may be detected and quantified by applying a specific enzyme-linked antibody on this prepared surface to grant antigen binding. Finally, a substance acting as substrate to the before mentioned enzyme is added and converted, evoking a detectable signal to occur, most commonly a colour change in a chemical substrate. Performing an ELISA involves at least one antibody with specificity for a particular antigen.

Samples with unknown amounts of antigen are immobilized on a solid support (i.e. a 96-well microtiter plate) either non-specifically - via adsorption to the surface, or specifically -via binding to a capture antibody specific to the same antigen (= so-called Sandwich-ELISA).

The antigen being immobilized, a detection antibody is added, forming antigen-antibody-complexes. The detection antibody can be covalently linked to an enzyme,

or it may itself be detected in a subsequent step by another enzyme-conjugated antibody.

Between each step of the procedure, the plate is washed using a mild detergent solution to remove any proteins or antibodies that are not specifically bound.

After a final washing step, the plate is developed by adding an enzymatic substrate to produce a visible signal, which indicates the quantity of antigen in the sample.

Most ELISAs involve chromogenic reporters and substrates that produce an observable color change to indicate the presence of antigen. Quantitation is performed via photometric measurement of absorption, the intensity of color change being proportional to the desired measurement parameters, e.g. concentration of a cytokine. Values measured from samples of unknown concentration are compared and range in the spectrum of a standard curve obtained from measurement of a dilution series of control samples of a defined concentration.

#### **3.2.1.12.2. Mouse albumin ELISA**

Sandwich-ELISA was performed to quantify the albumin concentration in mouse urine specimen using a commercially available kit (Bethyl Laboratories, Inc.).

Preliminarily, samples and albumin standard were diluted according to the manufacturer's protocol. The given standard is an albumin-solution of known concentration and values measured from its dilution series served as calibration curve for the urine samples.

Starting the procedure, 100 µl of 1:100 prediluted anti-albumin capture antibody in binding buffer were added into each well of the microtiter plate, using a multi-channel-pipet. Incubation of the antibody for 1 hour at room temperature led to its non-covalent binding on the well bottom. After discarding the supernatant and washing the plate 5 times, a sufficient amount of blocking solution containing BSA (bovine serum albumin) was pipetted into each well and incubated for 30 minutes at RT, leading to saturation of non-specific binding sites. Following another washing procedure, albumin standard in serial dilution and prediluted urine samples (depending on their Urine-stix-estimated albumin concentration which had to be inside the standard range) were applied on the plate and incubated for 1 hour at RT, granting the albumin contained in each specimen to specifically bind to its capture antibody. Subsequently, the plate was washed again to discard any non-specifically bound macromolecules. After washing, the secondary, HRP-conjugated so-called "detection antibody" was pipetted onto the plate in a 1:35.000 dilution and again incubated for 1 hour. The epitope of this antibody is directed against a different site of the albumin molecule than the epitope of the capture antibody. Binding of the detection antibody to the albumin in each well leads to the formation of antibody-antigen-antibody complexes.

Following the incubation period, the secondary antibody was discarded and the plate was washed anew to remove excess antibody. Afterwards, 100 µl of a

chemiluminescent substrate solution was pipetted on the plate and incubated for 15 minutes at RT in the dark. This substrate solution is enzymatically converted by the HRP bound to the detection antibody and is thus transformed from a colourless to a coloured, quantifiable substance. The enzymatic reaction was stopped after 15 minutes by adding 2 M sulfuric acid to each well.

The plate was then read out and measured using an ELISA plate reader (BioTek), which photometrically detects and calculates each well's absorption. The intensity of colour change is directly proportional to albumin concentration in the solution.

Extinction was measured at 450nm. The urinary albumin concentration was calculated according to the formula for absorption =  $(A-D)/1 + (x/C)^B + D$ , where A and D are values from the standard curve. Regression values for the standard curve were calculated to assess the accuracy of the measured values. Standard curves with r-values 0.9950 were used. The urinary albumin values were standardized against urinary creatinine values of the same probes.

### **3.2.12.3. Cytokine ELISA**

To determine the levels of IL-1 $\beta$ , MCP-1 and IL-6 in various specimen (mouse urine samples, kidney lysates, mouse serum samples), Sandwich ELISA was performed according to the manufacturer's protocol provided in each kit. The basic procedure largely resembles the above-described principle of the mouse albumin ELISA.

Due to rather low levels observed via pretesting, urine and serum samples were pipetted on all ELISA plates in the cytokine ELISA kits undiluted. 50-100  $\mu$ l of probe material were used, depending on the respective available amount that had been obtained from each animal. Kidney lysates were prediluted 1:3-1:5 in the respective sample buffer contained in the particular kit. Dilution levels depended on the respective protein content of each lysate that had been measured before ELISA via BioRad Protein Assay (see above). 100  $\mu$ l of lysate were used, respectively. Cytokine concentrations measured in kidney lysates were related to the particular protein content of the sample. Cytokine levels detected in mouse urine samples were related to serum creatinine values of the respective mouse to avoid measurement error due to concentration differences among urine samples.

### **3.2.13. RNA isolation and real-time PCR analysis**

#### **3.2.13.1. PCR – general principle**

Polymerase chain reaction (PCR) is a biomolecular technique that allows selective and exponential amplification of destined short DNA sequences within a longer molecule of double stranded DNA (Mullis 1990). So-called “primers” (short DNA fragments) containing sequences complementary to the selected target region on each of the two DNA strands along with a DNA polymerase are key components to enable selective and repeated amplification. After denaturation of the sample DNA, primers bind to their specific target region on each of the single strands and the DNA polymerase enzyme synthesizes new DNA sequences originating from these primers. The method relies on thermal cycling, consisting of cycles of repeated heating and cooling of the reaction for DNA melting and enzymatic replication of the DNA. As PCR progresses, the DNA generated is itself used as a template for replication, setting in motion a chain reaction in which the DNA template is exponentially amplified. Thanks to this exponential enrichment, selected DNA sequences may be detected in spite of very poor starting content of DNA in a sample. In order to detect messenger RNA (mRNA) in a sample, the method may be extended using reverse transcriptase to convert mRNA into complementary DNA (cDNA), which may then be amplified by PCR.

Starting the PCR procedure, a reaction mix is set up which includes a heat-stable DNA polymerase, specific primers for the gene of interest, deoxynucleotides and a suitable buffer. This mix is combined with the respective (c)DNA samples to be analyzed. Entering the PCR process, (c)DNA is denatured at more than ~94 degrees so that the two strands separate. The sample is then cooled to 50 to 60 degrees and specific primers are annealed that are complementary to a particular site on each strand. The temperature is then again raised to 72 degrees and the DNA polymerase extends the DNA from the primers. Since it is necessary to raise the temperature to separate any double stranded DNA, the DNA polymerase used must be thermo-stable. Taq polymerase was isolated from *Thermophilus aquaticus*, a bacterium that lives in hot springs and hydrothermal vents and the enzyme hence endures all rounds of heating and cooling throughout PCR process. The number of (c)DNA molecules doubles at each round of synthesis (exponentially), thus after N cycles the resulting outcome is  $2^N$  times as much DNA product as the amount started with. After 30-40 of these cycles, in PCR, the reaction products are analyzed by agarose gel electrophoresis. The amplicon is stained with ethidium bromide. Traditional PCR is a method of analysis that is only semi-quantitative and the amount of product is often not related to the amount of input DNA. Usual PCR hence solely is a qualitative tool for detecting the presence or absence of a particular DNA. In order to give evidence about not only the presence or absence but also about the quantity of a target sequence in a given sample, real-time quantitative PCR (qPCR) was invented. Real-time PCR based on fluorophores, such as SYBRGreen, permits measurement of the amplified product at each PCR cycle (in “real time”). The DNA-binding dye, e.g.

SYBRGreen, intercalates with any double-stranded DNA in the sample, causing fluorescence of the colourant. An increase in DNA product during PCR therefore leads to an increase in fluorescence intensity, which is measured at each new cycle, thus allowing DNA concentrations to be quantified. The higher the starting copy number of the nucleic acid target, the sooner a significant increase in fluorescence is observed.

The data generated by qPCR can be analyzed by computer software to calculate relative gene expression or mRNA copy number in given samples.

Real-time PCR technology was used in the APN model to determine how the expression of particular targets changed or responded over the experimental course, along with the onset of glomerular inflammation and proteinuria.

### **3.2.13.2. RNA isolation from mouse kidney tissue**

RNA isolation is the purification of RNA from a biological sample. This procedure is complicated by the ubiquitous presence of ribonuclease enzymes in cells and tissues, which can degrade RNA. Several methods are used in molecular biology to isolate RNA from samples. The most common is Guanidinium thiocyanate-phenol-chloroform extraction (Siebert et al. 1993).

This technique utilizes the ability of the chemical guanidinium isothiocyanate (commercially available as TRIzol) to lyse cells and denature proteins while simultaneously inactivating RNases. Phenol chloroform is used to partition the RNA from DNA, proteins and lipids.

A quarter snap-frozen mouse kidney ( $\approx 50 \mu\text{g}$ ) was placed into an Eppendorf tube filled with 500  $\mu\text{l}$  of TRIzol reagent. Homogenization of the tissue was obtained using tungsten carbide beads (3mm diameter, Qiagen) for shredding in a tissue lyser at 30 Hz for 1 minute. 100  $\mu\text{l}$  of phenol chloroform were then added to the homogenate. After thoroughly shaking the mixture, samples were centrifuged for 15 minutes at 10000 rpm and 4°C. The centrifugation step led to phase separation, partitioning RNA (upper phase, aqueous supernatant) from DNA (white interphase) and proteins and lipids (red bottom sediment).

The supernatant was pipetted and separated into new tubes, interphase and sediment were discarded. To induce RNA precipitation, 200  $\mu\text{l}$  of isopropanol were added and samples were incubated for 30 minutes on ice.

After another centrifugation step for 15 minutes at 10000 rpm, a RNA pellet became visible at the tube bottom. Supernatants were discarded and 3 washing steps using 500  $\mu\text{l}$  of 80% EtOH were performed, a 10 minute centrifugation step between each washing.

Finally, any liquid supernatant was discarded from the RNA pellet and pellets were dried using a spinning vacuum dryer for 1 minute. Subsequently, 30  $\mu\text{l}$  of sterile water containing RNase inhibitor were pipetted on the pellet and dissolving of the pellet was induced by tapping gently against the tube. Samples were then incubated on ice for 1 hour to allow complete redissolving. Quantification of RNA concentration was performed by photometric measurement. Each RNA sample was therefore diluted

1:200 in sterile water. 100  $\mu$ l of the dilute solution were pipetted into the photometer cuvette and RNA concentrations were measured via extinction and absorption assessment according to the Beer-Lambert-law.

### **3.2.13.3. cDNA Synthesis**

Subsequently to RNA isolation, complementary DNA was reversely transcribed from each sample to obtain real-time PCR-compatible specimen by a reverse transcriptase (RNA-dependent DNA polymerase).

Mastermixes containing enzymes and buffers were prepared and added to the isolated RNA material to gain a total volume of 20  $\mu$ l of cDNA from each RNA sample.

First, mastermix 1 was pipetted into Eppendorf tubes by adding random hexamer primers (1 microliter per sample) in a concentration of 100 ng/mL, 10 mM dNTPs [ (deoxynucleoside triphosphates, the building blocks from which the enzyme synthesizes a new DNA strand), (1 microliter per sample)] and sterile water (10,5  $\mu$ l per sample) to each sample of isolated RNA. 2  $\mu$ l of sample RNA were sufficient to synthesize 20  $\mu$ l of cDNA.

The mixture was incubated on a PCR-cycler at 65°C for 5 minutes and then put on ice until a second mastermix was added, designated at initiating the actual reverse transcription.

The first step was directed at building “starting points” for the reverse transcriptase along the single stranded RNA, from which the enzyme may synthesize double stranded cDNA by pairing of RNA base pairs to their DNA complements that were delivered from dNTPs and random hexamer primers contained in the first mastermix. Mastermix 2 consisted of First Strand Buffer [(a buffer that provides a suitable chemical environment for optimum activity and stability of the enzyme), (4  $\mu$ l per sample)] the M-MLV (named after Moloney murine leukemia virus, the retrovirus from which the enzyme was originally isolated) reverse transcriptase enzyme (1 microliter per sample) and RNase inhibitor (0,5  $\mu$ l per sample). A defined volume (5,5  $\mu$ l per sample-mastermix-mixture) of Mastermix 2 was pipetted into the tubes containing RNA and Mastermix 1 and the whole preparation was then again put on a PCR-cycler for 85 minutes, passing through different temperature levels and hence reaction steps (10 minutes 25°C, 60 minutes 42°C, 15 minutes 75°C). Throughout these steps, reverse transcriptase generates double-stranded DNA complementary to the single stranded sample RNA. The thus synthesized cDNA was stored at 4°C for future analysis.

### **3.2.14. Real-time PCR**

Real-time PCR was performed using the StepOne Plus realtime PCR System by AB Applied Biosystems and analysis was accomplished with the corresponding software. SYBRGreen dye was used as nucleic acid stain. It is an asymmetrical cyanine dye which binds to DNA, the resulting DNA-dye-complex absorbs blue light ( $\lambda_{max}$  = 488 nm) and emits green light ( $\lambda_{max}$  = 522 nm).

Two primers complementary to the 3' ends of each of the sense and anti-sense strand of the particular cDNA target were required as replication start point for the DNA polymerase enzyme. All primers were used in a 1  $\mu$ M concentration.

The PCR preparation was pipetted into 96-well microplates supplied by AB Biosystems, each specimen being assayed in duplicate.

First, a mixture of sterile water (2,25  $\mu$ l per 1,5  $\mu$ l of cDNA sample), the required primer pair (1,25  $\mu$ l of each primer) and SYBRGreen reagent (6,25  $\mu$ l per cDNA sample) was prepared for each target of interest, the amount of each component being multiplied by the number of cDNA probes to be analyzed. A defined volume of this preparation was pipetted into the plate wells, repeating the step for all primer pairs. Subsequently, a given amount (1,5  $\mu$ l) of each cDNA sample was added into the PCR plate wells in duplicates. "Blank" samples containing sterile water instead of cDNA were pipetted at the end of each primer analysis row on the plate.

18s served as invariant endogenous control. By using this control as an active reference, quantitation of mRNA targets could be normalized for differences in the amount of total RNA added to each reaction. Before entering the PCR system, the plate was shortly centrifuged to ensure the mixture liquid to completely cover the plate bottom.

## 4. Results

### 4.1. UCH-L1 KO mice develop a more severe Glomerulonephritis than mice heterozygous for UCH-L1.

The results shown in section 4.1. represent data obtained from experiments performed on homozygous (d/d) and heterozygous (d/+) UCH-L1 KO mice comprised in the first animal set analyzed. This animal set was monitored 20d following preimmune- or anti-podocyte serum injection respectively. The given data depicts the aggravated disease formation observed in homozygous UCH-L1 KO mice past anti-podocyte serum injection observed throughout all animal sets. This tendency is shown on the basis of the analysis of survival post anti-podocyte serum injection and of three clinical parameters – blood urea nitrogen levels, albuminuria and serum cholesterol levels.

#### 4.1.1. Survival past anti-podocyte serum injection

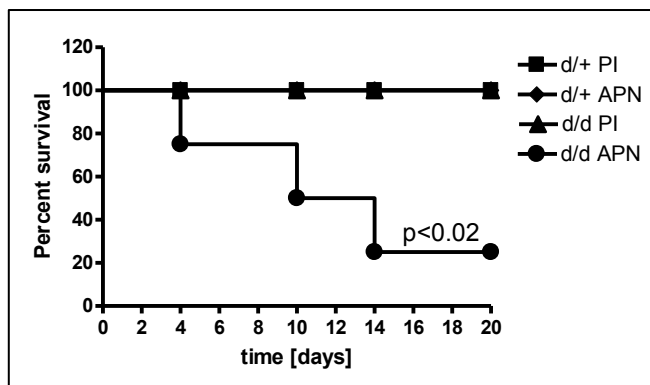


*Figure 10: UCH-L1 KO mice are more vulnerable towards APN induction than heterozygous control animals. Kaplan survival curve of heterozygous (d/+) and homozygous (d/d) UCH-L1 KO mice after injection of PI (n=2 per genotype) or APN (n=4 per genotype) serum. Heterozygous UCH-L1 KO mice were sacrificed 20 d past AP-serum injection. 3 homozygous UCH-L1 KO mice died prematurely throughout the monitoring period (see graph)*

Vulnerability towards anti-podocyte nephritis induction was assessed by monitoring the period (in days) of survival past anti-podocyte serum injection. This period was significantly shorter in UCH-L1 KO mice compared to heterozygous control animals (figure 10). While no sacrifice had to be denoted in the heterozygous control group consisting of 4 animals injected with anti-podocyte serum, the UCH-L1 KO population was diminished by 80% of the initial animal set. 3 heterozygous UCH-L1 KO mice died prematurely – on days 3, 9 and 14 respectively, one sole animal surviving throughout the whole disease monitoring period. Heterozygous UCH-L1 KO mice exhibited first symptoms (weight loss, matted fur) on day 4 past APN induction, their condition rapidly deteriorating from that time point on, while control animals remained stable until days 6-9, then showing slight signs of disease.

### 4.1.2. Evaluation of clinical parameters

#### 4.1.2.1. Blood Urea Nitrogen (BUN)

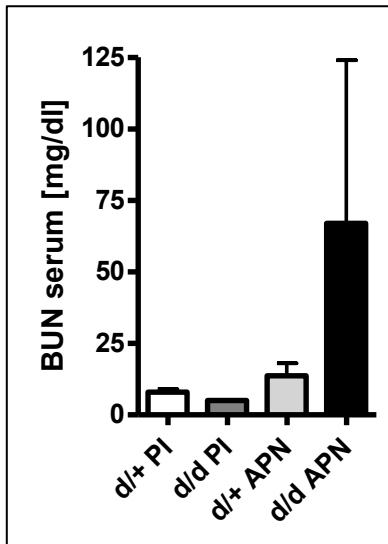


Figure 11: **UCH-L1 KO APN mice exhibit higher BUN levels than heterozygous control animals.** BUN levels (mg/dL) measured in the Dept. of Clinical Chemistry in UCH-L1 het (d/+) vs. UCH-L1 KO (d/d) PI and APN serum samples collected on day 14. Values are indicated as mean mean +/- SEM.

Elevated levels of serum creatinine and blood urea nitrogen are indicative of an impaired kidney functions as seen in glomerulonephritis. These parameters were measured in blood samples in UCH-L1 KO and heterozygous control PI and APN serum treated animals collected on the day of sacrifice (d20 in all mice injected with PI-serum; d20 in 4 d/+ and 1 d/d mice injected with AP-serum, d3,9,14 in the remaining 3 d/d animals injected with AP-serum) to assess renal condition past anti-podocyte serum injection.

UCH-L1 KO mice exhibited an increase in BUN levels when treated with APN levels compared to PI control animals, indicating a highly impaired kidney function in these mice. Heterozygous control mice did not exhibit an upregulation in BUN levels comparing PI and APN values, arguing for a better-preserved kidney function in this genotype after the onset of APN.

#### 4.1.2.2. Albuminuria

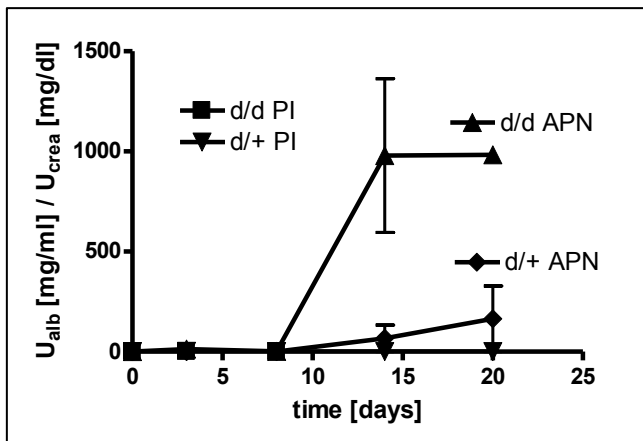


Figure 12: **Albuminuria is increased in UCH-L1 deficient mice treated with APN serum.** Urinary albumin levels were measured by ELISA and normalized against creatinine levels of the same urine samples. Values are plotted as mean +/- SEM.

Albuminuria is a cardinal sign of glomerular damage and was measured to assess renal integrity past anti-podocyte injection in mouse urine samples.

## Results

Urinary albumin values (mg/dl), obtained via ELISA from mouse urine samples collected periodically throughout the APN monitoring period, were standardized against urinary creatinine values (mg/dl) of the same probes to avoid measurement errors originating from differences in urine concentration to occur.

UCH-L1 KO and heterozygous control animals representing the PI group did not exhibit any proteinuria consistently throughout the monitoring period (graphs parallel to zero baseline).

APN animals of both genotypes remained free of proteinuria until day 8 past nephritis induction. From day 8 forth, APN serum treated UCH-L1 KO mice showed a rapid and steep augmentation in their albuminuria levels, cumulating in peak values around 1000 (albumin/creatinine ratio) on day 14 and remaining constant until the day of sacrifice. Heterozygous controls similarly exhibited first augmentations in albuminuria levels from day 8 forth, linearly increasing until the day of sacrifice, when a peak value of 200 (albumin/creatinine ratio) was measured.

The heavy extent and rapid velocity of proteinuria onset observed in the UCH-L1 KO APN group indicated the formation of a fulminant nephrotic syndrome and severe kidney damage in mice lacking Ubiquitin C-terminal Hydrolase L1.

### 4.1.2.3. Serum Cholesterol

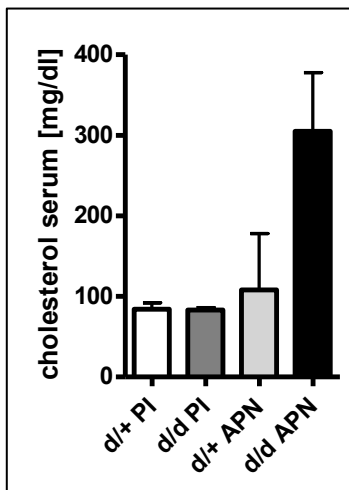


**Figure 13: UCH-L1 KO APN mice exhibit higher Cholesterol levels than heterozygous control animals.** Cholesterol serum levels measured in the UKE Dept. of Clinical Chemistry in UCH-L1 het (d/+) vs. UCH-L1 KO (d/d) PI and APN serum samples collected on the day of sacrifice. Values are indicated as mean +/- SEM.

Measurement of serum cholesterol (figure 12) and triglycerides (not shown) serve as diagnostic tools in

detecting a potential nephrotic syndrome in the context of kidney disease.

Evaluation of cholesterol and triglyceride levels in sera obtained from UCH-L1 KO and UCH-L1 heterozygous control animals revealed a clear tendency.

While there was an increase in the serum levels of both lipoprotein parameters in UCH-L1 KO APN mice compared to PI controls, UCH-L1 heterozygous mice showed little to no increase of serum cholesterol or triglycerides after APN treatment.

UCH-L1 KO mice of all animal sets that were experimented also showed signs of severe glomerulonephritis in all other experimental parameters analyzed, i.e. histology of kidney sections and assessment of inflammatory cytokines in urine, serum and kidney. These results will be illustrated in the following section 4.2. in comparison to wildtype and P2X7 KO mice.

### **4.2.P2X7 KO mice are protected against severe kidney damage.**

Results section 4.2. comprises a comparative evaluation of clinical parameters, i.e. body weight development, serum parameters and albuminuria, as well as histologic assessment of glomerular damage, podocyte counts and infiltration with inflammatory cells, among wildtype, P2X7 KO and UCH-L1 KO mice.

Additionally, the levels of the inflammatory cytokines MCP-1, IL-1 $\beta$  and IL-6 in urine, serum and kidney tissue of mice of all three genotypes investigated are shown.

The working idea behind these results was to gain hint of the severity of disease expressed by the different mouse types following anti-podocyte (AP-) serum injection. It was also directed at investigating the activation of the “inflammasome axis”, a downstream axis affected by stimulation of the proinflammatory P2X7-receptor, in wildtype versus UCH-L1 versus P2X7 KO animals and hence evaluates a possibly altered P2X7-activation in wildtype and UCH-L1 KO mice following AP-serum injection.

#### **4.2.1. Evaluation of clinical parameters**

##### **4.2.1.1. Body weight**

Mouse body weight was monitored on days 3, 8 and 14 (day of sacrifice) past anti-podocyte serum injection as a clinical parameter giving information on both general health condition and kidney function. A loss of weight in the course of GN formation gives hint of extensive systemic disease expressed by cachexia, a weight gain might account for the formation of a nephrotic syndrome, i.e. highly impaired kidney function, expressed by ascites or peripheral edema.

PI serum treated animals of all three genotypes did not exhibit any significant alterations in body weight.

The changes in body weight observed among the anti-podocyte serum treated mouse groups throughout the monitoring period were mildest in P2X7 KO animals compared to wildtype and UCH-L1 KO mice. The maximum weight reduction among P2X7 KO animals that were injected with anti-podocyte serum was 1,5 g (Figure 14B).

## Results

Wildtype mice that received anti-podocyte serum exhibited an average weight loss of approximately 3,5 g (26 g start weight to 22,5 g minimal weight on day 13) (Figure 14A).

Weight curves for P2X7 KO mice injected with anti-podocyte serum ran parallel to the developing seen in their PI-serum treated littermates, there was no significant weight loss to be denoted. In contrast, there were significant divergences between UCH-L1 KO mice that received PI- and those that received anti-podocyte serum, wildtype mice exhibited the same tendency (Figure 14 A and C).

Loss of body weight was most significant and earliest among the UCH-L1 KO anti-podocyte serum treated population. Compared to PI-serum treated littermates and PI and anti-podocyte serum treated wildtype control mice, UCH-L1 KO AP-serum animals showed the most significant and earliest loss of body weight, declining to a minimal mean weight of 19 g (day 8) from original average start weights around 24 g. This 21% reduction of body weight was a strong hint of the increased vulnerability of UCH-L1 KO mice towards anti-podocyte nephritis induction. UCH-L1 KO mice manifested slight weight gains throughout the final days of GN monitoring. This augmentation in body weight might argue for the extent of ascites and interstitial edema, which was observed in both wildtype and UCH-L1 KO animals upon sacrifice as a sign of the formation of nephrotic syndrome.

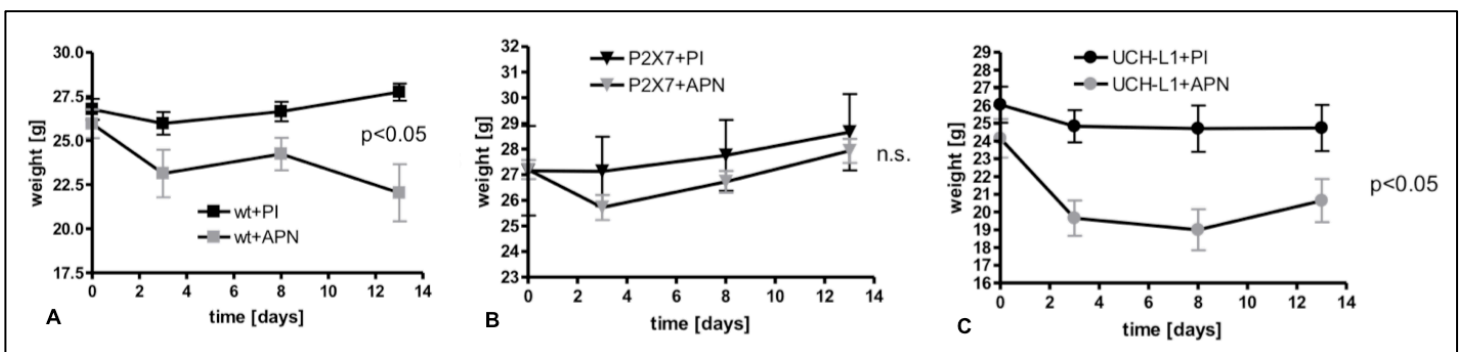


Figure 14: **P2X7 KO mice show no significant changes in body weight past anti-podocyte serum injection.** Course of body weight in wildtype (A), P2X7 KO (B) and UCH-L1 KO (C) animals. Mice were weighed before APN induction (day 0) and at three subsequent times (day 3, 8, 13) throughout the APN monitoring period. Values are expressed as mean  $\pm$  SEM. Statistical significance was measured using the ANOVA-Test.

### 4.2.1.2. Blood Urea Nitrogen (BUN)

Comparison between BUN levels in wildtype, P2X7 KO and UCH-L1 KO mice revealed an increase of urea levels in sera of anti-podocyte serum treated animals of all three genotypes compared to preimmune serum treated littermates. The extent of increase was strongest in wildtype animals. Variations between the three different

## Results

groups injected with anti-podocyte serum exhibited significance when comparing WT to P2X7 KO mice. P2X7 KO AP-serum treated animals showed significantly lower BUN levels than WT conspecifics. There was no significant variation between UCH-L1 KO AP-serum treatment group BUN levels and the other two genotypes respectively.

Measurement of serum creatinine levels also showed an increase of the retention parameter in AP-serum treated mice compared to control animals injected with preimmune serum among all three genotypes (not shown), without significant variations between the different genotypes.

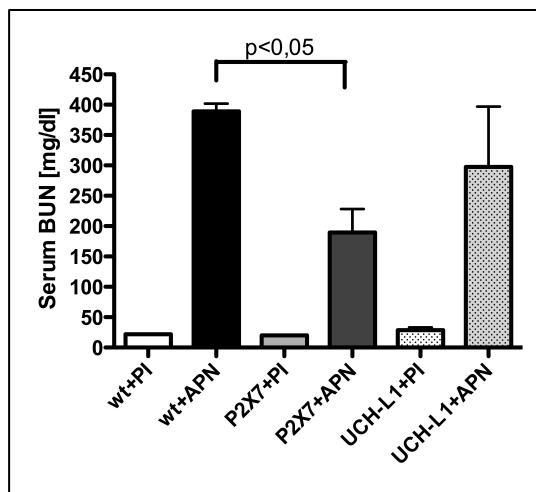


**Figure 15: P2X-deficient mice exhibit a significantly milder increase in blood urea nitrogen levels than wildtype conspecifics, 14d after anti-podocyte serum injection.** BUN levels measured in sera of wildtype, P2X7 KO and UCH-L1 KO mice collected on the day of sacrifice. Values are expressed as mean  $\pm$  SEM. Statistical significance was calculated using the Mann-Whitney-U-test. A  $p < 0.05$  was accepted statistically significant.

### 4.2.1.3. Serum Cholesterol

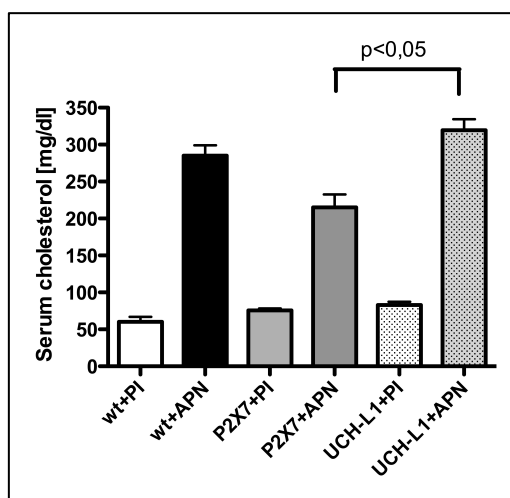


**Figure 16: P2X7 KO mice exhibit significantly lower serum cholesterol levels than UCH-L1 KO conspecifics, 14d after anti-podocyte serum injection.** Serum cholesterol levels in mg/dl measured in sera of wildtype, P2X7 KO and UCH-L1 KO mice collected on the day of sacrifice. Values are expressed as mean  $\pm$  SEM. Statistical significance was calculated using the Mann-Whitney-U-test. A  $p < 0.05$  was accepted statistically significant.

context of kidney disease.

Evaluation of cholesterol levels showed an increase in blood samples of mice injected with anti-podocyte serum compared to control animals treated with preimmune serum among all three genotypes investigated. The extent of increase

Measurement of serum cholesterol and triglyceride levels serve as diagnostic tools in detecting a potential nephrotic syndrome in the

## Results

varied significantly between UCH-L1 KO AP-serum treated mice, who exhibited highest cholesterol levels, and P2X7 KO animals injected with AP-serum, who showed the mildest increase compared to PI-serum treated littermates.

Comparing triglyceride levels (not shown) also revealed an upregulation between PI-serum- to AP-serum treatment groups in all three genotypes, whereas differences between the three AP-serum treated groups were not significant.

### 4.2.1.4. Albuminuria

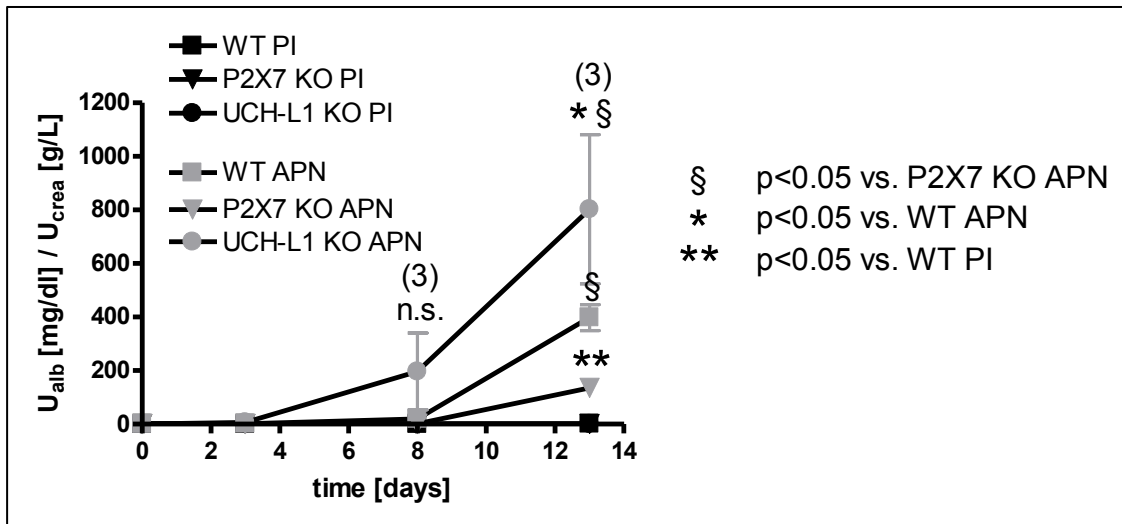


**Figure 17: The formation of albuminuria, a cardinal symptom of kidney damage, is mildest among P2X7-deficient mice compared to wildtype and UCH-L1 KO animals throughout a time span of 14 days after anti-podocyte serum injection.** Albuminuria in WT, UCH-L1 KO and P2X7 KO mice. Urinary albumin levels were measured by ELISA and normalized against creatinine levels of the same urine samples. Values are plotted as mean  $\pm$  SEM. Statistical significance was measured using the Mann-Whitney-U test. Urine of PI-serum treated mice of all three genotypes remained free of albumin throughout the APN monitoring period = graphs parallel to baseline.

Albuminuria was measured in wildtype, UCH-L1 KO and P2X7 KO mice on days 3, 8 and 13 past serum injection (Figure 17). Urinary albumin levels were measured by ELISA and normalized against creatinine levels of the same urine samples.

Preimmune serum treated mice of all three genotypes remained free of proteinuria throughout the disease monitoring period (graphs parallel to zero baseline).

Wildtype and P2X7 KO anti-podocyte-serum treated animals remained free of proteinuria until day 8 past serum injection. From day 8 forth, AP-serum treated wildtype mice showed a steady augmentation in their albuminuria levels throughout the monitoring period, cumulating in an average peak value around 400 (albumin/creatinine ratio) on day 13. P2X7 KO animals injected with anti-podocyte serum similarly exhibited first augmentations in albuminuria levels from day 8 forth, linearly increasing until day 13, when an average peak value of 180 (Albumin/Creatinine ratio) was measured.

In contrast, UCH-L1 KO mice injected with AP-serum showed first detectable proteinuria from day 3 forth, increasing to an average value around 200

(albumin/creatinine ratio) on day 8 and steadily accelerating until an average peak value of 800 (albumin/creatinine ratio) was measured in urine samples collected on day 13.

Albuminuria in the UCH-L1 KO AP-serum treated group proved to be significantly higher than those measured among WT and P2X7 KO animals ( $p < 0,05$ ) injected with anti-podocyte serum.

These results indicated severe kidney damage among UCH-L1 KO mice injected with AP-serum, while equally treated P2X7 KO animals exhibited only mild proteinuria.

These findings, together with the evaluation of serum parameters shown above (Figures 15 and 16) also suggested that P2X7 KO mice are protected against the development of a nephrotic syndrome, while wildtype and UCH-L1 KO animals develop a fully pronounced nephrotic state.

#### 4.2.1.5. Histology

##### 4.2.1.5.1. PAS

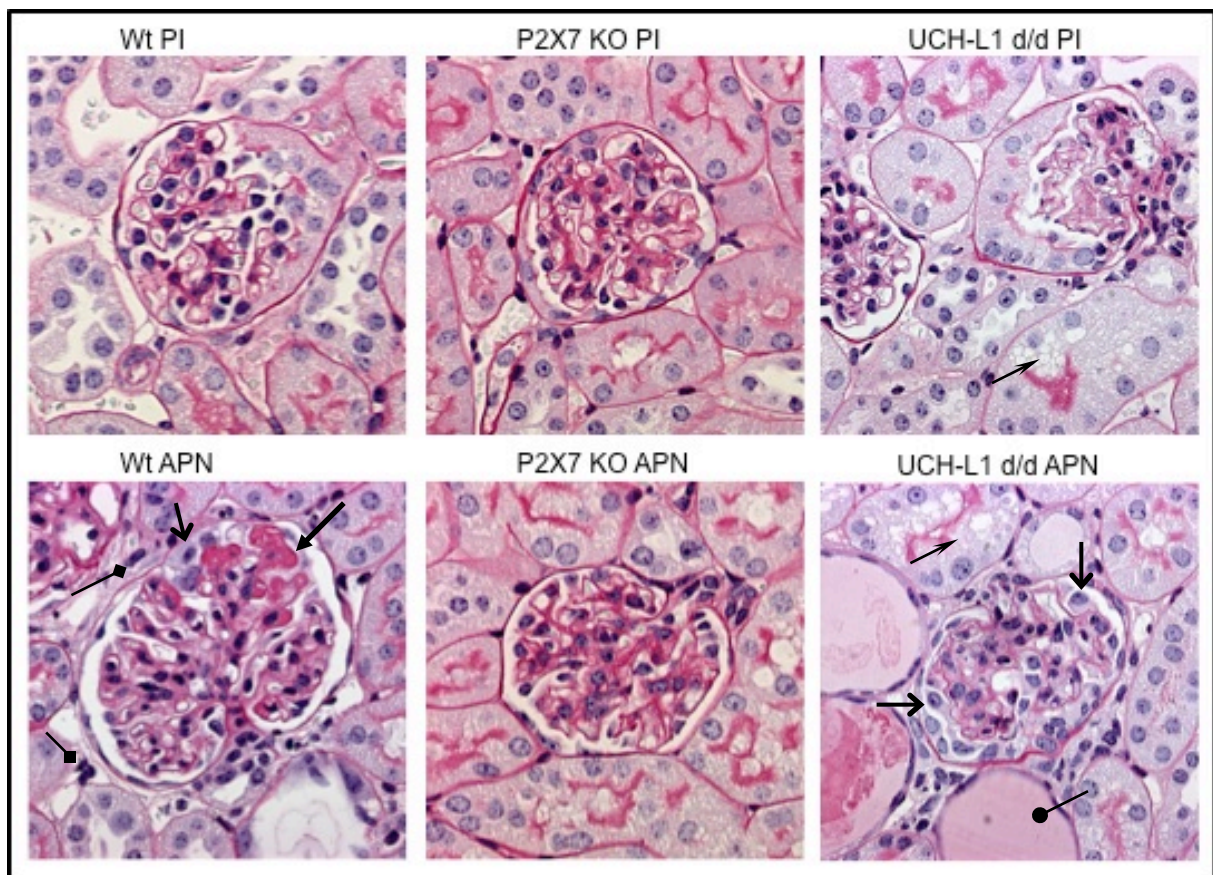


**Figure 18: P2X7-deficient mice show mildest glomerular damage in glomerular cross sections, 20d after anti-podocyte serum injection.** Representative photographs (400X) of Wt, P2X7 and UCH-L1 KO PI and APN PAS stained glomeruli. Open arrows → point to swollen podocytes. Closed arrow → points to PAS-positive material. Rhomboid ◊ points to infiltrating leucocytes. Circle ● points to protein casts. Narrow open arrow → points to tubular vacuolization.

## Results

To assess the severity of kidney damage in the six mouse groups investigated, PAS-stained kidney cross sections were analyzed for signs of glomerular damage. These signs comprised alterations in glomerular size, tubular vacuolization, capillary obliteration and the swelling of GBM and podocytes. 20 glomeruli per section from 4 animals per mouse group were examined via light microscopy (Figure 18) under blind trial conditions and glomerular damage was scored (Figure 19).

Cross sections from preimmune serum treated mice of all three groups investigated did not show significant signs of altered glomerular morphology. Glomerular size was increased compared to wildtype preimmune-serum treated mouse kidney cross sections. Tubular vacuolization was observed (Figure 18).

Among the animals injected with anti-podocyte serum, glomerular integrity was best conserved in P2X7 KO mice compared to UCH-L1 KO and wildtype animals. Cross sections of P2X7 KO AP-serum treated mice were rated with an average glomerular damage score of 8, which proved significantly lower than average scores reached in wildtype and UCH-L1 KO groups injected with AP-serum. Capillary lumina presented with only mild obliteration, podocyte and GBM swelling were discrete and glomerular size was considered relatively normal (Figure 18).

Sections from wildtype mice injected with anti-podocyte serum showed significant damage, rated with an average glomerular damage score of 14. Patency of capillary lumina was significantly reduced, podocytes and GBM appeared swollen, glomerular size was increased. A strong deposition of PAS-positive material argued for glomerular thrombosis. Infiltrating leucocytes were seen in the vicinity of damaged glomeruli.

The most significant loss of glomerular integrity was detected among cross sections of UCH-L1 KO mice injected with anti-podocyte serum. Glomeruli were distended, capillary lumina showed almost complete obliteration, podocytes and GBM appeared swollen. Glomerular damage scores reached an average value of 19. Protein casts congesting tubules could be observed just as tubular vacuolization.

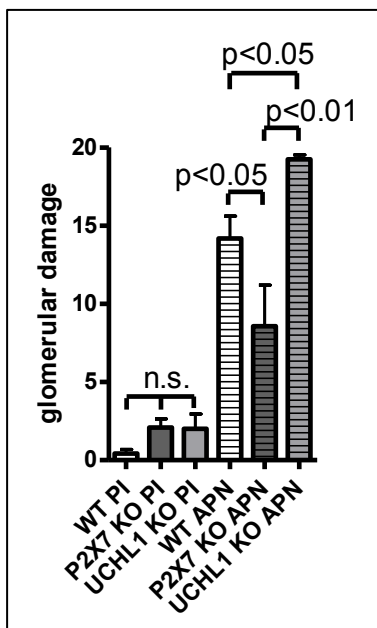


**Figure 19: Glomerular damage is in P2X7-deficient mice is significantly milder than in wildtype and UCH-L1 KO conspecifics, 14d after AP-serum injection.**

20 glomeruli per section were scored for glomerular damage on 4 animals per mouse group via light microscopy under blind trial conditions. The scoring system ranged between 3 grades of glomerular disease from healthy glomerulus (0 points) to severe glomerular damage (1 point per glomerulus).

All animals being examined, glomerular disease scores were summed up and the obtained results for a total of 80 glomeruli per group were compared.

Values are plotted as mean  $\pm$  SEM. Statistical significance was measured using the Mann-Whitney-U test. A  $p < 0.05$  was accepted statistically significant.

#### 4.2.1.5.2. Podocyte counts

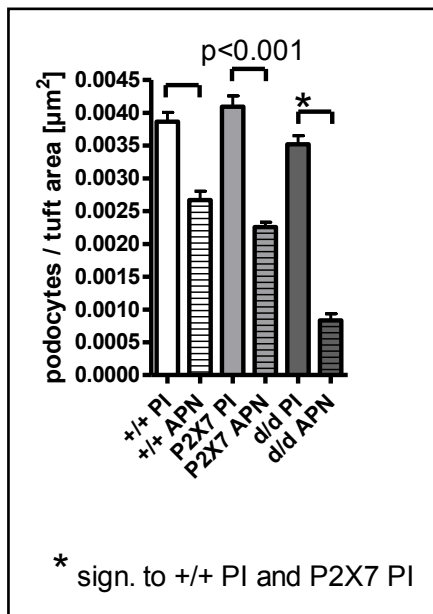


**Figure 20: UCH-L1 KO APN mice exhibit podocytopenia, while P2X7-deficient and wildtype animals show moderate podocyte loss, 14d after anti-podocyte serum injection.** WT-1 positive podocytes were counted in 20 glomeruli per mouse in n=4 mice per group. Podocyte counts were normalized against the respective tuft area in  $\mu\text{m}^2$ . Values are plotted as mean  $\pm$  SEM. Statistical significance was measured using the Mann-Whitney-U test. A  $p < 0.05$  was accepted statistically significant. +/+ = wildtype, d/d = UCH-L1 KO

Podocyte number is considered a critical determinant for the development of glomerulosclerosis and a decrease in podocyte number has been found to lead to progressive renal failure (Mundel and Shankland 2002).

Podocytes were visualized via WT-1 staining and counted in 40 glomeruli per animal and 4 animals per group (Figures 20 and 21). Podocyte counts were compared as an indicator of glomerular health and filtration barrier integrity.

Podocyte loss was apparent in all three genotypes investigated. Mildest loss was denoted in wildtype mice injected with anti-podocyte serum compared to preimmune serum treated littermates. P2X7 KO AP-serum treated animals showed moderate podocyte depletion, but values ranged significantly higher than those counted in wildtype anti-podocyte serum treated mouse sections. Podocyte loss was most severe ( $p < 0,01$ ) among UCH-L1 KO AP-serum treated mice compared to the UCH-L1 KO preimmune-serum treated group. This finding corresponded to the severe extent and early onset of proteinuria and strong weight loss observed in this group.

In a preimmune-serum treated state, wildtype and P2X7 KO mice did not exhibit significant differences in podocyte number or morphology. UCH-L1 KO preimmune serum treated mice (average 0,0035 podocytes/ $\mu\text{m}^2$  tuft area) initially showed significantly lower counts than wildtype (average 0,0039 podocytes/ $\mu\text{m}^2$  tuft area) and P2X7 KO conspecifics (average 0,004 podocytes/ $\mu\text{m}^2$  tuft area).

Among anti-podocyte serum treated mice, podocyte loss was mildest in wildtype animals compared to their preimmune-serum treated littermates, with an average count of 0,0028 podocytes/ $\mu\text{m}^2$  tuft area. In the P2X7 KO AP-serum treated group, podocyte depletion was significantly higher with an average number of 0,0024 podocytes/ $\mu\text{m}^2$  tuft area. UCH-L1 KO mice injected with anti-podocyte serum showed significantly lowest podocyte counts (0,0009 podocytes/ $\mu\text{m}^2$  tuft area), arguing for highly reduced filtration barrier integrity. This finding coincided with the clear clinical

appearance of fulminant nephrotic syndrome observed among this group via albuminuria, weight loss and serum parameter measurement.

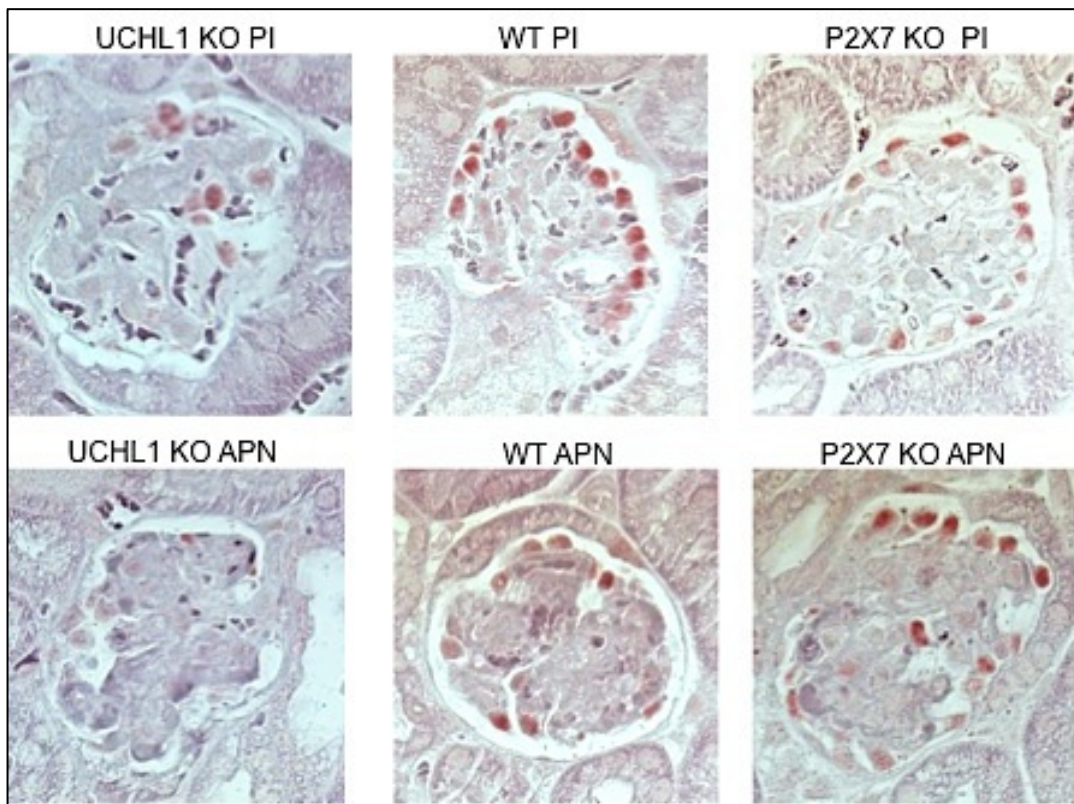


*Figure 21: WT1 stained glomeruli, podocyte depiction. Photographs (40X) are representative of the respective genotype and treatment group. WT-1 positive cells exhibit red nuclear staining.*

#### **4.2.1.5.3. Inflammatory cells**

To compare the severity of peripheral and glomerular inflammation among wildtype, P2X7 KO and UCH-L1 KO animals, interstitial and glomerular macrophages, T- and B-lymphocytes were stained and counted in 20 glomeruli per animal and 4 animals per group. Visualization of interstitial macrophages was obtained via F4/80 staining, glomerular macrophages were coloured via Mac2 stain. CD3 staining was used to visualize glomerular T-cells, glomerular B-cells were stained via B220 Immunohistochemistry.

### Interstitial Macrophages - F4/80

Basal periglomerular infiltration with interstitial macrophages in preimmune serum treated mice of all three genotypes investigated was insignificant with average values of 0,9 (WT, P2X7 KO) to 1,7 (UCH-L1 KO) cells per high power field (hpf) (Figure 22). After the onset of APN, the number of F4/80 positive cells per hpf increased mildly in P2X7 KO mice injected with anti-podocyte serum (average 1,6 cells per hpf). Kidney sections of wildtype animals treated with AP-serum were infiltrated with an average of 3,3 F4/80 positive cells per hpf (Figures 22 and 23). Infiltration increased most significantly in UCH-L1 KO animals injected with anti-podocyte serum, where an average of 4,2 cells per hpf was counted ( $p < 0,01$  compared to WT AP-serum and P2X7 KO AP-serum, Figure 22).

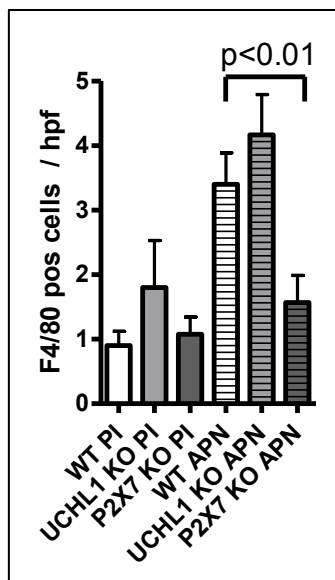


**Figure 22: Macrophage infiltration is strongest in UCH-L1 KO APN mice.** Quantification of periglomerular interstitial macrophages per high power field by F4/80 staining. Values are expressed as mean  $\pm$  SEM. A n of 20 glomeruli in 4 animals per group was counted. the p-value was calculated by Mann-Whitney-U-test. A p-value of  $< 0.05$  was accepted statistically significant.

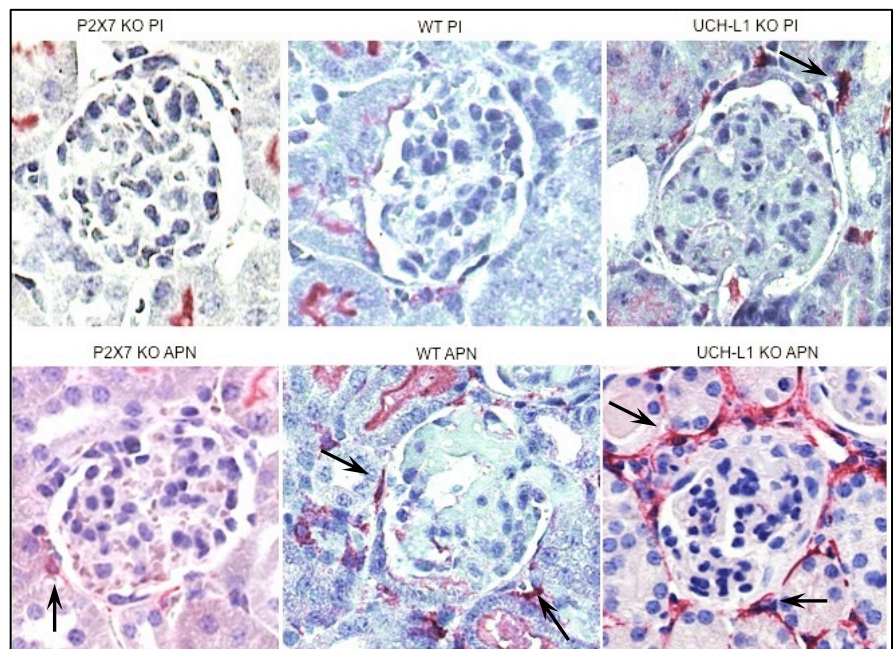


**Figure 23: Immunohistochemistry against F4/80,** for the depiction of interstitial macrophages (indicated by arrows). Photographs (400X) are representative of periglomerular macrophage infiltration in the respective genotype and treatment group.

## Glomerular Macrophages - Mac2

Basal infiltration with glomerular macrophages, as counted in healthy control mice of all three genotypes injected with preimmune serum investigated, was insignificant with average values of 0,2 (P2X7 KO) to 0,5 (WT, UCH-L1 KO) cells per hpf (Figures 24 and 25).

After the injection of AP-serum, the number of Mac2 positive cells per hpf increased in mice of all three genotypes (Figure 24). Glomeruli of wildtype anti-podocyte serum animals were infiltrated with an average of 0,8 Mac2 positive cells per hpf. P2X7 KO AP-serum treated mice showed a slightly, but insignificantly stronger average infiltration of 1 cell per hpf. Infiltration was strongest in UCH-L1 KO animals injected with anti-podocyte serum, where an average of 1,3 cells per hpf was counted.

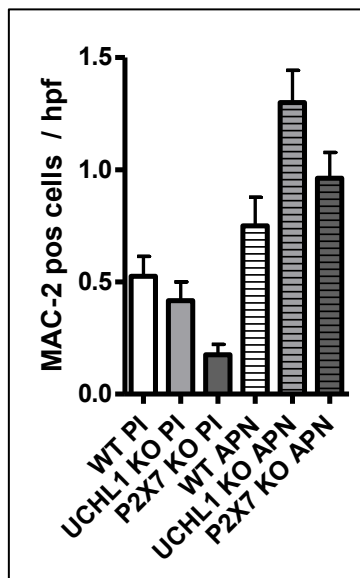


Figure 24: **Glomerular macrophage infiltration is strongest in UCH-L1 KO APN mice.** Quantification of glomerular macrophages per high power field by Mac2 staining in n=20 glomeruli per 4 mice per group. Values are plotted as mean +/- SEM.

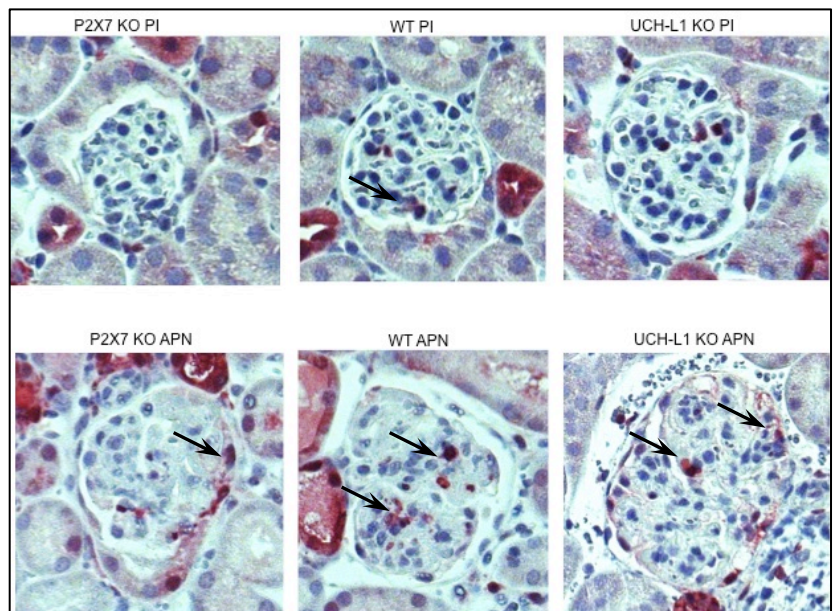
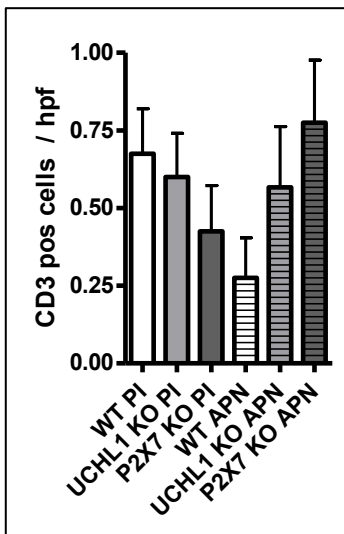
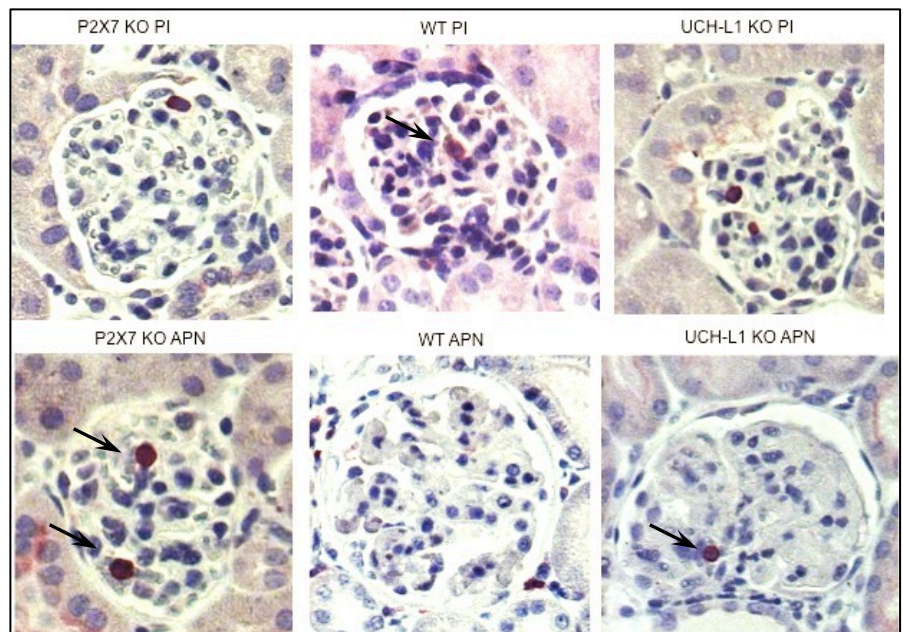


Figure 25: **Immunohistochemistry against Mac2**, for the depiction of glomerular macrophages (indicated by arrows). Photographs (400X) are representative of intraglomerular macrophage infiltration in the respective genotype and treatment group.

**T-Cells - CD3**



**Figure 26: Glomerular T-cell infiltration is strongest in P2X7-deficient mice, 14d after anti-podocyte serum injection.** Quantification of glomerular T cells per high power field by CD3 staining in  $n=20$  glomeruli per 4 mice per group. Values are plotted as mean mean  $\pm$  SEM.



**Figure 27: CD3 stained kidney cross sections, depiction of glomerular T cells (indicated by arrows).** Photographs (400X) are representative of intraglomerular T cell infiltration in the respective genotype and treatment group.

T cell counts turned out to be relatively low among all PI and APN mouse kidney sections analyzed. T cell infiltration did not show a significant increase in APN compared to PI animals (Figure 26).

A basal infiltration with CD3 positive T cells was counted in PI animals of all three genotypes investigated. Initial counts were highest in wildtype PI animals (0,7 cells/hpf), followed by UCH-L1 KO PI mice (0,6 cells/hpf). P2X7 KO PI animals showed lowest initial T-cell counts (0,45 cells/hpf). Interestingly, a lower amount of T cells was counted in wildtype APN mice compared to PI littermates (0,25 cells/hpf), though this tendency was not significant. UCH-L1 KO APN mice did not exhibit any differences in T-cell infiltration compared to PI littermates. The strongest infiltration was counted among P2X7 KO APN mice (0,8 cells/hpf) (Figures 26 and 27).

**B-cells – B220**

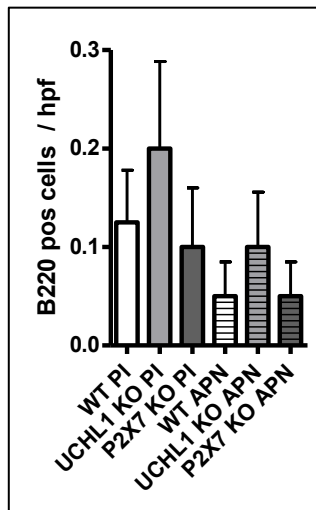


**Figure 28: Glomerular B-cell infiltration is stronger in mice injected with preimmune serum than in animals treated with anti-podocyte serum, 20d after injection.** Quantification of glomerular B cells per high power field by B220 staining in  $n=20$  glomeruli per 4 mice per group. Values are plotted as mean  $\pm$  SEM.

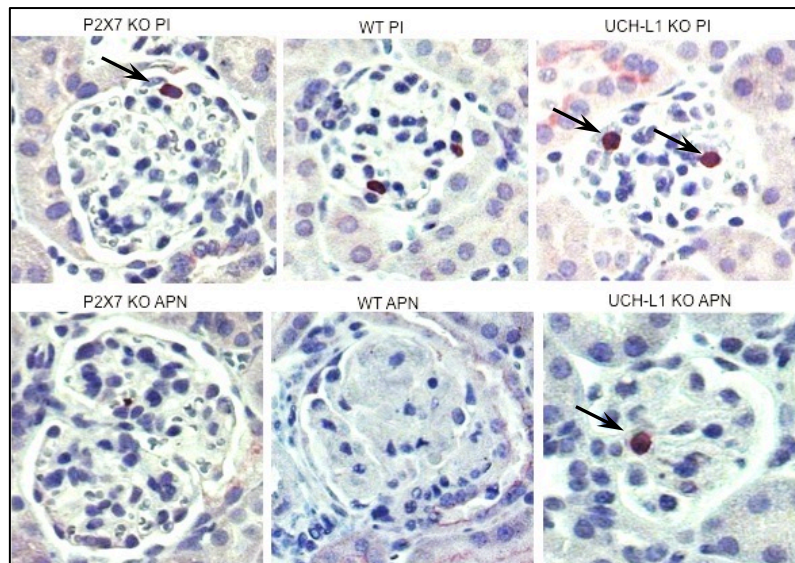


**Figure 29: B220 stained kidney cross sections, depiction of glomerular B cells (indicated by arrows).** Photographs (400X) are representative of intraglomerular B cell infiltration in the respective genotype and treatment group.

B-cell counts were low throughout all PI and APN mouse kidney sections analyzed (Figures 28 and 29).

Basal infiltration with B220 positive B-cells was highest in UCH-L1 KO PI animals (0,2 cells/hpf). Wildtype PI and P2X7 KO PI animals showed similar infiltration levels (0,1 cells/hpf). Interestingly, lower amounts of B-cells were denoted in all APN mouse compared to PI littermates ( $\approx 50\%$  lower counts), but tendencies proved insignificant. As in the PI state, UCH-L1 KO APN mice exhibited highest B cell infiltration compared to wildtype and P2X7 KO APN animals (0,1 compared to 0,05 cells/hpf).

**4.2.1.6. Proinflammatory cytokine levels**

The assessment of the proinflammatory cytokines MCP-1, IL-1 $\beta$  and IL-6 was performed on both mRNA and protein levels, in mouse serum, urine and kidney tissue pieces. This approach aimed at analyzing the severity of inflammatory response after anti-podocyte serum injection. Cytokine levels were compared between wildtype, P2X7-deficient and UCH-L1 KO mice to gain insight in the individual inflammatory response to renal injury presented by each genotype.

#### 4.2.1.6.1. MCP-1

##### Urinary MCP-1 levels

To determine whether the particular extent of macrophage recruitment among the different mouse cohorts was associated with corresponding levels of the pro-inflammatory chemokine MCP-1, ELISA measurement was performed on spendable urine samples collected on the day of sacrifice of mice representing the 6 different PI and APN groups.

MCP-1 levels (pg/mL) were detectable in undiluted urine samples and were grounded against urinary creatinine levels (mg/dL) to avoid measurement errors to occur.

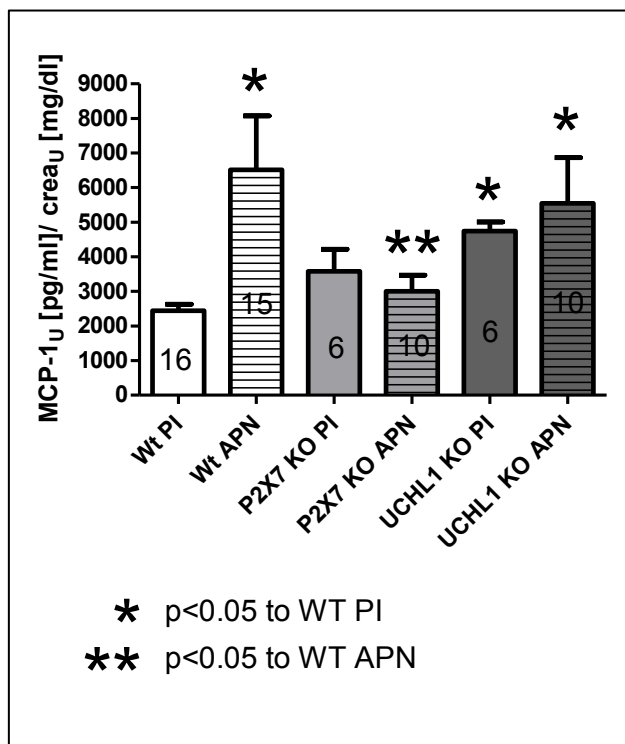


*Figure 30: P2X7 KO mice exhibit the mildest urinary levels of MCP-1, 14d after anti-podocyte serum injection. Urinary MCP-1 levels in PI and APN mouse groups of the three genotypes investigated. MCP-1 measurement was accomplished using a commercially available ELISA Kit. Urine samples collected on the day of sacrifice were used undiluted. Values were grounded against urinary creatinine levels to avoid measurement errors due to concentration differences.*

*Values are plotted as mean +/- SEM. P-values were calculated using the Mann-Whitney-U-test. A p-value <0.05 was accepted statistically significant. Figures in bars = n of mouse urine samples measured per group.*

Congruously to the macrophage counts denoted among this genotype (Figures 22 and 24), wildtype animals

showed a significant increase in MCP-1 levels from preimmune- to anti-podocyte treatment state ((Figure 30)(p<0.05, 62% augmentation)).

P2X7 KO mice showed low macrophage counts and a mild increase in infiltration from PI- to AP-serum treatment state (Figures 22 and 24). Interestingly, MCP-1 levels were detected slightly lower in urine samples of P2X7 KO anti-podocyte serum-treated animals than in probes collected from their preimmune-serum treated littermates, but did not differ significantly. P2X7 KO AP-serum treatment group MCP-1 levels were significantly lower than those of wildtype AP-serum treatment group controls (p<0,05). This finding convened with macrophage infiltration extent, which was counted lowest in P2X7 KO anti-podocyte serum treated animals compared to wildtype and UCH-L1 KO AP-serum treated mice.

## Results

Among UCH-L1 KO animals, preimmune serum treated mice showed basal levels significantly higher than those of wildtype or P2X7 KO preimmune serum treated conspecifics. Preimmune serum treatment group levels in this genotype even exceeded MCP-1 levels measured in urine samples of P2X7 KO injected with anti-podocyte serum. Levels obtained from probes of UCH-L1 KO animals injected with anti-podocyte serum were insignificantly higher than those of their preimmune serum treated littermates, but significantly exceeded WT PI-serum treatment group levels ( $p < 0,05$ ).

### MCP-1 mRNA expression/qPCR

Realtime PCR for MCP-1 from mouse kidney samples (Figure 31) was accomplished to verify the results obtained from urinary MCP-1 ELISA (Figure 30).

Expression levels were calculated as a ratio to the expression of the housekeeping gene 18S and control values were normalized to 1,0.

Results obtained via qPCR largely corresponded with the findings from macrophage counting and urinary MCP-1 ELISA.

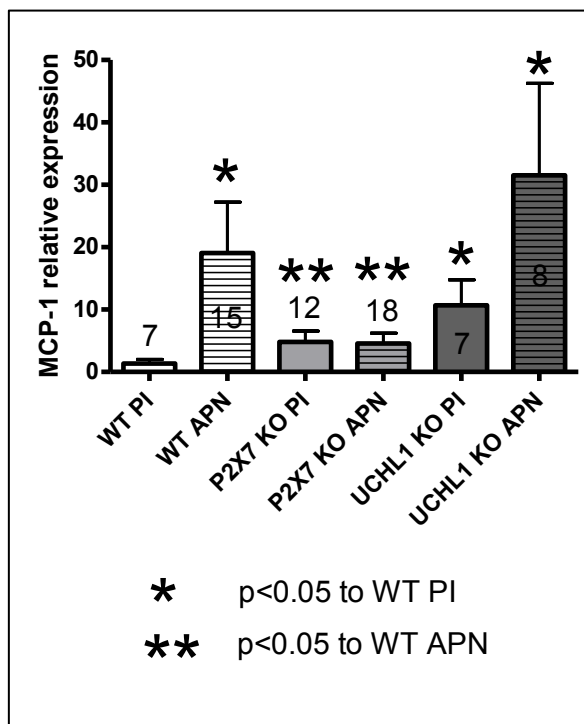


*Figure 31: Relative renal expression of MCP-1 mRNA is lowest in P2X7-deficient mice compared to wildtype and UCH-L1 KO mice, 14d after injection of anti-podocyte serum. Expression levels measured via qPCR in kidney tissues of wildtype, P2X7 KO and UCH-L1 KO mice in PI- and APN-serum treated groups. Values are plotted as mean  $\pm$  SEM. P-values were calculated using the Mann-Whitney-U-test. A p-value  $< 0.05$  was accepted statistically significant. Figures in/above bars = n of mouse urine samples measured per group.*

Wildtype animals exhibited lowest MCP-1 expression in the preimmune-serum treatment state compared to UCH-L1 KO and P2X7 KO mice injected with preimmune serum. Wildtype mice injected with anti-podocyte serum showed a significant, 20fold higher expression of the chemokine than their PI-serum treated littermates, which convened with the increase in urinary MCP-1 from preimmune-serum- to anti-podocyte serum treatment state (Figure 30) and the stronger macrophage infiltration detected (Figures 22 and 24).

In the P2X7 KO group, MCP-1 expression did not differ between mice injected with preimmune serum and those that obtained anti-podocyte serum. Both PI- and AP-

serum treatment group levels were significantly lower ( $p < 0,05$ ) than the value measured in wildtype mice injected with AP-serum, but higher than WT preimmune-serum treated MCP-1 expression. This result coincided with the observations made in macrophage counting and urinary MCP-1 ELISA, where levels mostly were lowest among P2X7 KO animals, especially when comparing anti-podocyte-serum treated P2X7 KO to wildtype and UCH-L1 KO mice injected with anti-podocyte serum.

UCH-L1 KO animals injected with preimmune serum exhibited the highest MCP-1 mRNA content among the three preimmune-serum treatment groups compared ( $p < 0,05$  to WT PI). Similarly, among the anti-podocyte serum treated groups, MCP-1 mRNA content was highest in UCH-L1 KO to wildtype and P2X7 KO mice. Levels increased significantly from preimmune-serum- to anti-podocyte serum-treated state and proved significantly ( $p < 0,05$ ) higher than WT PI-serum- and AP-serum-treatment levels. This outcome was congruous with the most severe macrophage infiltration and high urinary MCP-1 levels observed among UCH-L1 KO animals.

### **4.2.1.6.2. IL-1 $\beta$**

#### **IL-1 $\beta$ levels (urine, serum)**

Macrophages are a major source of the pro-inflammatory cytokine IL-1 $\beta$ , a mediator that has been shown to play an important role in glomerular crescent formation and subsequent tubulointerstitial injury. Moreover, IL-1 $\beta$  is released from macrophages following stimulation of the P2X7 receptor.

IL-1 $\beta$  levels in urine and serum samples (Figure 32 A and B) as well as the relative expression of IL-1 $\beta$  mRNA measured via qPCR (Figure 33) were hence considered indicators of both the severity of inflammation just as the activity of the P2X7 receptor in wildtype, P2X7 KO and UCH-L1 KO mice.

## Results

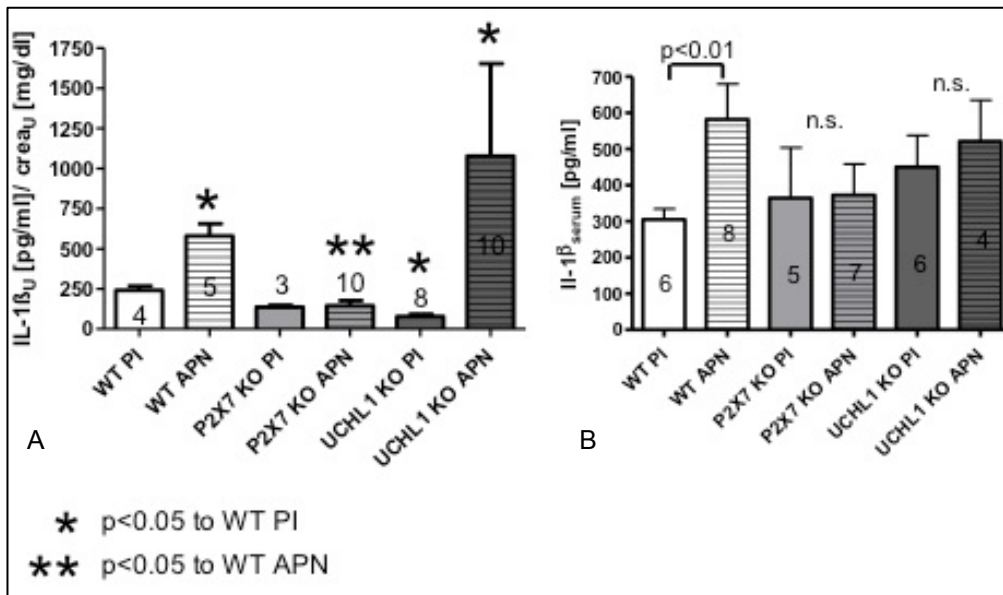


**Figure 32: Urinary IL-1 $\beta$  levels are significantly lower in P2X7 KO than in wildtype mouse urine samples, 14d after anti-podocyte serum injection.** IL-1 $\beta$  levels in urine (A) and serum (B) (ELISA measurement) obtained from wildtype, P2X7 KO and UCH-L1 KO mice on the day of sacrifice. Measurement was accomplished using a commercially available ELISA Kit. Urine sample values were grounded against urinary creatinine levels to avoid measurement errors due to concentration differences. Values are plotted as mean  $\pm$  SEM. Statistical significance was calculated using the Mann-Whitney-U-test. A p-value <0.05 was accepted statistically significant. Figures in bars = n of mouse urine or serum samples measured per group.

IL-1 $\beta$  measurement in wildtype urine samples revealed a significant increase in cytokine levels between preimmune- and anti-podocyte serum treated animals ( $p < 0,05$ ), accounting for the severe inflammation provoked via APN-serum administration.

Urinary levels of IL-1 $\beta$  indicated the most severe inflammatory reaction in UCH-L1 KO anti-podocyte serum treated mice (Figure 32A). Among the UCH-L1 KO genotype, the strongest augmentation between preimmune-serum treated and anti-podocyte-serum treated group levels was detected (increase of 93%). Basal cytokine levels in UCH-L1 preimmune-serum urine samples were significantly lower than those measured in WT preimmune-serum treated mice.

P2X7 KO animals did not exhibit any differences in urinary IL-1 $\beta$  levels when comparing preimmune- and AP-serum-treatment group values. Both PI- and AP-serum injected mice of this genotype showed values ranging below WT preimmune-serum treatment levels, P2X7 KO AP-serum treated mouse values were significantly lower than those obtained from WT AP-serum treatment group samples ( $p < 0,05$ ).

When comparing serum IL-1 $\beta$  levels, tendencies were less clear (Figure 32B). A significant increase between preimmune- and anti-podocyte serum treatment state could again be observed in wildtype mice. In contrast, measurement of sera from P2X7 KO and UCH-L1 KO did not exhibit any significant motion from PI- to AP-serum treatment states. All measurements ranged on a similar level, UCH-L1 KO values slightly above those detected in P2X7 KO probes.

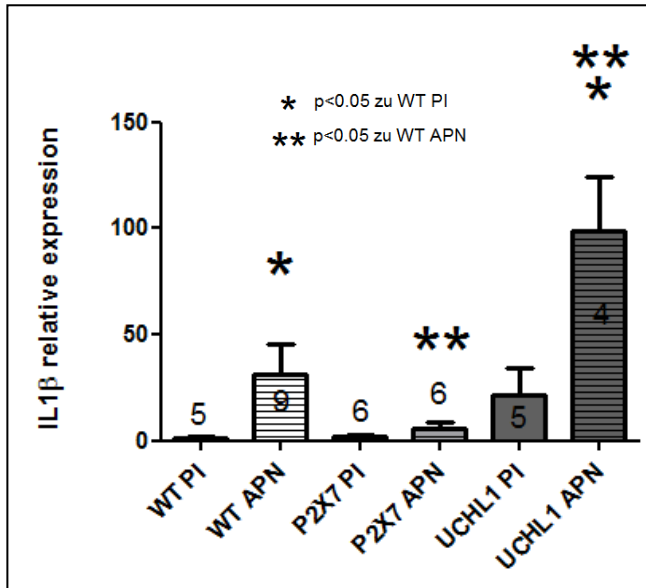


Figure 33: **The increase in relative renal expression of IL-1β mRNA is significantly lower in P2X7 KO mice than in wildtype and UCH-L1-deficient conspecifics, 14d after anti-podocyte serum injection.** Expression levels measured via qPCR in kidney tissues of wildtype, P2X7 KO and UCH-L1 KO mice in PI- and APN-serum treated groups. Values are plotted as mean +/- SEM. P-values were calculated using the Mann-Whitney-U-test. A p-value < 0.05 was accepted statistically significant. Figures in/above bars = n of samples measured per group.

Relative IL-1β expression measured via qPCR in whole kidney preparations supported the findings

obtained from urine ELISA (Figure 33). While a significant increase in cytokine levels from PI- to AP- serum treatment state was denoted in both wildtype and UCH-L1 KO mouse groups. P2X7 KO mice expressed constantly low levels of IL-1β, independent of the type of serum that had been administered. UCH-L1 KO anti-podocyte serum treated animals expressed significantly higher amounts of IL-1β than wildtype conspecifics injected with anti-podocyte serum (p < 0,05). Basal IL-1β expression was highest in UCH-L1 KO PI mice compared to WT and P2X7 KO PI animals.

#### 4.2.1.6.3. IL-6

##### IL-6 serum levels

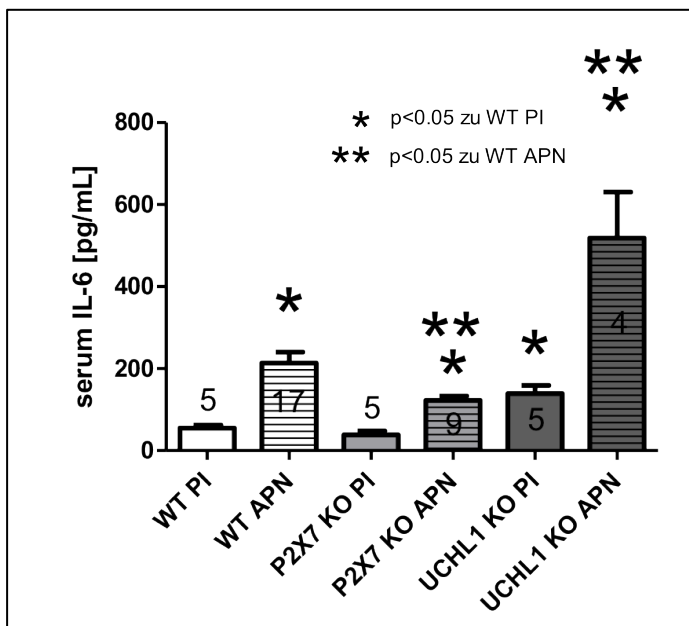


Figure 34: **P2X7-deficient animals show the mildest - UCH-L1 KO mice exhibit highest IL-6 serum levels, 14d after anti-podocyte serum injection.** IL-6 serum levels (pg/mL) in WT, P2X7 KO and UCH-L1 KO PI and APN mice. IL-6 levels were obtained via ELISA from serum samples collected on the day of sacrifice. Values are plotted as mean +/- SEM. P-values were calculated using the Mann-Whitney-U-test. A p-value < 0.05 was accepted statistically significant. Figures in/above bars = n of mouse serum samples measured per group.

## Results

---

IL-6 is a pro-inflammatory cytokine of which the release is induced by IL-1 $\beta$ . To reassess the arguable serum levels of IL-1 $\beta$  (Figure 32B), mouse serum samples were reanalyzed for IL-6 via ELISA, which offered more sensitive values than those obtained from IL-1 $\beta$  determination (Figure 34).

IL-6 serum levels convened with the results gained from qPCR (Figure 33) and urinary ELISA for IL-1 $\beta$  (Figure 32A).

Wildtype animals showed a significant augmentation in IL-6 levels after the induction of GN when comparing preimmune- and anti-podocyte serum treated samples ( $p < 0,05$ ). The most significant increase in serum IL-6 levels was denoted in probes representing the UCH-L1 KO anti-podocyte serum treated group ( $p < 0,05$  compared to WT AP-serum;  $p < 0,05$  compared to UCH-L1 KO preimmune serum). Basal IL-6 levels measured in UCH-L1 KO preimmune serum treated animals were significantly higher than the initial levels of wildtype controls ( $p < 0,05$ ).

Evaluation of P2X7 KO sera showed a slight, but low augmentation in IL-6 levels from preimmune- to anti-podocyte serum treated state. IL-6 values measured in P2X7 KO AP-serum probes proved significantly lower than those obtained from WT AP-serum blood samples ( $p < 0,05$ ) and UCH-L1 KO AP-serum blood samples.

### 4.3.UCH-L1 and P2X7 are both upregulated in the glomerulonephritic kidney.

Results section 4.3. shows the upregulation of both P2X7 and UCH-L1 in the glomerulonephritic kidney. This upregulation upon kidney injury is depicted via immunohistochemistry staining and comparison of glomerular cross sections of wildtype mice treated with preimmune- and anti-podocyte serum respectively and via the assessment of the protein and mRNA levels of UCH-L1 and P2X7 in preimmune serum- compared to anti-podocyte serum treated animals.

#### 4.3.1. Immunohistochemistry

To distinguish the expression and distribution patterns of P2X7 and UCH-L1 in glomerulonephritic and healthy kidney cross sections, immunohistochemistry staining was performed on kidney sections of wildtype PI and APN animals.

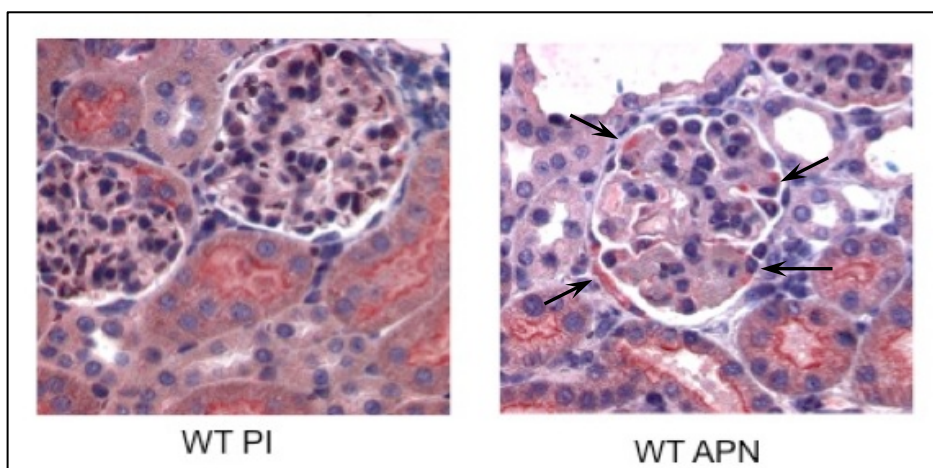


**Figure 35: P2X7 expression is upregulated in the glomerulonephritic kidney of wildtype mice, 14d after anti-podocyte serum injection.** P2X7 immunohistochemistry. P2X7 staining on an exemplary WT PI and WT APN kidney cross section using the K1G antibody in a 1:400 dilution, depiction via DAKO pH 9, PolAP Kit. Red staining pattern of P2X7-positive glomerular areas, indicated by arrow. While kidney cross-sections (400X) from wildtype PI-serum treated mice did not show any distinct P2X7 staining patterns, glomeruli of wildtype animals that were treated with APN-serum exhibited immunopositive areas. P2X7 staining seemed glomeruli-specific, with dye distributed among podocytes, lining the glomerulus (indicated by arrows).

Analysis of stained sections revealed an upregulation or rather de-novo detectability of both proteins in inflamed glomeruli of anti-podocyte serum treated mice compared to bland kidney tissue seen in sections of animals treated with preimmune serum. In case of UCH-L1, the majority of immunopositive staining was found in the glomeruli, particularly in podocytes. P2X7 immunostaining could also be found predominantly in glomerulonephritic glomeruli, expressing a pattern which might suggest podocyte involvement.

No immunoreactivity against either P2X7 or UCH-L1 was seen in mice glomeruli of wildtype animals that had been treated with preimmune serum.

## Results

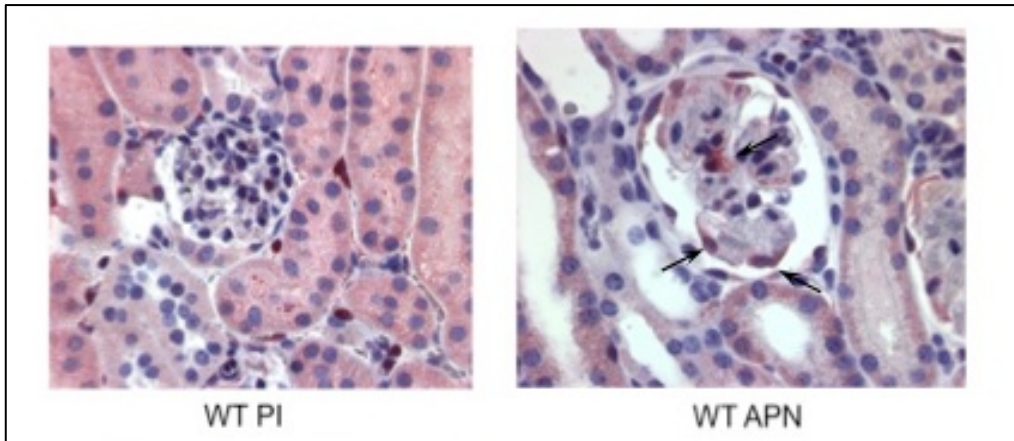


**Figure 36: UCH-L1 expression is upregulated in the glomerulonephritic kidney of wildtype mice, 14d past anti-podocyte serum injection.** UCH-L1 immunohistochemistry. UCH-L1 staining of an exemplary WT PI and WT APN kidney cross section (400X) using the U104 antibody in a 1:20 dilution, depiction via Dako pH9, PoIAP Kit. Wildtype PI glomeruli were completely UCH-L1 negative. APN-treated wildtype kidneys expressed glomeruli-specific staining patterns, immunopositivity was most significant in podocytes (indicated by arrows).

### 4.3.2. Western Blot Analysis

#### UCH-L1

Western blotting against UCH-L1 (figure 37) revealed an upregulation of UCH-L1 protein levels when comparing PI to APN kidney lysates in both wildtype and P2X7 KO mouse samples. UCH-L1 protein was absent in UCH-L1 KO mice. Densitometry of protein bands showed that the amount of UCH-L1 protein was similar in wildtype and P2X7 KO PI and wildtype and P2X7 KO APN mouse groups. The increase of UCH-L1 protein amounts detected when comparing to APN kidney lysate levels was significant ( $p < 0,01$ ) among both wildtype and P2X7 KO animal groups to the same extent.

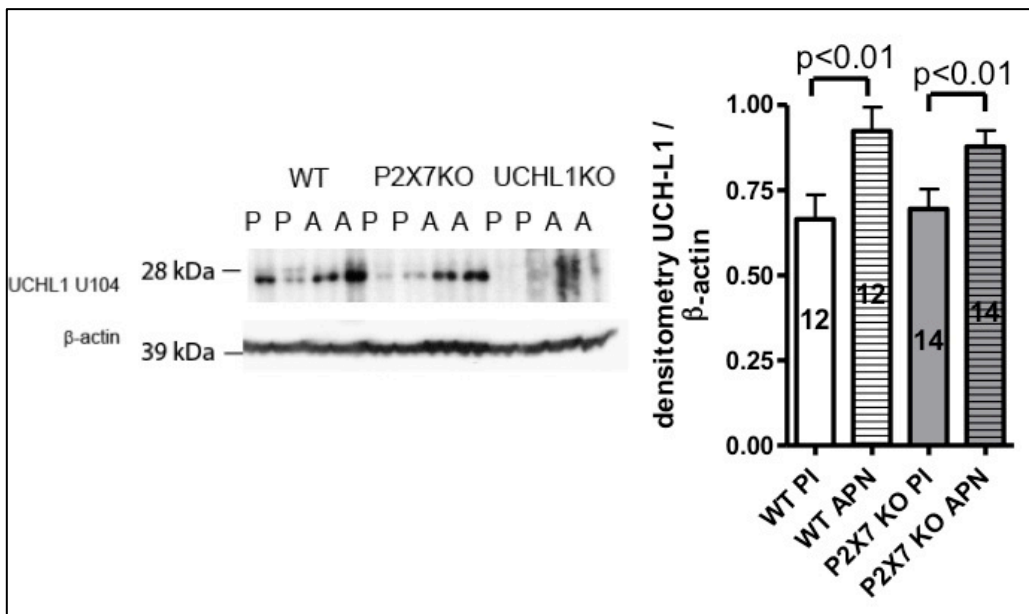


**Figure 37: UCH-L1 expression is upregulated in the glomerulonephritic kidney of wildtype and P2X7 KO mice, 14d past anti-podocyte serum injection.** Representative Western Blot from kidney lysates of wildtype, P2X7 KO and UCH-L1 KO mice; UCH-L1 detection; densitometry of UCH-L1 bands against  $\beta$ -actin bands of the same sample. Values are expressed as mean  $\pm$  SEM. Statistical significance was calculated using the Mann-Whitney-U-test. A  $p$ -value  $< 0.05$  was accepted statistically significant. Figures in bars = n of samples measured per group.

## P2X7

Western blotting against P2X7 (Figure 38) revealed that UCH-L1 KO mice express significantly higher levels of P2X7 protein than wildtype animals, independent of the respective serum injected ((preimmune or anti-podocyte serum) ( $p < 0,01$ )).

Wildtype mouse kidney lysates of preimmune- and anti-podocyte serum treated animals contained less P2X7 protein than lysates prepared from UCH-L1 KO preimmune- and anti-podocyte serum treated mouse kidneys. Densitometry of protein bands from whole kidney lysates showed that the extent of increase in P2X7 protein levels between preimmune- and anti-podocyte serum treatment state was similarly insignificant in both genotypes.

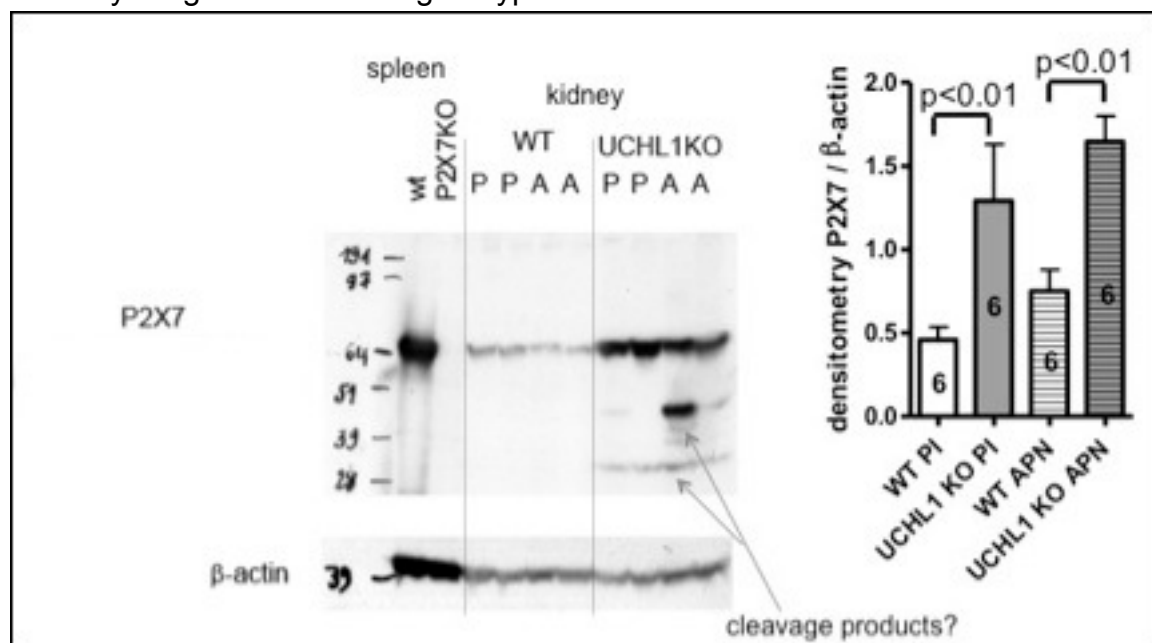


**Figure 38: UCH-L1 KO mice exhibit higher P2X7 expression than wildtype animals in kidney tissue, obtained on d14 past anti-podocyte serum injection.** Representative Western Blot from kidney lysates of wildtype, P2X7 KO and UCH-L1 KO mice; P2X7 detection; densitometry of P2X7 bands against  $\beta$ -actin bands: P2X7 was absent in spleen lysate of P2X7 KO mice, which served as negative control. Spleen lysate of a wildtype APN mouse served as positive control. Values are expressed as mean  $\pm$  SEM. Statistical significance was calculated using the Mann-Whitney-U-test. A  $p$ -value  $< 0.05$  was accepted statistically significant. Figures in bars =  $n$  of samples measured per group.

P2X7 was absent in kidney lysates of P2X7 KO mice. Preimmune-serum treated wildtype kidneys showed moderate P2X7 expression (light, narrow protein bands, moderate density). As densitometry of several Western blots for P2X7 ( $n=6$  per group) revealed, there was no significant upregulation of P2X7 protein in wildtype anti-podocyte serum treated compared to wildtype preimmune-serum treated mice. P2X7 protein amounts were significantly higher in PI-treated UCH-L1 KO animals than in wildtype PI conspecifics (thicker, intensely black bands,  $p < 0,01$ ). As observed in wildtype anti-podocyte-serum-treated kidney lysates, densitometry showed no significant but a tendency towards upregulation of P2X7 protein in UCH-L1 KO AP-serum lysates compared to preimmune-serum values. As seen in preimmune-serum lysates, UCH-L1 KO anti-podocyte serum lysates exhibited significantly higher amounts of P2X7 protein than WT AP-serum probes ( $p < 0,01$ ). P2X7 band intensity

visually appeared a lot stronger in UCH-L1 KO mouse kidney lysates than in wildtype preparations.

Interestingly, additional protein bands running below the estimated P2X7 kDa size appeared on WB lines where UCH-L1 KO kidney lysate had been blotted. These additional bands, stronger in UCH-L1 KO AP-serum than in PI-serum lysates, might be proofs of P2X7 cleavage products in mice lacking UCH-L1, accounting for an altered P2X7 activation in this genotype.

### 4.3.3. Realtime PCR

#### UCH-L1

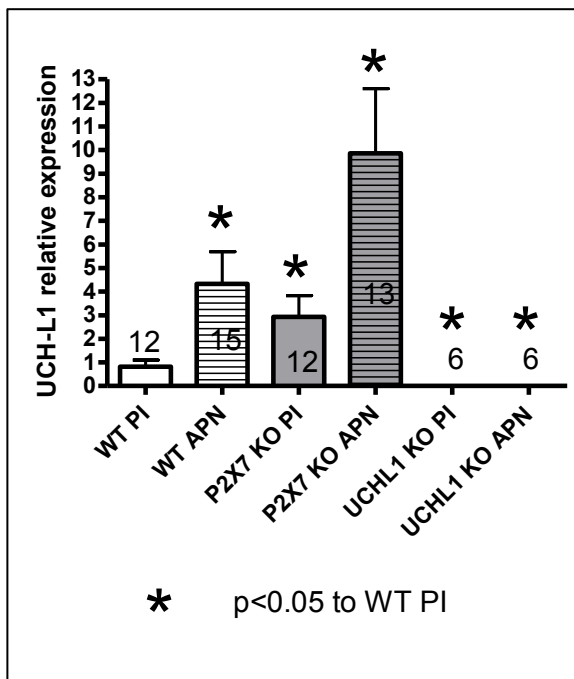


**Figure 39: UCH-L1 expression is upregulated in the glomerulonephritic kidney of wildtype and P2X7-deficient mice, 14d past injection of anti-podocyte serum.** Relative renal expression of UCH-L1 mRNA. Expression levels measured via qPCR in kidney tissues of wildtype, P2X7 KO and UCH-L1 KO mice in PI- and APN-serum treated groups. Values are expressed as mean +/- SEM. Statistical significance was calculated using the Mann-Whitney-U-test. A p-value < 0.05 was accepted statistically significant. Figures in bars = n of samples measured per group.

Relative renal expression of UCH-L1 mRNA. was measured via qPCR in kidney tissues of wildtype, P2X7 KO and UCH-L1 KO mice in preimmune- and anti-podocyte-serum treated groups (Figure 39).

UCH-L1 mRNA expression was absent in UCH-L1 KO animals. Wildtype animals treated with anti-podocyte serum showed a significant upregulation of UCH-L1 compared to littermates that had been injected with preimmune serum.

P2X7 KO animals showed basal expression levels of UCH-L1 mRNA in healthy control preimmune-serum treated probes that ranged significantly higher than those detected in wildtype PI samples. Analysis of P2X7 KO mouse probes exhibited a significant 10-fold upregulation in the relative UCH-L1/18S ratio when comparing preimmune- and anti-podocyte serum treated group values in this genotype. UCH-L1 mRNA expression levels measured in P2X7 KO anti-podocyte serum probes were significantly higher than in wildtype anti-podocyte serum samples, though this tendency proved insignificant.

P2X7

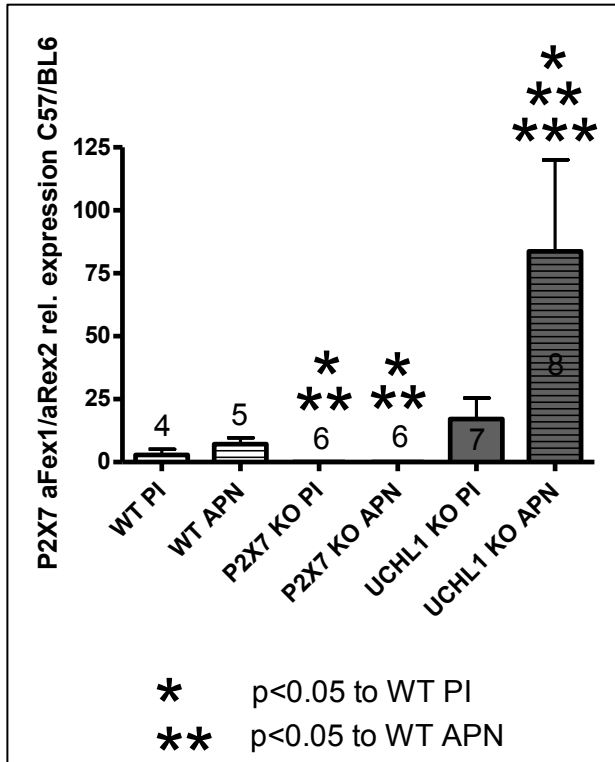


Figure 40: **P2X7 mRNA content is significantly upregulated in UCH-L1 KO mouse kidneys, 14d after anti-podocyte serum injection.** Relative renal expression of P2X7 mRNA. Expression levels measured via qPCR in kidney tissues of wildtype, P2X7 KO and UCH-L1 KO mice in PI- and APN-serum treated groups. Values are expressed as mean +/- SEM. Statistical significance was calculated using the Mann-Whitney-U-test. A p-value <0.05 was accepted statistically significant. Figures in/above bars = n of samples measured per group.

Relative renal expression of P2X7 mRNA. was measured via qPCR in kidney tissues of wildtype, P2X7 KO and UCH-L1 KO mice in preimmune- and anti-podocyte-serum treated

groups (Figure 40).

P2X7 receptor mRNA expression was absent in P2X7 KO animals. Wildtype animals treated with anti-podocyte serum showed a slight upregulation of P2X7 compared to littermates that had been injected with preimmune serum, but levels proved insignificant. This finding coincided with the upregulation of P2X7 depicted via immunohistochemistry staining in wildtype APN compared to PI mouse kidney sections (Figure 35), as well as with the increased amounts of P2X7 protein in kidney lysates representing wildtype APN animals observed by Western blotting (Figure 38). In contrast, UCH-L1 KO animals showed basal expression levels of P2X7 mRNA in healthy control preimmune serum treated animal probes that already ranged higher than those detected in wildtype anti-podocyte treated mouse samples and exhibited a significant 80-fold increase when comparing PI- and AP-serum values in this genotype. P2X7 mRNA expression measured in UCH-L1 KO anti-podocyte serum treated mouse probes was significantly higher than in wildtype AP-serum samples. This finding coincided with the early onset and severe degree of detectable proteinuria and the peak in macrophage infiltration, as well as the increased expression of MCP-1 and IL-1 $\beta$ , urinary levels of IL-1 $\beta$  and serum levels of IL-6 (see above) among this mouse group.

#### 4.4.P2X7 activation is altered in UCH-L1 KO mice.

As an indicator of P2X7 activity, the “ADAM17 axis”, a downstream axis affected by stimulation of the P2X7 receptor, was investigated. This axis is focused on the shedding activity of ADAM17 and its downstream effects on EGFR and proteins involved in the Notch1-pathway, such as HeyL.

In particular, we chose to investigate mRNA and protein levels of ADAM17, mRNA and protein levels of EGFR and mRNA levels of HeyL.

##### 4.4.1. ADAM17

##### 4.4.1.1. ADAM17 Western blot

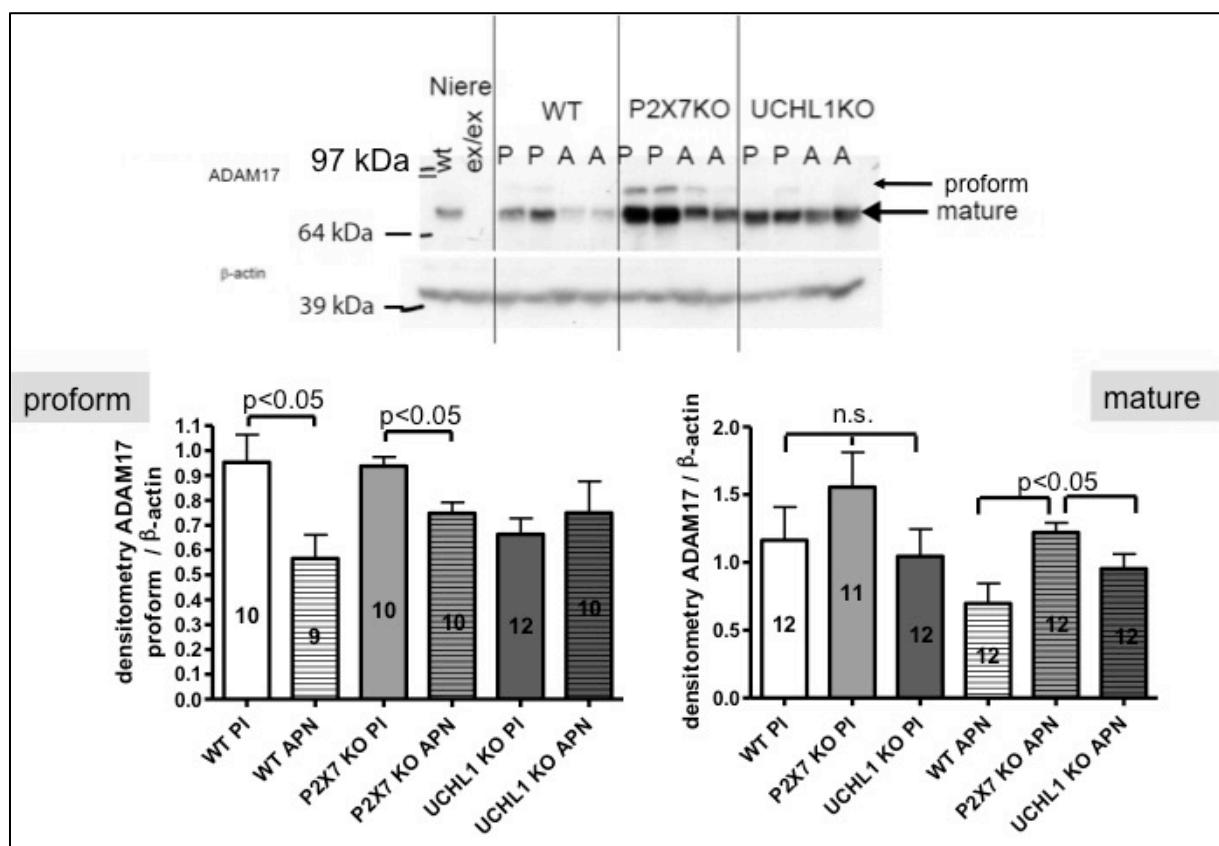


Figure 41: Levels of ADAM17 and its preform are significantly higher in P2X7 KO mice than in wildtype and UCH-L1 KO conspecifics, 14d after injection of preimmune- or anti-podocyte serum respectively. Representative Western blot from kidney lysates of wildtype, P2X7 KO and UCH-L1 KO mice; ADAM17 detection – the mature as well as the preform of ADAM17 are detectable with the antibody used; densitometry of pro-ADAM17 and ADAM17 bands against  $\beta$ -actin bands. Values are expressed as mean  $\pm$  SEM. Statistical significance was calculated using the Mann-Whitney-U-test. A p-value  $<0.05$  was accepted statistically significant. Figures in bars = n of samples measured per group.

Detection of ADAM17 on Western blots prepared from wildtype, UCH-L1 KO and P2X7 KO mouse kidney lysates was performed to gain indication of potentially altered P2X7 activation in preimmune-serum treated animals compared to mice injected with anti-podocyte serum. A comparison was also made between UCH-L1 KO, wildtype and P2X7 KO animals (Figure 41).

The antibody applied detects both the proform and activated mature ADAM17. ADAM17 activation is P2X7-co-mediated.

Analyzing the blotting pattern and densitometry of pro-ADAM17 in wildtype and P2X7 KO mice, more intense bands and significantly ( $p < 0,05$ ) higher density of pro-ADAM17 were observed in wildtype PI compared to wildtype APN and P2X7 KO PI to P2X7 KO APN lysates respectively. This finding may account for an enhanced ADAM17 activation in glomerulonephritic kidneys compared to healthy tissue. In UCH-L1 KO kidney lysates, pro-ADAM17 bands do not show any significant difference in intensity or density when comparing PI and APN samples. This observation might be indicative of an impaired ADAM17 activation due to altered P2X7 function in mice lacking UCH-L1.

Bands of mature ADAM17 showed similar features as those of pro-ADAM17. While in wildtype and P2X7 KO kidney lysates, protein amounts were diminished in APN compared to PI preparations both band-wise as density-wise, UCH-L1 KO samples were inert concerning ADAM17 band intensity and density between PI and APN state. P2X7 KO animals showed most intense ADAM17 bands and highest density compared to wildtype and UCH-L1 KO mice. In P2X7 KO APN kidney lysates, mature ADAM17 content was significantly ( $p < 0,05$ ) higher than in wildtype APN and UCH-L1 KO APN preparations respectively.

#### 4.4.1.2. ADAM17 mRNA expression

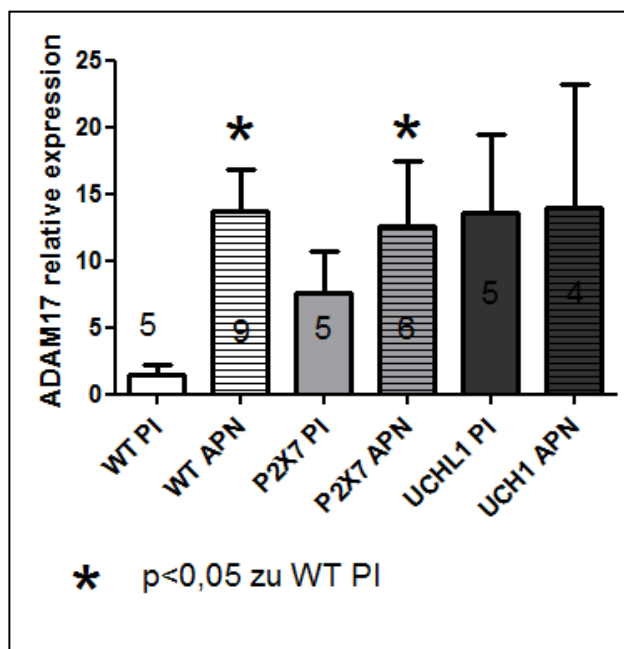


Figure 42: **Relative renal expression of ADAM17 mRNA.** Expression levels measured via qPCR in kidney tissues of wildtype, P2X7 KO and UCH-L1 KO mice in PI- and APN-serum treated groups. Values are expressed as mean  $\pm$  SEM. Statistical significance was calculated using the Mann-Whitney-U-test. A  $p$ -value  $< 0.05$  was accepted statistically significant. Figures in bars = n of samples measured per group.

In contrast to ADAM17 protein content, which showed a decline in tissue lysates prepared from kidneys of animals that had been issued anti-podocyte serum (Figure 41), ADAM17 mRNA expression was upregulated in

anti-podocyte serum treated compared to preimmune-serum treated wildtype and P2X7 KO mouse kidneys. While basal ADAM17 expression was low in wildtype preimmune-serum mouse kidneys, a significant, 7-fold increase could comparatively be denoted in anti-podocyte-serum treated tissues. The same tendency, yet without significance, could be observed in P2X7 KO anti-podocyte serum treated compared

to P2X7 KO preimmune-serum treated littermates (3-fold increased ADAM17 expression).

Relative ADAM17 expression coincided with ADAM17 protein levels among the UCH-L1 KO groups. There was no significant upregulation in ADAM17 expression between preimmune- and anti-podocyte serum treated animals, but basal expression in UCH-L1 KO preimmune-serum kidney lysates was already as high as wildtype and P2X7 KO anti-podocyte serum values. UCH-L1 KO anti-podocyte serum tissue preparations showed similar ADAM17 expression levels. These findings argue for a proper ADAM17 regulation in wildtype animals, whereas mice lacking UCH-L1 seem unable to adjust expression and function of the sheddase. This observation might be indicative of an altered P2X7 activation or function in UCH-L1 KO animals.

#### 4.4.2. EGFR

##### 4.4.2.1. EGFR Western Blot

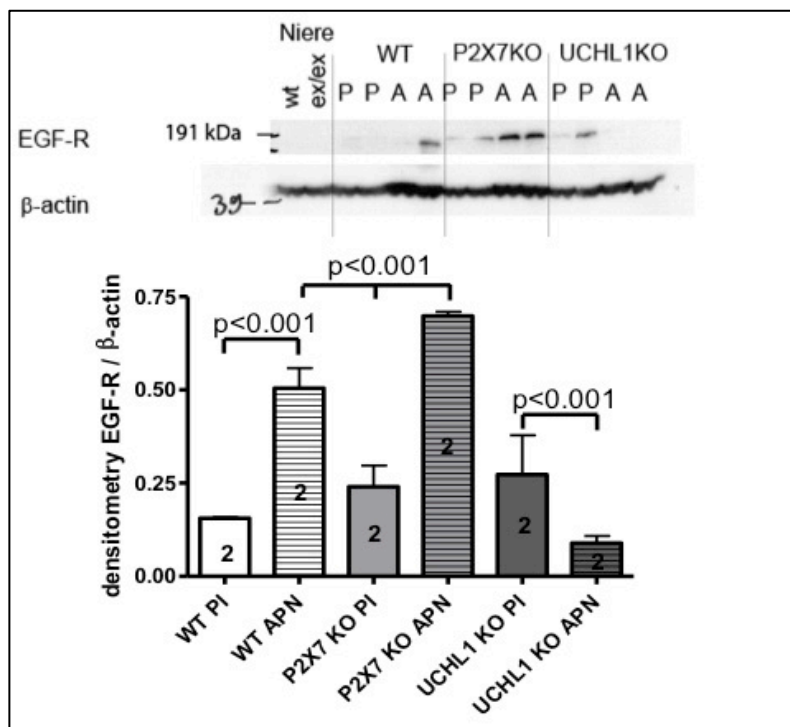


**Figure 43: EGFR Western blot in P2X7 KO and UCH-L1 KO kidney lysates.** Representative Western blot from kidney lysates of wildtype, P2X7 KO and UCH-L1 KO mice; EGFR detection. Densitometry of  $n=2$  Western Blots per mouse group. Values are expressed as mean  $\pm$  SEM. Statistical significance was calculated using the Mann-Whitney-U-test. A  $p$ -value  $<0.05$  was accepted statistically significant. Figures in bars =  $n$  of samples measured per group.

ADAM17 activation results in proinflammatory signals in most systems through shedding of  $\text{TNF}\alpha$ .

However, ADAM17 has also been described to function antiinflammatorily via the activation of the notch pathway and EGFR. EGFR protein content was hence considered an indicator of ADAM17 - and, in consequence, P2X7 - function in wildtype, P2X7 KO and UCH-L1 KO mouse kidneys.

Evaluation of protein bands and densitometry after EGFR antibody detection (Figure 43) showed a significant ( $p<0,001$ ) increase of EGFR protein amounts in lysates prepared from wildtype and P2X7 KO anti-podocyte serum-treated mouse kidneys compared to kidney preparations obtained from their respective preimmune-serum-treated littermates. This finding coincided with the upregulated ADAM17 mRNA expression seen among wildtype and P2X7 KO animals mice injected with anti-

podocyte serum described above. P2X7 KO anti-podocyte serum treated mouse kidney lysates contained the highest amounts of EGFR protein ( $p < 0,001$  to WT APN).

In contrast, UCH-L1 KO anti-podocyte serum kidney lysates contained less EGFR protein than lysates prepared from preimmune-serum treated mouse tissues. This observed decrease was significant ( $p < 0,001$ ) and corresponded to the impaired ADAM17 regulation found via ADAM17 Western blot and qPCR.

#### 4.4.2.2. EGFR expression/qPCR

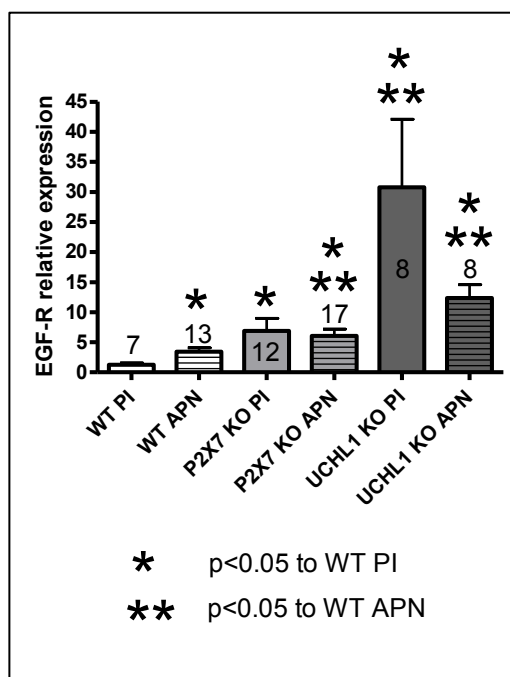


Figure 44: Relative renal expression of EGFR mRNA is highest in UCH-L1 KO mice injected with preimmune serum, 14d past serum injection. Expression levels measured via qPCR in kidney tissues of wildtype, P2X7 KO and UCH-L1 KO mice in PI- and APN-serum treated groups. Values are expressed as mean  $\pm$  SEM. Statistical significance was calculated using the Mann-Whitney-U-test. A  $p$ -value  $< 0.05$  was accepted statistically significant. Figures in bars = n of samples measured per group.

Among wildtype mice injected either with preimmune(PI)- or anti-podocyte(APN) serum, results obtained from qPCR for EGFR (Figure 44) corresponded with EGFR protein contents evaluated via WB (Figure 43). Kidney lysates prepared from anti-podocyte serum-treated

wildtype mice showed a significantly higher (5-fold) EGFR mRNA expression than preimmune-serum-treated littermates ( $p < 0,05$ ). In contrast, results differed from WB findings in the P2X7 KO mouse group. EGFR mRNA expression was significantly higher than in in WT anti-podocyte serum treated mouse kidneys ( $p < 0,05$ ), but did not alter between P2X7 KO preimmune- and anti-podocyte serum treated kidneys. P2X7 KO animals treated with preimmune serum and those that obtained anti-podocyte serum expressed the same amounts of EGFR mRNA.

Among UCH-L1 KO animals, Western blotting observations were approved by qPCR. UCH-L1 KO preimmune-serum treated animals expressed 2,8-fold higher levels of EGFR mRNA than anti-podocyte-serum-treated littermates. Interestingly, UCH-L1 KO PI kidneys exhibited the highest EGFR expression levels of all mice investigated ( $p < 0,05$  to WT APN).

## 4.4.3. HeyL

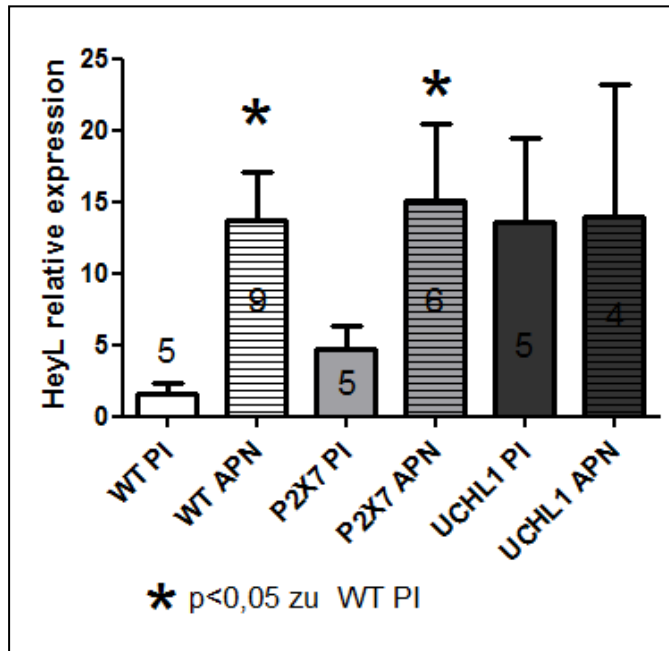


Figure 45: Relative renal expression of HeyL mRNA is significantly higher in wildtype and P2X7-deficient mice injected with anti-podocyte serum than in wildtype and P2X7 KO animals treated with preimmune serum. Expression levels measured via qPCR in kidney tissues of wildtype, P2X7 KO and UCH-L1 KO mice in PI- and APN-serum treated groups. Values are expressed as mean  $\pm$  SEM. Statistical significance was calculated using the Mann-Whitney-U-test. A p-value  $< 0.05$  was accepted statistically significant. Figures in bars = n of samples measured per group.

HeyL is a member of the Hes and Hey families of basic helix-loop-helix transcription factors, that are regarded as Notch target genes and mediate EGFR expression. HeyL is among the last links of the intracellular Notch1-involving reaction chain activated by ADAM17. HeyL expression was hence considered an indicator of ADAM17 activity.

HeyL mRNA expression levels among wildtype, P2X7 KO and UCH-L1 KO mice injected with either preimmune- or anti-podocyte serum coincided with ADAM17 mRNA expression patterns among the different mouse groups (Figure 45).

HeyL mRNA expression was upregulated in anti-podocyte serum treated mice compared to wildtype and P2X7 KO mouse kidneys of animals that received preimmune serum. While basal HeyL expression was low in wildtype preimmune-serum mouse kidneys, a significant ( $p < 0,05$  to WT PI), 8-fold increase could comparatively be denoted in anti-podocyte-serum treated tissues. The same tendency, yet without significance, could be observed in P2X7 KO mice injected with anti-podocyte serum compared to preimmune-serum-treated P2X7 KO littermates (3-fold increased HeyL expression).

Among the two UCH-L1 KO group, there was no significant upregulation in HeyL expression between preimmune- and anti-podocyte-serum treated animals, but basal expression in UCH-L1 KO preimmune-serum kidney lysates was already as high as in wildtype and P2X7 KO anti-podocyte serum conspecifics. UCH-L1 KO anti-podocyte serum tissue preparations showed similar HeyL expression levels. These findings again argue for a proper ADAM17 regulation in wildtype animals, whereas mice deprived of UCH-L1 seem incapable to adjust expression and function of the enzyme.

#### 4.5. Therapeutic antagonization of the P2X7 receptor attenuates the development of anti-podocyte nephritis.

Results section 4.5. shows the outcome of the nanobody experiment and arouses suspicion of the efficacy of therapeutically antagonizing the P2X7 receptor in anti-podocyte nephritis. Albuminuria as a clinical sign of severe kidney damage and IL-6 serum levels as indicator of the extent of inflammatory response are compared among wildtype mice injected with anti-podocyte serum that additionally received either a P2X7 agonistic or antagonistic nanobody or the so-called “dummy”.

##### 4.5.1. Albuminuria

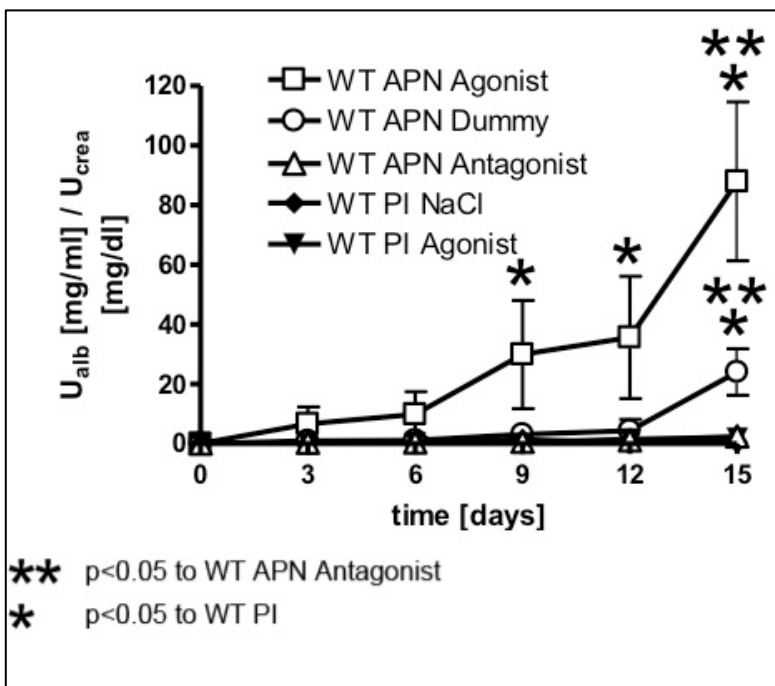


Figure 46: WT APN mice treated with P2X7 antagonistic nanobodies do not exhibit albuminuria, 14d past injection of anti-podocyte serum. Albuminuria in wildtype mice of 5 different treatment groups. Urinary albumin levels were measured by ELISA and normalized against creatinine levels of the same urine samples. Values are plotted as mean mean +/- SEM. Statistical significance was measured using the Mann-Whitney-U test. A  $p < 0.05$  was accepted statistically significant. Urine of PI-serum treated mice of all three genotypes and WT APN urines remained free of albumin throughout the APN monitoring period = graphs parallel to baseline.

Preimmune-serum treated wildtype mice that received either saline (black diamond)

or agonistic P2X7 nanobody (black triangle) remained free of albuminuria throughout the monitoring period (Figure 46, graphs parallel to baseline). Wildtype animals injected with anti-podocyte serum that were treated with antagonistic P2X7 nanobody did not exhibit any proteinuria throughout the monitoring period, similar to the development in healthy Preimmune-serum-treated animals (graph = white triangle, parallel to baseline). Mice injected with anti-podocyte serum that had been administered the placebo dummy nanobody (represented by white circle) showed first detectable proteinuria from day 8 forth and exhibited the highest increase in albuminuria within days 12 to 15, then reaching a moderate peak value that ranged significantly higher than proteinuria levels in preimmune-serum-treated and antagonist groups ( $p < 0.05$ ). Wildtype animals injected with anti-podocyte serum that received the agonistic P2X7 nanobody (represented by white square) developed the

## Results

most severe proteinuria, with levels significantly higher than in WT dummy animals injected with anti-podocyte serum, antagonist and preimmune-serum-treated groups ( $p < 0,05$ ). The onset of proteinuria was very early, with first detectable values from day 1 forth. The incline of the curve was steady, with enhanced augmentation between days 6 and 9 and days 12 and 15.

Preimmune-serum-treated wildtype mice that had been administered either saline or agonistic P2X7 nanobody stayed free of proteinuria throughout the monitoring course. This observation was similarly made in wildtype animals that been administered anti-podocyte serum but that were treated with nanobodies antagonizing the pro-inflammatory P2X7 receptor. This finding indicated an effective, anti-inflammatory and renoprotective impact of the agent. Wildtype mice injected with anti-podocyte serum and treated with ineffective dummy nanobody exhibited moderate proteinuria, with a rather late onset around day 8 and a very gentle augmentation of the graph. Earliest and most significant proteinuria was denoted among wildtype mice injected with anti-podocyte serum that had been administered agonistic P2X7 nanobodies. These findings suggest a pro-inflammatory, noxious role of the P2X7 receptor in the context of GN development, just as the therapeutic potential of inhibiting it. Overall proteinuria levels remained low among this experimental mouse set compared to the P2X7 KO and UCH-L1 KO involving sets. This finding is probably due to the young age of the wildtype mice enrolled in the experiment.

### 4.5.2. IL-6 serum levels

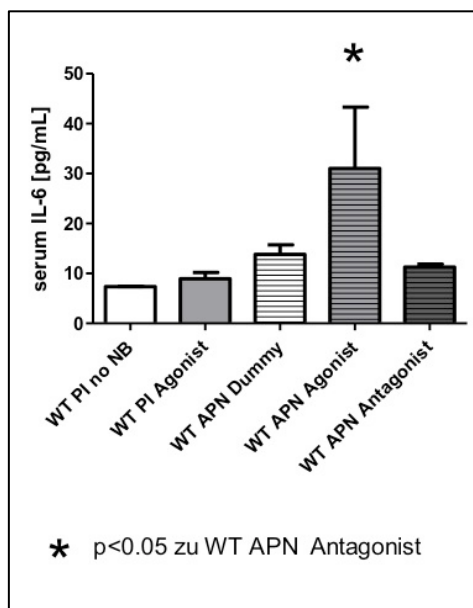


*Figure 47: WT APN mice treated with P2X7 agonistic nanobodies exhibit highest IL-6 serum levels, 14d past anti-podocyte serum injection. IL-6 serum levels (pg/mL) in nanobody experiment mice. IL-6 levels obtained via ELISA from serum samples collected on the day of sacrifice in all mice of all treatment groups. Values are expressed as mean  $\pm$  SEM. Statistical significance was calculated using the Mann-Whitney-U-test. A  $p$ -value  $< 0.05$  was accepted statistically significant.*

IL-6 was considered a surrogate parameter for P2X7 activation and had proven a suitable measurement parameter to assess the severity of renal inflammation after the onset of anti-podocyte nephritis in animal sets involving P2X7 KO and UCH-L1 KO mice (see above). It was

therefore measured similarly in wildtype mice treated with nanobodies in addition to preimmune and anti-podocyte serum injection.

IL-6 levels measured among the 5 different mouse groups largely corresponded to the observations made via albuminuria assessment (Figure 47).

## Results

---

Preimmune-serum treated wildtype mice, either injected with saline or agonistic P2X7 NB, had normal IL-6 serum levels. Values assessed in sera of wildtype animals that had received anti-podocyte serum and were treated with P2X7 antagonist ranged in the same healthy level. This finding was similarly made in wildtype conspecifics injected with anti-podocyte serum, that had received the dummy NB. This observation did not correspond to the development of proteinuria and hence apparent kidney damage found in albuminuria measurement (Figure 46).

Coinciding with the early and severe proteinuria detected in this group, WT anti-podocyte serum treated agonist mice exhibited highest IL-6 levels and a significant increase when comparing to WT anti-podocyte serum treated antagonist mice values ( $p < 0,05$ ).

## 5. Discussion

The aim of this thesis was to investigate the respective roles of UCH-L1 and the P2X7 receptor in the glomerulonephritic kidney, with particular focus on podocytes. A de novo expression of the Ubiquitin C-terminal Hydrolase L1 has been shown to occur in podocytes in several entities of human glomerulopathy associated with foot process effacement, such as FSGS or LN (Meyer-Schwesinger et al 2008; Liu et al. 2008). It to date remains elusive whether this new expression of the hydrolase in diseased podocytes embodies a protective mechanism to shield the cell against glomerulonephritic injury, or whether it enhances podocyte damage. UCH-L1 activity has recently been identified to induce polyubiquitin accumulation in podocytes and increase proteinuria in a rat model of membranous nephropathy (Meyer-Schwesinger et al. 2011). However, the nature of its role in the diseased podocyte remains equivocal, hitherto existing findings giving indication rendering both renoprotective and noxious capacities of the enzyme possible.

Ubiquitin C-terminal Hydrolase L1 is a protein potently expressed throughout the nervous system and has been shown to interact with P2X receptors in neurons (Manago et al., 2005). As published by Turner et al. (Turner, Tam et al., 2007), the P2X7 receptor promotes renal inflammation in human and rodent forms of GN, just as its deficiency or therapeutic antagonization has been shown to attenuate glomerulonephritic kidney injury (Taylor, Turner et al., 2009). P2X7 is assumed to exert malevolent effects on the diseased kidney, promoting severe inflammation (Turner, Tam et al., 2007; Vonend, Turner et al. 2004).

In this present work, we approached the hypothesis that UCH-L1 and P2X7, both having separately been identified to play a role in the pathogenesis of GN, might possibly interact in the inflamed kidney, as described in the nervous system.

The anti-podocyte-nephritis (APN) model was used to induce experimental GN in mice. UCH-L1 and P2X7 KO animals were involved in the study and respectively compared to wildtype conspecifics, to monitor possibly altered disease courses in mice lacking either the Ubiquitin C-terminal Hydrolase L1 or the P2X7 receptor.

### 5.1. UCH-L1 KO mice are more vulnerable towards APN.

To gain insight into the function of UCH-L1 in the onset and development of glomerulonephritis, anti-podocyte nephritis was induced in mice lacking the Ubiquitin C-terminal Hydrolase L1. Severity of disease observed among these animals was compared to the situation found in mice heterozygous for UCH-L1, that had similarly been injected with the anti-podocyte serum. Mice representing both genotypes

treated with pre-immune PI serum served as internal controls. Evaluation of clinical parameters measured in this first experiment indicated UCH-L1 deficiency to expose the mouse kidney to enhanced vulnerability towards glomerulonephritic injury. General health condition among UCH-L1 KO mice injected with anti-podocyte serum rapidly deteriorated following the induction of APN. UCH-L1 KO AP-serum treated animals exhibited a poor overall survival throughout the 14-day-monitoring period compared to heterozygous AP-serum treated controls (Fig.10).

UCH-L1 KO animals injected with AP-serum also expressed significantly higher levels of albuminuria and showed the serum parameter constellation pathognomonic for a nephrotic syndrome (Fig.11-13). Assessment of proinflammatory cytokines, such as MCP-1, IL-1 $\beta$  and IL-6, on both mRNA and protein levels, accounted for severe inflammation in UCH-L1 KO AP-serum treated mice (Fig.30-34).

Concluding from the aggravated disease condition observed among mice lacking the Ubiquitin C-terminal Hydrolase L1, UCH-L1 was, in the context of this study, considered a protector against GN, whose absence drastically increased vulnerability of experimental subjects towards the onset of glomerulonephritis. This conclusion is discrepant to the findings observed in a recent study by Meyer-Schwesinger et al. (Meyer-Schwesinger et al., 2011), where the pharmacologic inhibition of UCH-L1 resulted in decreased proteinuria and preserved Ubiquitin-proteasome-system (UPS) function in a rat model of membranous nephropathy (MN), passive Heymann-nephritis (PHN). Vice versa, increased UCH-L1 expression in diseased podocytes after the onset of PHN caused UPS impairment, the noxious formation of durable podocytic polyubiquitin aggregates and consequentially high levels of albuminuria. Nevertheless, comparing the two works one has to consider the difference in systemic consequence between pharmacologic inhibition of UCH-L1 on the one hand and ubiquitous knockout of the hydrolase on the other hand. Although UCH-L1 KO mice show normal development and weight at birth, these mice develop a severe neurological phenotype at 6-8 weeks of age. Their UPS function and systemic reactivity in response to disease could be declined. One also has to regard the typical differences in UCH-L1 expression in rats versus mice as well as the pathophysiologic differences in the APN and PHN disease models.

In an earlier publication by Meyer-Schwesinger et al., UCH-L1 overexpression in podocyte culture had been shown to compromise cellular differentiation and integrity, with inhibitory effects on the proteasome and the formation of polyubiquitin aggregates. The published de novo expression of UCH-L1 in the diseased podocyte of the rat (Meyer-Schwesinger et al., 2009; Liu et al., 2009) was similarly observed in murine podocytes in the present study. While control kidney sections did not show any UCH-L1-positive staining patterns by immunohistochemistry, podocytes in glomeruli of mice treated with AP-serum exhibited marked immunopositivity for the hydrolase (Fig.36). Significantly upregulated levels of UCH-L1 in wildtype mice treated with AP-serum compared to WT PI-serum-treated littermates were also detected on protein and mRNA levels in Western Blot and qPCR experiments of

whole kidney lysates (Fig.37,39). These findings confirmed the enhancement of UCH-L1 expression in diseased kidneys and podocytes. However, its causality remains elusive. It stays questionable whether the observed UCH-L1 upregulation and activity in the diseased podocyte protects the cell from the negative effects of damaged protein aggregation occurring during glomerulonephritic injury, or whether it itself leads to disease aggravation via polyubiquitin accumulation and proteasome inhibition.

Enhanced susceptibility of UCH-L1 KO mice towards anti-podocyte nephritis formation as witnessed in the present study could possibly be due to several pathognomonic phenomena observed distinctively among animals of this genotype in response to GN induction. Three of these are discussed in the following section:

#### **5.1.1. UCH-L1 KO mice treated with anti-podocyte serum exhibit podocytopenia.**

Mice lacking UCH-L1 exhibited serious podocytopenia after AP-serum treatment, which significantly exceeded podocyte loss measured among WT mice (Fig.20,21). This characteristic finding observed in mice lacking UCH-L1 was suggestive of a podocyte-protective function of the hydrolase in the context of GN. Podocyte number is considered a critical determinant for the development of glomerulosclerosis and a decrease in podocyte number has been found to lead to progressive renal failure (Mundel and Shankland 2002). Interestingly, podocyte counts were also profoundly lowered among UCH-L1 deficient mice treated with PI-serum compared to wildtype mice treated with PI-serum (Fig.20). This finding was unexpected, since according to the given literature on renal UCH-L1 expression, the hydrolase is not expressed in podocytes of healthy glomeruli (Shirato, Asanuma et al. 2000). Immunohistochemical studies demonstrated UCH-L1 expression in tubular epithelial cells, collecting duct cells, and parietal epithelial cells (Shirato, Asanuma et al. 2000; Diomedi-Camassei, Rava et al. 2005). It is thought that, in these cell types, UCH-L1 contributes to nephrogenesis, cell differentiation, and the regulation of the cell cycle (Debigare, Price et al. 2003; Franch 2002). During nephrogenesis of the rat kidney, UCH-L1 has been found to be diffusely expressed in progenitors of parietal epithelial cells. In contrast, UCH-L1 expression decreases in cells that later develop into podocytes. In the mature glomerulus of the rat, parietal epithelial cells exhibit UCH-L1, whereas podocytes are negative. In podocyte culture, differentiation into an arborized cell is accompanied by down-regulation of UCH-L1 and monoubiquitin, and functional inhibition of UCH-L1 leads to increased process formation (Meyer-Schwesinger et al., 2008). Recent studies were able to show that injury-activated podocytes possess the capability to de-differentiate, re-enter the cell cycle and compensatorily proliferate in response to certain glomerular diseases (Barisoni, Kriz et al. 1999; Moeller, Soofi et al. 2004; Griffin, Krofft et al. 2005). In various forms of GN, the onset of proteinuria is closely linked to podocyte damage and the detachment of podocytes from the GBM, resulting in urinary podocyte loss (Yu,

Petermann et al. 2005).

Yu et al. (Yu, Petermann et al. 2005) could show that podocyuria might provide clinically relevant information on disease activity in rodent models of acute glomerular disease. Counterintuitively, in this study, urinary podocyte loss was not accompanied by a reduction in the number of glomerular podocytes. Yu et al. concluded that initial podocyte loss could possibly act as a repair stimulus in surviving glomerular podocytes. By thus triggered cell division, they might cover the cellular gaps resulting from initial podocyte loss.

In response to injury, podocytes may undergo several cell fates, which include proliferation, de-differentiation and hypertrophy. Cell cycle regulators, e.g. cyclin-dependent kinase 5 (CDK5) or the mitotic cycle-activating enzyme p27, are components of the protein apparatus coordinating the podocyte's growth and cell cycle and are hence thought to play a major role in diseased podocytes (Petermann, Pippin et al. 2003; Srivastava, Garola et al. 2006; Mashall and Shankland, 2007; Griffin, Hiromura et al., 2004; Griffin, Krofft et al. 2005; Hiromura, Haseley et al. 2001; Shankland, Eitner et al. 2000). UCH-L1 has been reported to play an important role in regulating p27 degradation (Caballero, Resto et al. 2002). Therefore, it could be speculated that the upregulation of UCH-L1 in damaged podocytes may be a cellular reaction to immune injury, promoting the degradation of p27 and supporting regenerative endeavours of the podocyte.

Present research on UCH-L1 focuses on its activity within the ubiquitin–proteasome pathway and other ubiquitin-involving pathways, which enables it to modify the function and control the quantity of targeted proteins in normal cells (Wilkinson, Lee et al. 1989). Research on UCH-L1 and its possible involvement in the pathogenesis of certain diseases, e.g. in neurologic maladies like Parkinson's or Alzheimer's disease (Lowe, McDermott et al. 1990; Choi, Levey et al. 2004; Gong, Cao et al. 2009) or in various tumor entities, such as non-small-cell lung cancer (Hibi, Westra et al. 1999; Seliger, Fedorushchenko et al. 2007; Liu, Lashuel et al. 2003; Seliger, Fedorushchenko et al. 2007) suggests that there might exist a relationship between UCH-L1 expression and cellular proliferation, particularly in disease conditions. A knockout of the hydrolase might hence embody a threat to the cellular proliferation and regeneration apparatus, possibly provoking tissue damage and impaired organ function and, in the context of GN, promote podocytopenia.

Further possible fates met by podocytes in response to glomerulonephritic injury are apoptosis and necrosis. A major hypothesis to be investigated in this study was the possible existence of a relationship between UCH-L1 and the pro-apoptotic P2X7 receptor in the glomerulonephritic kidney, particularly in podocytes. A such relationship had already been demonstrated in the nervous system by Manago et al., where UCH-L1 stimulates ATP-induced currents through P2X receptors in neurons (Manago et al., 2005). The distinct causal mechanisms, just as the importance of this stimulation, to date remain elusive. Whereas Manago et al. reported cooperativeness between P2X7 and UCH-L1 in neurons, in the present study it was hypothesized

that, in the diseased podocyte, UCH-L1 inhibits P2X7 to protect the cell from the inflammatory damage and apoptotic cell death promoted by P2X7 activation. This hypothesis was based on the published literature on UCH-L1 and P2X7 in GN and on the results obtained in this study. An upregulation of P2X7 has been reported to occur in the glomerulonephritic kidney in various publications (Turner, Tam et al. 2007; Vonend, Turner et al. 2004), just as it has been shown in this present work (Fig.35,40). It is generally accepted that stimulation of the P2X7 receptor after exposure to ATP leads to apoptosis in a variety cell types, including macrophages or mesangial cells (Harada, Chan et al., 2004). The upregulation of P2X7 mRNA and protein in the glomerulonephritic mouse kidney has been published to coincide with increased mRNA levels of the pro-apoptotic p53 and bax genes and increased numbers of apoptotic cells in diseased glomeruli, revealed via immunohistochemistry against Caspase-3 and TUNEL-assay in a murine model of ANTN (Turner, Tam et al., 2007). A co-localization of immunoreactivity against P2X7 and Caspase-3 could be detected in wildtype mouse glomeruli, including their podocytes, past nephritis induction.

An increased expression and activity of the P2X7 receptor might hence contribute to the increased apoptosis rates among glomerular cells, e.g. podocytes, following GN induction. Levels of P2X7 protein and mRNA measured among UCH-L1 KO mice treated with AP-serum in this study significantly exceeded the upregulated levels seen in control mice treated with AP-serum. One could thus assume that UCH-L1 KO animals concomitantly suffer from increased apoptotic cell loss, which would plausibly, among other cell types such as mesangial cells, affect podocytes. An excessive activation and expression of the pro-apoptotic P2X7 could accordingly account for the increased podocytopenia observed in UCH-L1 KO APN mice.

### **5.1.2. UCH-L1 KO mice treated with anti-podocyte serum develop severe proteinuria.**

A further occurrence observed notably among UCH-L1 KO mice in response to treatment with AP serum was the development of severe proteinuria. The onset of proteinuria was significantly earlier in UCH-L1 KO animals than in WT mice and its degree drastically exceeded the extent of proteinuria in WT conspecifics (Fig.13,17). Many proteinuric glomerular diseases share podocyte injury as their key element, characterized by alterations in the molecular composition of the slit diaphragm or by reorganization of the foot process structure with fusion of filtration slits. The podocyte slit diaphragm is a delicate extracellular protein structure that requires constant renewal. Podocytes can retract and reform their foot processes in response to several cellular stresses (Endlich, Kriz et al. 2001). These dynamics require a tightly regulated interplay of signaling adaptors that orchestrate the tight regulation of protein trafficking and turnover, which is regulated by the Ubiquitin-Proteasome-System. The knockout of UCH-L1 as a deubiquinating enzyme and member of the

UPS could possibly lead to an impairment of this apparatus. In a study on slit diaphragm turnover in podocytes and proteinuria published in 2010, Tossidou, Teng et al. examined a mechanism of nephrin endocytosis via CIN85/Ruk(L)-mediated ubiquitination (Tossidou, Teng et al. 2010). They demonstrated that the loss of nephrin expression and the onset of proteinuria in CD2AP(-/-) mice involved in their study correlated with an increased accumulation of ubiquitinated proteins and expression of CIN85/Ruk(L) in podocytes. They were able to show that, in cultured murine podocytes, CD2AP deficiency leads to an early ubiquitination of nephrin and podocin after stimulation with fibroblast growth factor-4. They detected an increase of ubiquitin- and CIN85/Ruk(L) positive podocytes in diseased CD2AP(-/-) mice that correlated with the beginning of proteinuria. Furthermore, they could show an accumulation of ubiquitinated proteins in diseased kidneys of CD2AP(-/-) mice and in cultured CD2AP(-/-) podocytes. These findings were consistent with the work published by Meyer-Schwesinger et al. (Meyer-Schwesinger, Meyer et al. 2009) where an increase in podocytic UCH-L1 and ubiquitin content was demonstrated in a subset of glomerulopathies that correlated with an internalization of nephrin and podocin. These studies support the hypothesis that the activated UPS might be a contributor to glomerulopathies with proteinuria via an increased ubiquitination of nephrin and podocin.

UCH-L1 is a deubiquitinating enzyme holding the capability to deubiquitinate and recycle once degradation-doomed proteins. Cell surface transmembrane molecules are primarily ubiquitinated, which alters their subcellular localization or targets them for degradation. It has been hypothesized that the increased ubiquitination of nephrin and podocin may destabilize the slit diaphragm. UCH-L1 KO mice lack the enzymatic capacity to revise or reengineer the potential damages caused by the constant ubiquitination of proteins and their accumulation. A progressive destabilization of the slit diaphragm via the ubiquitination of nephrin and podocin might hence contribute to the severe proteinuria observed among mice lacking UCH-L1 in this present study (Fig.13,17).

### **5.1.3. UCH-L1 KO mice treated with anti-podocyte serum show severe glomerular damage and enhanced inflammatory response.**

Another phenomenon observed among UCH-L1 KO mice during APN was severe glomerular damage, as histologically evaluated in PAS-stained kidney sections (Fig.18,19). Assessment of proinflammatory cytokines, such as MCP-1, IL-1 $\beta$  and IL-6, on both mRNA and protein levels, accounted for excessive inflammation contributing to the observed glomerular damage in these mice (Fig.30-34). The extent of both glomerular damage and inflammatory response in UCH-L1 KO AP-serum treated mice exceeded those seen in WT AP-serum treated animals (Fig.18,19,22-25).

A further hypothesis on a possible role for UCH-L1 in the glomerulonephritic kidney

to be investigated in this thesis was that the hydrolase protects the podocyte via an attenuation of the proinflammatory P2X7 receptor. Manago et al. showed a potentiation of ATP-induced currents through P2X receptors mediated by UCH-L1 in neuronal cells. In UCH-L1 transfected PC12-cells, they found a stimulation of P2X receptors by UCH-L1 via the upregulation of monoubiquitin and the activation of Protein kinase A (PKA) and Calcium/Calmodulin Protein kinase II (CaMKII). The distinct causal mechanisms accounting for this stimulation remain elusive. Manago et al. assumed that PKA activation might lead to P2X receptor phosphorylation and activation. CaMKII has been proven to promote the trafficking of P2X receptors. The possible relationship between UCH-L1 and P2X receptors suggested by Manago et al. would exhibit a collaborative character as to which UCH-L1 stimulates P2X receptors. In contrast, we opposingly hypothesized that, in the diseased podocyte, UCH-L1 inhibits P2X7 to protect the cell from inflammatory damage and apoptosis promoted by P2X7 activation. Both UCH-L1 and the proinflammatory P2X7 receptor are upregulated in the glomerulonephritic kidney. The effects of UCH-L1 upregulation in the inflamed kidney remain questionable, but present data offers to hypothesize both benevolent and deleterious roles. In the APN model used in this study, UCH-L1 KO mice clearly exhibited increased vulnerability towards nephritis induction (Fig.10-14), which led to the possible conclusion of a protective function for the hydrolase. P2X7 activity has been shown to aggravate renal inflammation. The linkage of these findings against the background of a hypothetical interaction of the two molecules in the diseased kidney led to the hypothesis that UCH-L1 inhibits P2X7 and therefore protects against glomerular inflammation. However, this hypothesis does not necessarily dissent the findings by Manago et al., since the experimental settings used in their study highly differed from the approach used in this thesis. While Manago et al. investigated the relationship of UCH-L1 and P2X receptors *in vitro* in a neuronal cell model mimicking the occurrences in neurons under healthy conditions, the APN model of GN embodies an *in vivo* experiment where a multitude of surrounding factors may alter molecular reciprocities. Furthermore, UCH-L1 function in podocytes seems to oppose its role in neurons. While in neuronal progenitor cells, *in vitro* experiments have shown UCH-L1 to enhance differentiation and promote neurogenesis (Sakurai, Aykawa et al., 2006), upregulation of the hydrolase has been observed in and might hence contribute to de-differentiation in podocytes *in vitro* (Meyer-Schwesinger, Meyer et al., 2009).

We detected significantly higher levels of P2X7 protein and mRNA in UCH-L1 KO mice than in wildtype conspecifics (Fig.38,40). We also found a strong upregulation of P2X7 to occur after the onset of anti-podocyte nephritis in UCH-L1 KO mice, which might act as an enhancer of the systemic inflammatory reaction induced by APN-serum injection in mice lacking UCH-L1 (Fig.38,40). This upregulation was stronger in UCH-L1 KO AP-serum treated mice than in equally treated WT conspecifics, where it was similarly observed at a milder degree. UCH-L1 KO mice treated with AP-serum in the present study exhibited most severe kidney damage when compared to wildtype and P2X7 KO conspecifics, as reflected e.g. in highest levels of

proteinuria (Fig.13,17). UCH-L1 KO APN-serum treated animals also exhibited strongest macrophage infiltration and correspondingly highest levels of MCP-1, IL-1 $\beta$  and IL-6 (Fig.22-25,30-34). Wildtype animals in contrast did not react as drastically to APN-serum injection, showing a milder inflammatory reaction. These findings offered the possible deduction that the excessive inflammatory reaction observed in UCH-L1 KO mice after the onset of APN might partly be due to excessive P2X7 activation. In the wildtype state, where renal inflammation was markedly present, but not as severe as in UCH-L1 deficient mice, UCH-L1 might exert attenuating effects on P2X7, buffering the occurrence of such severe inflammation. UCH-L1 expression might help the podocyte compensate and fight injuries occurring in the setting of immune-mediated glomerulonephritis. However, this conclusion needs to be tested in thorough further research.

The distinct function of UCH-L1 in the healthy and the diseased (e.g. glomerulonephritic) kidney to date remains unclear. The pathological features of injured podocytes include foot process effacement and slit diaphragm reorganization, which are closely linked to the development of proteinuria and glomerulosclerosis (Farquhar, Vernier et al. 1957). These pathologic podocytic changes have been observed in non-immunecomplex-mediated glomerular diseases, as minimal change disease (MCD), focal-segmental glomerulosclerosis (FSGS) or diabetic nephropathy (Chiang, Hawkins et al. 1988; Schiffer, Bitzer et al. 2001), and such severe damage to podocytes similarly occurs in immune-mediated forms of glomerulonephritis, as membranous nephropathy (mN), Lupus nephritis (LN) or IgA nephropathy (Kerjaschki and Neale, 1996; Trivedi, Zeier et al. 2009). UCH-L1 expression in podocytes could scarcely be detected in non-immunecomplex mediated GN entities, whereas it was noticeably increased in immunecomplex-mediated nephritis forms (Meyer-Schwesinger et al., 2008; Liu et al., 2008). It has been demonstrated in podocyte cell culture that treatment with TGF $\beta$ , TNF $\alpha$  and IL-1 $\beta$ , common cytokines involved in inflammatory reactions, could not promote significant UCH-L1 expression in the cells (Liu, Wu et al. 2008). Similar findings were observed in human neural cell lines (Sato and Kuroda, 2001).

However, in podocytes, cocultured with mesangial cells, that were exposed to anti thymocyte serum (ATS) with normal human serum, UCH-L1 expression was promptly increased (Liu, Wu et al., 2008). It had previously been reported that ATS may interact with antigens on the cell membrane of mesangial cells to form immunecomplexes. Subsequently, the serum complement system is activated to form the sublytic C5b-9 membrane attack complex (MAC), which has in vitro been shown to cause cellular immune injury (Yamamoto and Wilson, 1987). Since podocytes have Fc and C3 receptors on their cell surface, it is possible that immune complexes and sublytic complement compounds are stimulatory factors affecting podocytes in inflamed glomeruli (Akilesh, Huber et al. 2008; Kazatchkine, Fearon et al. 1982). Thereby, one could assume that the deposition of immune complexes may cause the induction of a podocyte's UCH-L1 expression in immune-mediated forms of GN. The upregulated UCH-L1 expression in immune-mediated GN might embody

a compensatory reaction of the podocyte in response to glomerular inflammation. Altogether, these results might support the hypothesis that immune complexes could stimulate podocytes to compensatorily regenerate (or even proliferate) in order to replace damaged and lost cells in immune-mediated GN entities. Thus, considering the enhancing effects of UCH-L1 expression on cell proliferation, as studied e.g. in the context of malignant tumors, one might assume the possibility of a relationship between a podocyte's UCH-L1 expression and its regenerative, possibly proliferative endeavours following immune complex-mediated stimulation.

#### **5.1.4. Systemic deficiency of UCH-L1 might contribute to the aggravated course of glomerulonephritis in UCH-L1 KO mice.**

Eventually, one also has to be aware of the fact that the UCH-L1 KO mice used in the present study have a complete systemic UCH-L1 deficiency, which is not restricted to the podocyte but involved all cell types throughout the organism. This deficiency is reflected in the neurologic impairment observed among UCH-L1 KO mice, accounting for a poor general condition of the CNS and a lack of coping mechanisms of the latter in states of systemic disease. Kidney development was normal among UCH-L1 deficient mice, as reflected in normal kidney weights and the absence of pathologic urine or serum parameters in PI-serum treated control animals.

Nevertheless, UCH-L1 expression and contribution to nephrogenesis has been detected in parietal epithelial cells of Bowman's capsules and tubular epithelia in human and rodent kidneys. A deficiency of the hydrolase in these cells might affect renal integrity and might consequentially have contributed to the aggravated renal disease condition observed in UCH-L1 KO APN mice in this study. Anti-podocyte nephritis should hence be induced and studied anew in mice lacking UCH-L1 exclusively in the podocyte. This approach would enable a distinct investigation of UCH-L1 function in the podocyte and offer the opportunity to reconsider its questionable benevolence or malevolence.

#### **5.2.P2X7 KO mice are protected against several renal inflammation.**

Given the finding that UCH-L1 seemed to act as a renoprotector in the context of APN, this study's second experimental model aimed at comparatively analyzing the effects of P2X7 in glomerulonephritic mice, before finally linking the obtained results and investigating a possible relationship of the two molecules in the APN model. For this purpose, animals lacking the P2X7 receptor were integrated into the APN induction course and compared to UCH-L1 KO and wildtype mice.

### **5.2.1. P2X7 KO animals exhibit attenuated disease.**

Evaluation of clinical parameters, i.e. body weight development, serum parameters and albuminuria, as well as histologic assessment of PAS-stained glomeruli, clearly indicated a significantly mitigated glomerulonephritis development in P2X7-deficient mice (Fig.14-19). P2X7 KO mice treated with AP-serum did not exhibit significant weight loss compared to PI-treated controls. Serum parameters distinctive for a nephrotic syndrome, i.e. serum triglycerides, and kidney retention parameters indicating severe impairment in renal function, i.e. BUN, were not significantly elevated in probes of P2X7 KO mice injected with AP-serum. Most impressively, proteinuria levels measured among P2X7 KO mice proved significantly lower than those observed in wildtype and UCH-L1 KO groups throughout the APN monitoring period. P2X7 KO mice exhibited a later and significantly milder elevation of urinary protein levels than WT and UCH-L1 KO animals of the same treatment group.

Proteinuria is considered a hallmark of podocyte injury (Kriz, Gretz et al. 1998; Pavenstaedt 2000) and its extent highly correlates with the severity of renal impairment in the context of GN. These clinical results were consistent with the observation of less severe histologic injury in specimens from P2X7 KO mice injected with AP-serum than seen in equally treated WT and UCH-L1 KO mouse kidney cross sections (Fig.18,19). Attenuated disease severity was also reflected in low interstitial macrophage infiltration as well as in lowest urinary MCP-1 levels and MCP-1 mRNA content in P2X7 KO versus WT control and UCH-L1 KO mice (Fig.22-25,30,31). The proinflammatory cytokines IL-1 $\beta$  and IL-6 were only marginally increased in AP-serum treated P2X7 KO mice compared to PI-serum treated littermates on both protein and mRNA levels and proved significantly lower than values measured among UCH-L1 KO and wildtype conspecifics (Fig.32-34).

In summa, clinical and inflammatory parameter assessment in P2X7-deficient mice injected with AP-serum exhibited an appreciable attenuation of the severity of glomerulonephritis compared to wildtype mice and conspecifics lacking UCH-L1. P2X7 KO mice evidently were protected from severe inflammation and kidney injury induced by anti-podocyte serum injection. Vice versa, these findings provided indication of a significant proinflammatory role for the P2X7 receptor in immune-mediated renal injury.

The results we obtained corresponded to observations published by Taylor et al., who found decreased urinary MCP-1 in P2X7 deficient mice after induction of accelerated nephrotoxic nephritis (ANTN) as well as reduced renal MCP-1 in WKY rats treated with the selective P2X7 antagonist A-438079 (Taylor et al. 2009). Other publications have reported reduced tissue MCP-1 production in an adjuvant-induced model of paw inflammation in P2X7 KO mice (Chessell et al., 2005). Accordingly, reduced MCP-1 production and reduced urinary excretion of the chemokine could be direct consequences of P2X7 receptor deficiency or secondarily be due to a decrease in IL-1  $\beta$  secretion due to a lack of the proinflammatory receptor.

### **5.2.2. P2X7 mRNA and protein are upregulated in renal inflammation.**

A previous study by Turner et al. addressed the noxiousness of the presence and upregulation of P2X7 in renal inflammation in wildtype mice (Turner, Tam et al. 2006). Turner et al. observed an upregulation of the P2X7 receptor in rodent models of GN as well as in human lupus-related GN compared to healthy controls. P2X7 receptor mRNA was increased in a rat model of proliferative GN, coinciding with the onset of proteinuria. An increase in IL-1 $\beta$  mRNA and in mRNA of the pro-apoptotic markers p53 and bax was furthermore observed, as well as an increased number of apoptotic cells in mouse glomeruli. Increased P2X7 receptor protein levels were detected in glomeruli of ANTN mice, partially due to infiltrating macrophages.

Immunohistochemical evaluation of biopsies of lupus nephritis (LN) patients revealed P2X7 receptor protein detectability in glomeruli and renal tubules whereas the receptor was not detectable in healthy control tissue.

In the present work, we similarly found P2X7 receptor protein and mRNA amounts to be increased in wildtype kidney tissue obtained from APN-serum treated mice, coinciding with increased IL-1 $\beta$  and MCP-1 levels and aggravated glomerular damage respectively (Fig.18,19,30-33,38,40). Immunohistochemistry staining against the P2X7 receptor proved to be challenging, since a broad palette of commercially available antibodies binds nonspecifically to smooth muscle cells, e.g. vascular smooth muscle cells, giving an overlay of positive staining patterns on any glomerular cross section endowed with small vessels. Staining attempts with the Alomone anti-P2X7 antibody used for Western blotting in various dilutions (Alomone Laboratories, Israel) procured an excessive ubiquitous staining of the respective glomerular cross section in WT and P2X7 KO mice. The mentioned antibody has been used for immunohistochemistry experiments and published in various studies focused on P2X receptor expression in smooth muscle cells (Vial, Evans et al. 2000; Lewis, Gitterman et al. 2000, Gitterman, Evans et al. 2000). Staining attempts using the Roche anti-P2X7 antibody applied in the study by Turner et al. in our case similarly procured false positive staining patterns on P2X7 KO mouse kidney sections. It hence remains questionable whether the deductions Turner et al. drew from their staining experiments – clearly visible P2X7 receptor immunoreactivity in the glomeruli of mice with accelerated nephrotoxic nephritis, patterns suggesting mesangial staining, apical membrane distal tubule staining, no co-localization with the podocyte nuclear protein WT-1, co-localization with CD68-positive infiltrating macrophages – may be considered unconditionally reliable.

In the present study, credible P2X7 immunohistochemistry staining was accomplished using a rabbit anti-mouse antibody generated by genetic immunization in the Koch-Nolte lab at University Medical Center, Hamburg (Adriouch et al., 2005). P2X7 KO sections used as negative control remained free of any remarkable immunopositivity, tubular staining artefacts that occurred sporadically were not regarded specific. When applied in a 1:400 dilution on an exemplary cross section, sections from healthy wildtype PI mice did not show any distinct P2X7 staining

patterns, while glomeruli of wildtype animals that had been treated with AP-serum exhibited immunopositive areas. P2X7 staining seemed glomeruli-specific, with dye distributed among podocytes, lining the glomerulus (Fig.35). The P2X7 immunohistochemistry results hence are consistent with an upregulation of the receptor in the glomerulonephritic kidney.

The findings made by Turner et al., similarly to the observations in P2X7 KO mice by Taylor et al. and the results obtained from our study, suggested that an upregulation in the renal expression of P2X7 could be an important mediator of inflammatory tissue injury in the pathogenesis of GN, for example via the regulation of proinflammatory cytokine production or through apoptotic cell loss.

P2X7 is constitutively expressed on the majority of cells of the immune system. In non-immune cells, inflammatory mediators may upregulate expression of P2X7. One example is the TNF $\alpha$ -mediated stimulation of glomerular mesangial expression of P2X7 mRNA (Harada, Chan et al 2000). Evidence has also been given for altered distribution of P2X7 in diseased tissues. In spite of no appreciable detectability of P2X7 in healthy kidney tissue, upregulated P2X7 receptor expression has been observed in the glomeruli of different rodent models of renal disease and in human LN (Turner, Tam et al. 2007). In a streptozotocin-induced murine diabetes model, increased P2X7 receptor expression was colocalized in glomerular podocytes (Vonend, Turner et al. 2004). An increased expression of the P2X7 receptor was also detected in rodent models of anti-glomerular basement antibody-mediated glomerulonephritis in intrinsic glomerular cells and infiltrating macrophages (Vonend, Turner et al. 2004; Turner, Tam et al. 2007). In a model of ureteric obstruction, diseased P2X7 KO mice exhibited a decreased macrophage infiltration, lower expression of TGF $\beta$ , and reduced tubular apoptosis (Goncalves, Gabrich et al. 2006).

Under healthy tissue conditions with low levels of extracellular ATP, activation of P2X7 is not easily feasible. However, in disease states, ATP concentration is likely to increase noticeably because of leakage from damaged cells and release from nucleotide-rich granules in platelets recruited to the site of tissue injury and damage (Beigi, Kobatake et al. 1999; Bodin and Burnstock, 2001). P2X7-stimulated cells may, once activated, themselves act as a source of ATP. ATP concentrations released at the cell surface of living cells can reach 100–200  $\mu$ M (Turner, Ramesh et al. 2004), embodying a sufficient stimulus for further P2X7 activation. Prolonged stimulation of P2X7 leads to cytolysis (Surprenant, Rassendren et al. 1996) and uncontrolled release of the P2X7-agonist ATP from the apoptotic cell, which could reach millimolar concentrations. Such abundant levels of extracellular ATP may trigger excessive P2X7 stimulation, resulting in the promotion of fulminant inflammation as well as apoptotic cell death.

There is also evidence that the activity of the P2X7 receptor itself is increased under inflammatory conditions, independent of ATP levels. An increase in protein expression under the influence of inflammatory cytokines or bacterial products

(Humphreys and Dubyak, 1998; Narcisse, Scemes et al. 2005) supports this hypothesis, just as a decrease in activation threshold of the receptor in conditions of hypoxia (Franke, Guenther et al., 2004; Wirkner, Fischer et al. 2004).

Concluding from hitherto existing research data and the results obtained in this study, the P2X7 receptor is significantly upregulated following glomerular injury, e.g. in podocytes. Although the exact function and regulation of the receptor in the context of GN remain unclear, its association with inflammatory cytokine release and cell death suggests that increased expression of P2X7 might be involved in the pathogenesis of glomerular cell injury.

### **5.3.P2X7 activation is altered in UCH-L1 KO mice.**

We hypothesized in this study that the ubiquitin C-terminal hydrolase L1, itself upregulated in expression in the glomerulonephritic kidney, might contribute to P2X7 regulation in renal cells, particularly podocytes. To approach this hypothesis, P2X7 expression and activity were investigated in wildtype compared to UCH-L1 KO and in healthy PI-treated compared to diseased APN-treated mice. P2X7 mRNA and protein levels were assessed and compared in kidney lysates of wildtype and UCH-L1 KO PI- and AP-serum treated animals. As indicators of P2X7 activity, two downstream axes affected by stimulation of the receptor were investigated: The “inflammasome axis”, centered around P2X7-mediated release of IL-1 $\beta$  and IL-6, thus around enhanced inflammatory response, and the “ADAM17 axis”, focused on the shedding activity of ADAM17 and its downstream effects on EGFR and proteins involved in the Notch1-pathway, such as HeyL. In particular, we chose to investigate mRNA and protein levels of ADAM17, mRNA and protein levels of EGFR and mRNA levels of HeyL, just as mRNA and protein levels of IL-1 $\beta$  and IL-6 as proinflammatory cytokines. MCP-1 levels in urine and mRNA content via qPCR were measured to further assess inflammatory response, although it remains elusive whether P2X7 itself promotes MCP-1 release or whether the chemokine is secondarily produced in response to IL-1 $\beta$  secretion.

#### **5.3.1. P2X7 protein and mRNA are upregulated in UCH-L1 KO mice.**

Western blotting revealed significantly higher levels of P2X7 protein in lysates prepared from UCH-L1 KO mouse kidneys compared to lysates from WT mice, independent of the treatment with PI or AP serum (Fig.38). A slight upregulation of P2X7 protein was observed when comparing lysates from UCH-L1 KO mice treated with AP serum versus UCH-L1 KO mice treated with PI serum. We had expected statistical significance at this junction since P2X7 protein had been assumed to be upregulated in injured compared to healthy tissues.

However, the finding of enhanced P2X7-expression in UCH-L1 KO mice does support the hypothesis of UCH-L1 exerting attenuating effects on the P2X7 receptor in the wildtype state. Whereas wildtype animals showed moderate levels of the protein, abundant amounts of P2X7 were detected in UCH-L1 KO lysates. Animals lacking UCH-L1 might fail to buffer excessive P2X7 expression and activity, which reflects in significantly higher P2X7 protein levels. qPCR for P2X7 showed the same tendency (Fig.40). Whereas wildtype kidneys, independent of the type of serum injected, exhibited moderate levels of P2X7 mRNA and showed a slight upregulation of P2X7 mRNA when comparing AP- to PI-serum treatment state, UCH-L1 KO mice exhibited stronger P2X7 mRNA expression and a significant 80-fold upregulation in the APN-serum treated state. The upregulation of P2X7 upon inflammatory tissue injury was hence approved by qPCR. This finding, too, speaks for an altered regulation of P2X7 in mice lacking UCH-L1 in the sense of an excessive activation, promoting inflammation after the onset of APN.

These results supported the hypothesis that the severe extent of disease observed in UCH-L1 KO AP-serum treated mice when compared to equally treated WT animals was partly due to an excessive P2X7 activation. In the wildtype state, where renal inflammation was markedly present, but not as severe as in UCH-L1 KO mice, UCH-L1 might attenuate or even inhibit the proinflammatory capacities of P2X7, buffering the formation of severe glomerulonephritic injury. A knockout of the hydrolase could hence liberate the P2X7 receptor and trigger an excessive proinflammatory activity.

### **5.3.2. The “inflammasome axis” seems overactive in UCH-L1 KO mice injected with anti-podocyte serum.**

Focusing on the “inflammasome axis”, indicative of P2X7 activity, procured results that again supported the hypothesis of UCH-L1-involvement in P2X7 regulation. Among the three mouse groups treated with AP-serum, UCH-L1 KO mice exhibited the highest levels of MCP-1 mRNA, urinary amounts and mRNA content of IL-1 $\beta$  and serum levels of IL-6 (Fig.30-34). P2X7 KO animals treated with AP-serum showed barely any upregulation of the inflammatory parameters, while wildtype mice expressed levels accounting for a fully pronounced nephritic state, that nevertheless were appreciably lower than the excessive cytokine levels measured in UCH-L1 KO specimens. UCH-L1 deficient mice develop an aggravated disease state, with an overactive “inflammasome axis” fortifying the inflammatory tissue damage induced by AP-serum administration. It is possible that excessive P2X7 expression, observed among UCH-L1 KO mice via Western blot and qPCR analysis, is, to a questionable extent, responsible for this occurrence.

### 5.3.3. ADAM17 expression is altered in P2X7 KO and UCH-L1 KO mice.

Looking at the “ADAM17 axis” revealed interesting results. It is generally accepted, and has been shown in T lymphocytes, that P2X7 activation will lead to cleavage of the ADAM17 propeptide and thus activate the protease (Jamieson, Snook et al. 1996; Gu, Bendall et al. 1998; Labasi, Petrushova et al. 2002). Our expectations when analyzing ADAM17 expression in the different mouse groups on the one hand included an upregulation of the protease in AP-serum treated compared to PI-serum treated wildtype and possibly UCH-L1 KO animals, since ADAM17 induction had been reported before in podocytes, proximal tubules, and peritubular capillaries in various human renal diseases, such as membranous nephropathy or FSGS (Melenhorst, Visser et al., 2009; Gutwein, Abel-Bakky et al., 2009).

UCH-L1 KO mice, having proved to express higher P2X7 protein and mRNA levels than wildtype conspecifics, possibly alongside with an altered P2X7 activation, were expected to show modified ADAM17 expression as well, potentially in the sense of an upregulation.

Then again, we hypothesized that P2X7 KO mice would exhibit a somehow altered ADAM17 activation, since P2X7 has been recognized to be an important activator of the sheddase. Both down- and upregulation of ADAM17 were considered possible. On the one hand, a downregulation of the enzyme is plausible by being a potential consequence of the absence of P2X7 as an activator of ADAM17, serving as a systemic signal that might indicate a decreased necessity for the sheddase. On the other hand, one could also imagine an upregulation of ADAM17 as a compensatory attempt to balance the reduced ADAM17 activity caused by the lack of P2X7. Western Blotting for mature and pro-ADAM17 interestingly revealed significantly higher protein levels of the sheddase in kidney lysates from PI-serum treated animals than in those of AP-serum treated littermates among wildtype and P2X7 KO animals (Fig.41). Among UCH-L1 KO animals, no variations were denoted when comparing PI- to AP-serum treated animals. Interestingly, kidney lysates of P2X7 KO mice treated with AP-serum contained significantly higher ADAM17 protein levels than lysates of equally treated WT or UCH-L1 KO mice. This finding was unexpected, P2X7 being understood to activate ADAM17. P2X7 KO animals were assumed to exhibit low levels of the mature sheddase protein, whereas higher ADAM17 proform levels would have been plausible. Concerning pro-ADAM17, P2X7 KO animals expressed levels similarly high as those observed among WT conspecifics. Solely UCH-L1 KO mice expressed lower levels of ADAM17, both mature and proform. However, this observation might still support the hypothesis of an altered P2X7 and hence altered ADAM17 regulation in UCH-L1 KO mice.

In contrast, qPCR for ADAM17 (Fig.42) revealed the expected upregulation of ADAM17 mRNA content in AP-serum treated kidneys of wildtype and P2X7 KO mice compared to PI-serum treated tissues. Again, P2X7 KO animals showed similar mRNA expression levels as wildtype mice. UCH-L1 KO mice anew exhibited a different ADAM17 expression – no alterations were seen between PI- and AP-serum treatment, but kidney preparations from UCH-L1 KO mice treated with either PI- or

AP-serum both contained as much ADAM17 mRNA as WT and P2X7 KO kidneys. ADAM17 activates the EGF (epidermal growth factor) receptor by processing its ligand, pro-transforming-growth-factor- $\beta$ , (TGF- $\beta$ ) to TGF- $\beta$  (Peschon, Slack et al., 1998). EGFR protein and mRNA levels were measured and compared among the different genotypes and treatment groups to gain insight on ADAM17 and hence P2X7 activity (Fig.43,44). The EGF receptor is a transmembrane receptor with intrinsic tyrosinkinase activity. An upregulation or mutation of EGFR has been shown to occur in various tumour entities, promoting uncontrolled proliferation of cancer cells. EGFR-specific tyrosinkinase-inhibitors contribute to targeted therapies, e.g. in the treatment of non-small-cell lung cancer (NSCLC) (Martinez-Navarro, Rabollo et al. 2011). In the kidney, the EGF-EGFR system plays an important role in mediating renal hypertrophy, where it may regulate cell growth and proliferation and mediate the actions of angiotensin II through transactivation of the EGFR. In a study by Advani, Wiggins et al. (Advani, Wiggins et al. 2011) that investigated the effects of EGFR tyrosine kinase inhibition in an experimental model of diabetic nephropathy characterized by angiotensin II dependent hypertension, it was found that inhibition of the tyrosine kinase activity of the EGFR attenuates kidney and glomerular enlargement in association with podocyte preservation and reduction in albuminuria in diabetes. Furthermore, signalling via EGFR has recently been found to potentially play a role in the pathogenesis of proliferative glomerulonephritis (Bollee, Flamant et al. 2011). Conditional deletion of the EGFR gene from murine podocytes has been shown to alleviate the severity of rapid progressive glomerulonephritis (RPGN), an immune-mediated proliferative glomerulopathy. Likewise, pharmacological blockade of EGFR has been found to improve the course of RPGN.

Western Blotting for EGFR showed upregulated receptor protein in kidney lysates from WT and P2X7 KO animals compared to preparations from PI-serum treated conspecifics. Interestingly, AP-serum treated P2X7 KO kidneys even contained significantly higher EGFR protein levels than similarly treated WT mouse tissues. Evaluation UCH-L1 KO kidney lysates interestingly showed a significant downregulation of EGFR protein levels when comparing AP-serum treated to PI-serum treated mouse specimen. However, results obtained from evaluation of EGFR Western blotting may solely be referred to as approximate hints, since material was limited (n=2 for all mouse groups). EGFR qPCR (Fig.44) revealed unexpected measures. WT and P2X7 KO animals expressed rather low amounts of EGFR mRNA. Tissues from WT mice treated with AP-serum contained significantly higher mRNA amounts than probes from PI-serum treated animals. P2X7 animals expressed similar amounts of EGFR mRNA in PI- and AP-serum treatment state, but amounts were significantly higher than those measured in WT PI and AP animals. UCH-L1 KO mice exhibited significantly higher expression than PI- or AP-serum treated animals of the other genotypes and showed a significant downregulation from PI- to AP-serum treatment state.

qPCR for HeyL (Fig.45), as representative of the Notch1 axis, revealed the same tendency observed in ADAM17 qPCR. There was an upregulation of HeyL mRNA content in kidneys of AP-serum treated wildtype and P2X7 KO mice compared to PI-

serum treated animals. Again, P2X7 KO mice showed similar mRNA expression levels as wildtype mice. UCH-L1 KO mice anew exhibited a difference in expression levels – no alterations were seen in HeyL mRNA content between PI- and AP-serum treatment, but kidney preparations from UCH-L1 KO mice treated with PI- and from those treated with AP-serum contained as much HeyL mRNA as WT and P2X7 KO kidneys treated with AP-serum.

In summa, investigation of the “ADAM17 axis” procured results supporting the thesis that UCH-L1 is involved in the regulation of P2X7 and its downstream associates. Evaluation of UCH-L1 KO mouse samples exhibited results that consistently differed from the findings observed in wildtype and P2X7 KO probes. ADAM17, EGFR and HeyL regulation somehow appeared “inert” in UCH-L1 deficient animals, as there was no alteration in the expression of the molecules in healthy PI compared to severely diseased APN animals. This observation could be indicative of an impaired or anyhow altered P2X7 activation in animals lacking UCH-L1. Vice versa, this would lead to the conclusion that UCH-L1 physiologically influences P2X7 activity. Looking at the “inflammasome axis”, UCH-L1 KO animals exhibited excessive inflammatory conditions, which could possibly be the result of an excessive P2X7 activity. Comparatively, the “ADAM17 axis” gave results accounting for an impaired, but not necessarily excessive P2X7 function, since there was no increased cleavage of the downstream associate molecules of P2X7 stimulation, such as ADAM17. Nevertheless, an excessive stimulation of P2X7 might finally result in impaired function of the receptor, which might tentatively explain the occurrences seen in UCH-L1 KO mice when examining both downstream axes of P2X7 activity.

Focusing on these two axes revealed significant differences in P2X7 expression and activity in UCH-L1 KO animals, speaking for an altered P2X7 regulation in these mice. The distinct nature of this alteration and its causality remain to be elucidated. It also remains unanswered how UCH-L1 affects P2X7 function in a wildtype state and whether the two molecules solely interact in disease states or whether their relation is constitutive in healthy tissues.

In any case, it still remains equivocal whether P2X7 and UCH-L1 do interact in the healthy or diseased kidney and the questionable nature and importance of a such interaction respectively stays elusive.

Advanced in vivo and in vitro studies, e.g. in podocyte culture applying transfection approaches, would have to follow to provide answers to these questions.

#### **5.4. Therapeutic antagonization of the P2X7 receptor attenuates the development of anti-podocyte nephritis.**

The proinflammatory P2X7 receptor is already considered a viable therapeutic target in inflammatory diseases, such as arthritis or chronic obstructive pulmonary disease, and P2X7 antagonists for the treatment of rheumatoid arthritis are currently being tested in phase II clinical trials (Keystone et al., 2011; Lucattelli, Cicko et al., 2011). The selective P2X7 antagonist A-438079 was experimentally shown an efficient treatment option in rodent model studies of pathological pain and Huntington's disease (Diaz-Hernandez et al., 2009; McGaraughty, Chu et al., 2007).

However, the distinct role of P2X7 and its therapeutic inhibition in the etiology of renal diseases such as GN to date remains elusive (Hillman, Burnstock et al., 2005). An increase in glomerular expression of the P2X7 receptor has been reported at mRNA and protein levels in a rodent model of immune complex-mediated GN as well as in renal biopsy tissue from lupus nephritis patients (Turner, Tam et al., 2007). P2X7-deficient mice were shown to be protected against severe inflammatory kidney injury, as published by Taylor et al. (Taylor, Turner et al., 2009) and as observed in this present study. Taylor et al. have furthermore reported that treatment with the selective P2X7 antagonist A-438079 prevented rats from the development of severe nephritis upon induction of experimental ANTN. A-438079-treated rats exhibited reduced glomerular macrophage infiltration and expressed markedly lower renal and urinary levels of the chemokine. This outcome, together with the findings in P2X7 KO mice published by Turner et al. and the results obtained in the present study, provided evidence that P2X7 antagonists might possibly possess the capability to attenuate the severity of glomerulonephritic disease, rendering P2X7 a potential therapeutic target in the abatement of GN.

To reinvestigate the therapeutic potential of P2X7 antagonization in the APN model of glomerulonephritis, we directed the P2X7 receptor by the means of anti-albumin VHH coupled P2X7 nanobodies. SdABs are attractive therapeutic tools characterized by their small size and a good in vivo tissue penetration (Wesolowski et al., 2009). Tandem cloning of P2X7 nanobodies to a single domain antibody against serum albumin increased the reagents' in vivo half-life, protecting them from renal elimination. P2X7 nanobodies hence were assumed suitable devices for therapeutically targeting the glomerulonephritic kidney.

In order to test the efficiency of P2X7 nanobodies in glomerulonephritic animals, APN was induced in a population of wildtype mice treated with three different nanobodies – a P2X7 agonist, a P2X7 antagonist and an ineffective “dummy” nanobody. PI-serum treated wildtype mice served as controls receiving the same nanobodies.

Unfavorably, due to availability and scheduling difficulties, mice enrolled in the experimental course described were rather young of age (4-6 weeks) and consequentially lightweight (average bodyweight 18 g). Maturation of murine kidneys is usually completed by 8-10 weeks (Okada, Yakubi et al. 2005) and thus might not have been sufficient in these animals. The results obtained from APN-induction in

these mice hence have to be considered an approximate hint of the expected occurrence in mature mice. To mimick the proinflammatory effects of P2X7 activity, one wildtype AP-serum treated mouse group was treated with a nanobody acting as P2X7 agonist. Those animals were compared with WT AP-serum treated mice treated with a P2X7 antagonist, that was expected to attenuate renal inflammation after the onset of APN. The ineffective “dummy” nanobody was administered to a third mouse group as internal control to obviate the eventuality of any endogenous per se effects of the application of nanobodies.

Albuminuria and IL-6 serum levels were chosen as parameters indicative of kidney damage and inflammatory response (Fig.46,47). Assessment of albuminuria levels revealed highest urinary protein levels in WT AP-serum treated mice treated with the P2X7 agonist nanobody. Proteinuria occurred earlier and was significantly higher in this group than among WT AP-serum treated animals treated with dummy NB, which served as a control group mimicking the untreated APN state. This finding could be due to aggravated inflammatory damage in the glomerulonephritic kidney as a consequence of P2X7 agonization. One WT AP-serum treated mouse that had received the agonistic NB deceased on day 12 past APN induction with high proteinuria. Apart from this animal, the AP-serum treated mouse group receiving the agonistic NB exhibited a relatively stable health condition throughout the 15 days of APN monitoring. This observation, too, might be due to the limited potency of AP-serum in the young litter involved in the nanobody experiment.

WT mice treated with AP-serum that had been injected the P2X7 antagonist did not exhibit any proteinuria or deterioration of their health condition throughout the monitoring period, which might argue for the potency of the antagonizing nanobody and hence emphasize the importance of P2X7 in inflammatory disease.

PI-serum treated animals of all treatment groups, independent of the particular nanobody administered, similarly remained free of proteinuria and did not exhibit any signs of health impairment throughout the monitoring course. Neither P2X7 inhibition, nor agonization of the receptor hence seemed to affect a healthy kidney or healthy organism respectively.

IL-6 serum level measurement in AP-serum treated WT mice treated with the P2X7 agonist corresponded to the high extent of albuminuria observed in this group, which was considered an indicator of inflammatory response in the context of glomerular injury (Fig.46,47). Sera from AP-serum treated WT mice treated with the agonist NB contained significantly higher IL-6 levels than measured in any other mouse group. Disappointingly, all other mouse groups, independent of PI- or AP-serum treatment, exhibited similar amounts of IL-6 in their sera. AP-serum treated WT mice that had been administered the “dummy” NB showed similar IL-6 levels as PI-serum treated WT mice treated with saline, accounting for an attenuated potency of the AP-serum in these mice, since APN induction was expected to launch a significant systemic inflammatory response, normally reflected in elevated IL-6 serum levels. This finding probably was due to the young age of the litter enrolled in this experiment. However, evidence was gained of the tendency of P2X7 agonist treatment enhancing renal injury while P2X7 antagonist administration appeared to attenuate APN development.

To reappraise this promising tendency, the above described nanobody experiment has to be repeated in a set of mature mice.

On an advanced level, P2X7 inhibition or stimulation via antagonistic or agonistic nanobodies could be applied in UCH-L1 KO mice, to gain further insight on the possible relationship between P2X7 and UCH-L1. As mentioned, we assumed that P2X7 activity is altered, possibly by being excessively stimulated, in UCH-L1 KO animals. UCH-L1 KO mice exhibit a significantly aggravated APN progression compared to wildtype and P2X7 KO conspecifics. One hence would anticipate that antagonizing the P2X7 receptor in UCH-L1 KO mice, e.g. by the means of an antagonistic nanobody, might possess the capability to attenuate the perniciously enhanced glomerulonephritic damage in UCH-L1 KO animals. It will be interesting to realize such an approach and the obtained results might provide further insight in a possible interaction between UCH-L1 and P2X7.

In summa, nanobodies seem to embody suitable devices for agonizing and antagonizing the P2X7 receptor in a model of glomerulonephritis. P2X7 antagonization seemed to hold therapeutic potential, as urinary albumin and IL-6 serum levels were not increased in mice treated with the nanobody after APN induction, whereas animals treated with the P2X7 agonist exhibited severe albuminuria. This tendency corresponds to the promising observations published before on the selective P2X7 antagonist A-438079, which proved capable to attenuate experimental GN, pathologic nociception and Huntington's disease in rodent models.

Further in vivo studies on P2X7 inhibition in the context of glomerulonephritis should follow to finally conclude a definite statement on the therapeutic potential of antagonizing P2X7 in inflammatory kidney disease.

## 6. Summary

The aim of this thesis was to explore a possible role for UCH-L1 and P2X7 in glomerulonephritis, particularly in podocytes, using the murine anti-podocyte nephritis model. APN was induced in UCH-L1 KO, P2X7 KO and wildtype mice and disease severity was compared among the genotypes to gain insight in the function of UCH-L1 and P2X7 in the glomerulonephritic kidney via evaluation of the occurrences in diseased mice lacking the respective molecule. First, the overall degree of kidney damage was assessed by monitoring clinical parameters such as proteinuria or the formation of a nephrotic syndrome. This approach revealed an aggravated disease condition in UCH-L1 KO mice, while P2X7 KO animals exhibited attenuated GN formation. WT mice showed a fully pronounced nephritic state, which was milder than in UCH-L1 KO animals but significantly more severe than observed among P2X7 KO conspecifics. Given this tendency, it was analyzed whether an altered activity of UCH-L1 and P2X7 might have contributed to the observed disease condition in the respective mouse group. WT mice showed an upregulation of both UCH-L1 and P2X7 after the onset of APN, accounting for a possible involvement of both molecules in either the abatement or enhancement of GN. UCH-L1 KO mice exhibited significant upregulation of P2X7, P2X7 KO animals showed significant upregulation of UCH-L1 respectively, and levels of increase proved significantly higher than in WT mice. To approach the question whether an altered P2X7 regulation contributed to the aggravated disease condition in UCH-L1 KO mice, P2X7 activity was comparatively assessed in all three genotypes via evaluation of downstream associate parameters of P2X7, including indicators of inflammatory response (IL-1 $\beta$ , IL-6 or MCP-1) and parameters linked to the activation of ADAM17 (ADAM17, EGFR or HeyL). Results obtained from evaluation of P2X7 activity in the different mouse groups gave evidence of a possibly altered P2X7 regulation in UCH-L1 KO mice, which exhibited abundant levels of inflammatory parameters and significantly altered in ADAM17 regulation from wildtype and P2X7 KO mice.

In summa, these observations support the hypothesis of UCH-L1 and P2X7 contributing to the pathogenesis of GN just as to the assumption that UCH-L1 and P2X7 interact in the context of GN, possibly via an attenuation of P2X7 activity by UCH-L1 in physiological conditions, which would explain the aggravated kidney injury observed in UCH-L1 KO APN animals. However, thorough further research is required to verify the given hypotheses.

Finally, the importance of P2X7 in renal inflammation was evaluated by testing the therapeutic potential of P2X7 inhibition in the APN model. Single-domain antibodies (nanobodies), were applied as potential therapeutic agents and the effects of nanobody-mediated antagonization or agonization of P2X7 in WT mice after APN induction were investigated. Results indicated enhanced kidney injury in mice treated with the P2X7 agonist, while animals that had been treated with the P2X7 antagonistic nanobody showed attenuated disease parameters. This promising tendency should encourage further experimental application of P2X7 nanobodies in GN models.

## 7. List of abbreviations

AB	Antibody
ADAM17	A Disintegrin And Metalloproteinase 17
ANCA	Anti-Neutrophil Cytoplasmic Antibody
ANTN	Accelerated NephroToxic Nephritis
AP	Alkaline Phosphatase
AP-serum	Anti-Podocyte serum
APN	Anti-Podocyte Nephritis
ATP	Adenosine-5'-triphosphate
ATS	Anti-Thymocyte Serum
BSA	Bovine Serum Albumin
BUN	Blood Urea Nitrogen
BzATP	2'(3')-O-(4-Nezoyl-benzoyl)adenosin-5' triphosphat
BW	Body Weight
CD	Cluster of Differentiation - protocol for the identification of cell surface antigens present on white blood cells
CD2AP	CD2-associated protein
cDNA	complementary DNA
CKB	Chronic Kidney Disease
DAB	3,3'-Diaminobenzidine
DAPI	4',6-diamidino-2-phenylindole - fluorescent stain that binds strongly to A-T rich regions in DNA
DNA	Deoxyribonucleic acid
dNTP	Deoxynucleoside triphosphate
EDTA	Ethylenediaminetetraacetic acid

## List of abbreviations

---

EGFR	Epidermal Growth Factor Receptor
EGR-1	Early growth response protein 1 – mammalian transcription factor
ELISA	Enzyme-Linked ImmunoSorbent Assay
FITC	Fluorescein IsothioCyanate – fluorochrome
FSGS	Focal Segmental Glomerulosclerosis
GBM	Glomerular Basement Membrane
GFR	Glomerular Filtration Rate
GN	Glomerulonephritis
hcAB	heavy-chain Antibody
HRP	Horseradish-Peroxidase
ICE	IL-1beta Converting Enzyme
IHC	Immunohistochemistry
IL	Interleukin
K11/29/48/63	Lysine residues serving as points of polyubiquitylation
LDS	Lithium dodecyl sulfate
LN	Lupus Nephritis
LPS	Lipopolysaccharide
M-MLV	here: Reverse transcriptase from murine leukemia virus
MAC	Membrane Attack Complex
MCD	Minimal Change Disease
MCP-1	Monocyte Chemotactic Protein 1
MGN	membranous Glomerulonephritis
MN	membranous Nephropathy
monoUb	Monoubiquitin
MOPS	3-(N-morpholino)propanesulfonic acid

List of abbreviations

---

mRNA	messenger ribonucleic acid
N1IC	intracellular Notch1 fragment
NAD	Nicotinamide adenine dinucleotide
NALP3	NACHT, LRR and PYD domains-containing protein 3 – component of the inflammasome
NB	Nanobody
NTN	Nephrotoxic Nephritis
PAS	Periodic acid-Schiff
PBS	Phosphate-buffered Saline
PCNA	Proliferating Cell Nuclear Antigen
PCR	Polymerase Chain Reaction
PFA	Paraformaldehyde
PHN	passive Heymann-Nephritis
PI	Pre-Immune (serum)
PVDF	Polyvinylidene Fluoride
PYCARD	Apoptosis-associated speck-like protein containing a CARD – component of the inflammasome
PYD	Pyrin Domain – component of the inflammasome
qPCR	Quantitative real-time PCR
RT	Room Temperature
SA	Streptavidin
sdAB	single-domain Antibody
SDS	Sodium dodecyl sulfate
SLE	Systemic Lupus Erythematosus
TBS	Tris-buffered Saline
TBST	Tris-buffered Saline and Tween

List of abbreviations

---

TCR	T-cell receptor
TGF	Transforming Growth Factor
TLR	Toll-like Receptor
TMB	3,3',5,5'-Tetramethylbenzidine
TNF	Tumour Necrosis Factor
UBP	Ubiquitin specific protease
UCH	Ubiquitin C-terminal Hydrolase
UCH-L1	Ubiquitin C-terminal Hydrolase L1
UPS	Ubiquitin proteasome system
WB	Western Blot
WT	Wildtype
WT1	Wilms tumor protein 1
ZO-1	Zonula occludens 1 - Tight junction protein

## 8. List of references

- Adler, S., 1992. Characterization of glomerular epithelial cell matrix receptors. *The American Journal of Pathology*, 141(3), S.571-578.
- Adriouch, S. et al., 2005. Probing the expression and function of the P2X7 purinoceptor with antibodies raised by genetic immunization. *Cellular immunology*, 236(1-2), S.72–77.
- Advani, A. et al., 2011. Inhibition of the epidermal growth factor receptor preserves podocytes and attenuates albuminuria in experimental diabetic nephropathy. *Nephrology (Carlton, Vic.)*, 16(6), S.573-581.
- Akilesh, S. et al., 2008. Podocytes use FcRn to clear IgG from the glomerular basement membrane. *Proceedings of the National Academy of Sciences of the United States of America*, 105(3), S.967-972.
- Aswad, F. & Dennert, G., 2006. P2X7 receptor expression levels determine lethal effects of a purine based danger signal in T lymphocytes. *Cellular Immunology*, 243(1), S.58-65.
- Baricordi, O.R. et al., 1996. An ATP-activated channel is involved in mitogenic stimulation of human T lymphocytes. *Blood*, 87(2), S.682-690.
- Barisoni, L., Kriz, W, et al., 1999. The dysregulated podocyte phenotype: a novel concept in the pathogenesis of collapsing idiopathic focal segmental glomerulosclerosis and HIV-associated nephropathy. *Journal of the American Society of Nephrology: JASN*, 10(1), S.51-61.
- Basgen, J. & Nicholas, S., 2010. Comparison of Methods for Counting Podocyte Number in the Kidney. *Microscopy and Microanalysis*, 16(Supplement S2), S.1150–1151.
- Baumgart, A. et al., 2010. ADAM17 regulates epidermal growth factor receptor expression through the activation of Notch1 in non-small cell lung cancer. *Cancer Research*, 70(13), S.5368-5378.
- Beck, L.H., Jr et al., 2009. M-type phospholipase A2 receptor as target antigen in idiopathic membranous nephropathy. *The New England Journal of Medicine*, 361(1), S.11-21.
- Beigi, R. et al., 1999. Detection of local ATP release from activated platelets using cell surface-attached firefly luciferase. *The American Journal of Physiology*, 276(1 Pt 1), S.C267-278.

## List of references

---

- Berasain, C. et al., 2009. The epidermal growth factor receptor: a link between inflammation and liver cancer. *Experimental Biology and Medicine (Maywood, N.J.)*, 234(7), S.713-725.
- Betarbet, R., Sherer, T.B. & Greenamyre, J.T., 2005. Ubiquitin-proteasome system and Parkinson's diseases. *Experimental Neurology*, 191 Suppl 1, S.S17-27.
- Black, R.A., 2002. Tumor necrosis factor-alpha converting enzyme. *The international journal of biochemistry & cell biology*, 34(1), S.1-5.
- Blanchot-Jossic, F. et al., 2005. Up-regulated expression of ADAM17 in human colon carcinoma: co-expression with EGFR in neoplastic and endothelial cells. *The Journal of Pathology*, 207(2), S.156-163.
- Bodin, P. & Burnstock, G, 2001. Purinergic signalling: ATP release. *Neurochemical Research*, 26(8-9), S.959-969.
- Bollée, G. et al., 2011. Epidermal growth factor receptor promotes glomerular injury and renal failure in rapidly progressive crescentic glomerulonephritis. *Nature Medicine*, 17(10), S.1242-1250.
- Brou, C. et al., 2000. A novel proteolytic cleavage involved in Notch signaling: the role of the disintegrin-metalloprotease TACE. *Molecular Cell*, 5(2), S.207-216.
- Buisman, H.P. et al., 1988. Extracellular ATP induces a large nonselective conductance in macrophage plasma membranes. *Proceedings of the National Academy of Sciences of the United States of America*, 85(21), S.7988-7992.
- Caballero, O.L. et al., 2002. Interaction and colocalization of PGP9.5 with JAB1 and p27(Kip1). *Oncogene*, 21(19), S.3003-3010.
- Chadban, S.J. & Atkins, R.C., 2005. Glomerulonephritis. *Lancet*, 365(9473), S.1797-1806.
- Chessell, I.P. et al., 2005. Disruption of the P2X7 purinoceptor gene abolishes chronic inflammatory and neuropathic pain. *Pain*, 114(3), S.386-396.
- Chiang, M.L. et al., 1988. Diagnostic and prognostic significance of glomerular epithelial cell vacuolization and podocyte effacement in children with minimal lesion nephrotic syndrome and focal segmental glomerulosclerosis: an ultrastructural study. *Clinical Nephrology*, 30(1), S.8-14.
- Chiozzi, Paola et al., 1997. Spontaneous Cell Fusion in Macrophage Cultures Expressing High Levels of the P2Z/P2X7 Receptor. *The Journal of Cell Biology*, 138(3), S.697-706.

- Choi, J. et al., 2004. Oxidative modifications and down-regulation of ubiquitin carboxyl-terminal hydrolase L1 associated with idiopathic Parkinson's and Alzheimer's diseases. *The Journal of Biological Chemistry*, 279(13), S.13256-13264.
- Coffman, R.L., 1982. Surface antigen expression and immunoglobulin gene rearrangement during mouse pre-B cell development. *Immunological reviews*, 69, S.5–23.
- Collo, G et al., 1997. Tissue distribution of the P2X7 receptor. *Neuropharmacology*, 36(9), S.1277-1283.
- Cortez-Retamozo, V. u. a., 2002. Efficient tumor targeting by single-domain antibody fragments of camels. *International Journal of Cancer. Journal International Du Cancer*, 98(3), S.456-462.
- Couser, W G, 1999. Glomerulonephritis. *Lancet*, 353(9163), S.1509-1515.
- Danquah, Welbeck: Selection and characterization of llama-derived anti-P2X7 single domain antibodies. Dissertationsschrift, Universität Hamburg, 2012.
- Debigaré, R. & Price, S.R., 2003a. Proteolysis, the ubiquitin-proteasome system, and renal diseases. *American Journal of Physiology. Renal Physiology*, 285(1), S.F1-8.
- Debigaré, R. & Price, S.R., 2003b. Proteolysis, the ubiquitin-proteasome system, and renal diseases. *American Journal of Physiology. Renal Physiology*, 285(1), S.F1-8.
- Díaz-Hernández, M. et al., 2009. Altered P2X7-receptor level and function in mouse models of Huntington's disease and therapeutic efficacy of antagonist administration. *The FASEB Journal: Official Publication of the Federation of American Societies for Experimental Biology*, 23(6), S.1893-1906.
- Dietel, M., Suttorp, N. & Zeitz, M., 2008. *Harrisons Innere Medizin: Deutsche Ausgabe. In Zusammenarbeit mit der Charité, 3 Bände inkl. Registerband 17. Aufl.*, ABW Wissenschaftsverlag.
- Diomed-Camassei, F. et al., 2005. Protein gene product 9.5 and ubiquitin are expressed in metabolically active epithelial cells of normal and pathologic human kidney. *Nephrology, Dialysis, Transplantation: Official Publication of the European Dialysis and Transplant Association - European Renal Association*, 20(12), S.2714-2719.
- Dubyak, George R, 2003. Knock-out mice reveal tissue-specific roles of P2Y receptor subtypes in different epithelia. *Molecular Pharmacology*, 63(4), S.773-776.
- Dumoulin, M. u. a., 2003. A camelid antibody fragment inhibits the formation of amyloid fibrils by human lysozyme. *Nature*, 424(6950), S.783-788.

- Endlich, K., Kriz, W. & Witzgall, R., 2001. Update in podocyte biology. *Current Opinion in Nephrology and Hypertension*, 10(3), S.331-340.
- Engvall, E., Jonsson, K. & Perlmann, P., 1971. Enzyme-linked immunosorbent assay. II. Quantitative assay of protein antigen, immunoglobulin G, by means of enzyme-labelled antigen and antibody-coated tubes. *Biochimica et biophysica acta*, 251(3), S.427-434.
- Ermisch, B. & Schwechheimer, K., 1995. Protein gene product (PGP) 9.5 in diagnostic (neuro-) oncology. An immunomorphological study. *Clinical Neuropathology*, 14(3), S.130-136.
- Farguhar, M.G., Vernier, R.L. & Good, R.A., 1957. An electron microscope study of the glomerulus in nephrosis, glomerulonephritis, and lupus erythematosus. *The Journal of Experimental Medicine*, 106(5), S.649-660.
- Feldmann, M., 2002. Development of anti-TNF therapy for rheumatoid arthritis. *Nature Reviews. Immunology*, 2(5), S.364-371.
- Ferrari, D et al., 1997. Extracellular ATP triggers IL-1 beta release by activating the purinergic P2Z receptor of human macrophages. *Journal of Immunology (Baltimore, Md.: 1950)*, 159(3), S.1451-1458.
- Finley, D., Ciechanover, Aaron & Varshavsky, A., 2004. Ubiquitin as a central cellular regulator. *Cell*, 116(2 Suppl), S.S29-32, 2 p following S32.
- Fischer, K.G. et al., 2001. Extracellular nucleotides regulate cellular functions of podocytes in culture. *American Journal of Physiology. Renal Physiology*, 281(6), S.F1075-1081.
- Fleetwood, G. & Gordon, J.L., 1987. Purinoceptors in the rat heart. *British Journal of Pharmacology*, 90(1), S.219-227.
- Flotte, T.J., Springer, T.A. & Thorbecke, G.J., 1983. Dendritic cell and macrophage staining by monoclonal antibodies in tissue sections and epidermal sheets. *The American journal of pathology*, 111(1), S.112-124.
- Franch, H.A., 2002. Pathways of proteolysis affecting renal cell growth. *Current Opinion in Nephrology and Hypertension*, 11(4), S.445-450.
- Franke, H. et al., 2004. P2X7 receptor expression after ischemia in the cerebral cortex of rats. *Journal of Neuropathology and Experimental Neurology*, 63(7), S.686-699.
- Froldi, G. et al., 1997. P2X-purinoceptors in the heart: actions of ATP and UTP. *Life Sciences*, 60(17), S.1419-1430.

## List of references

---

- Garton, K.J., Gough, P.J. & Raines, E.W., 2006. Emerging roles for ectodomain shedding in the regulation of inflammatory responses. *Journal of Leukocyte Biology*, 79(6), S.1105-1116.
- Gitterman, D.P. & Evans, R.J., 2000. Properties of P2X and P2Y receptors are dependent on artery diameter in the rat mesenteric bed. *British Journal of Pharmacology*, 131(8), S.1561-1568.
- Gomori, G., 1952. The periodic-acid Schiff stain. *American journal of clinical pathology*, 22(3), S.277-281.
- Gonçalves, R.G. et al., 2006. The role of purinergic P2X7 receptors in the inflammation and fibrosis of unilateral ureteral obstruction in mice. *Kidney International*, 70(9), S.1599-1606.
- Gong, B. et al., 2006. Ubiquitin hydrolase Uch-L1 rescues beta-amyloid-induced decreases in synaptic function and contextual memory. *Cell*, 126(4), S.775-788.
- Gooz, M., 2010. ADAM-17: the enzyme that does it all. *Critical Reviews in Biochemistry and Molecular Biology*, 45(2), S.146-169.
- Griffin, S.V., Krofft, R.D., et al., 2005. Limitation of podocyte proliferation improves renal function in experimental crescentic glomerulonephritis. *Kidney International*, 67(3), S.977-986.
- Griffin, S.V. et al., 2005. Limitation of podocyte proliferation improves renal function in experimental crescentic glomerulonephritis. *Kidney International*, 67(3), S.977-986.
- Gu, B., Bendall, L.J. & Wiley, J.S., 1998. Adenosine triphosphate-induced shedding of CD23 and L-selectin (CD62L) from lymphocytes is mediated by the same receptor but different metalloproteases. *Blood*, 92(3), S.946-951.
- Gutwein, P. et al., 2009. CXCL16 Is Expressed in Podocytes and Acts as a Scavenger Receptor for Oxidized Low-Density Lipoprotein. *The American Journal of Pathology*, 174(6), S.2061-2072.
- Hamers-Casterman, C. u. a., 1993. Naturally occurring antibodies devoid of light chains. *Nature*, 363(6428), S.446-448.
- Harada, H et al., 2000. Induction of proliferation and apoptotic cell death via P2Y and P2X receptors, respectively, in rat glomerular mesangial cells. *Kidney International*, 57(3), S.949-958.
- Hershko, A. & Ciechanover, A., 1998. The ubiquitin system. *Annual Review of Biochemistry*, 67, S.425-479.

## List of references

---

- Hibi, K. et al., 1998. Serial analysis of gene expression in non-small cell lung cancer. *Cancer Research*, 58(24), S.5690-5694.
- Hibi, K. et al., 1999. PGP9.5 as a candidate tumor marker for non-small-cell lung cancer. *The American Journal of Pathology*, 155(3), S.711-715.
- Hicke, L., 2001. Protein regulation by monoubiquitin. *Nature Reviews. Molecular Cell Biology*, 2(3), S.195-201.
- Hickman, S.E. et al., 1994. P2Z adenosine triphosphate receptor activity in cultured human monocyte-derived macrophages. *Blood*, 84(8), S.2452-2456.
- Hillman, K.A., Burnstock, G & Unwin, R J, 2005. The P2X7 ATP receptor in the kidney: a matter of life or death? *Nephron. Experimental Nephrology*, 101(1), S.e24-30.
- Hiomura, K, Haseley, L.A., et al., 2001. Podocyte expression of the CDK-inhibitor p57 during development and disease. *Kidney International*, 60(6), S.2235-2246.
- Holzman, L.B. et al., 1999. Nephritin localizes to the slit pore of the glomerular epithelial cell. *Kidney International*, 56(4), S.1481-1491.
- Hughes, J.P., Hatcher, J.P. & Chessell, I.P., 2007. The role of P2X(7) in pain and inflammation. *Purinergic Signalling*, 3(1-2), S.163-169.
- Humphreys, B.D. & Dubyak, G R, 1998. Modulation of P2X7 nucleotide receptor expression by pro- and anti-inflammatory stimuli in THP-1 monocytes. *Journal of Leukocyte Biology*, 64(2), S.265-273.
- Jamieson, G.P. et al., 1996. Extracellular ATP causes loss of L-selectin from human lymphocytes via occupancy of P2Z purinoceptors. *Journal of Cellular Physiology*, 166(3), S.637-642.
- Kanellopoulos, J.M. u. a., 1983. Biosynthesis and molecular nature of the T3 antigen of human T lymphocytes. *The EMBO journal*, 2(10), S.1807-1814.
- Kawamura, H. et al., 2005. P2X7 receptor-dependent and -independent T cell death is induced by nicotinamide adenine dinucleotide. *Journal of Immunology (Baltimore, Md.: 1950)*, 174(4), S.1971-1979.
- Kerjaschki, D. & Neale, T.J., 1996. Molecular mechanisms of glomerular injury in rat experimental membranous nephropathy (Heymann nephritis). *Journal of the American Society of Nephrology: JASN*, 7(12), S.2518-2526.

- Keystone, E.C. et al., 2011. Clinical evaluation of the efficacy of the P2X7 purinergic receptor antagonist AZD9056 on the signs and symptoms of rheumatoid arthritis in patients with active disease despite treatment with methotrexate or sulphasalazine. *Annals of the Rheumatic Diseases*. Available at: <http://www.ncbi.nlm.nih.gov/pubmed/21406457> [Zugegriffen August 8, 2011].
- Kobayashi, N & Mundel, P, 1998. A role of microtubules during the formation of cell processes in neuronal and non-neuronal cells. *Cell and Tissue Research*, 291(2), S.163-174.
- Kobayashi, Naoto, 2002. Mechanism of the process formation; podocytes vs. neurons. *Microscopy Research and Technique*, 57(4), S.217-223.
- Kriz, W, Gretz, N. & Lemley, K.V., 1998. Progression of glomerular diseases: is the podocyte the culprit? *Kidney International*, 54(3), S.687-697.
- Kwon, J. et al., 2005. Ubiquitin C-terminal hydrolase L-1 is essential for the early apoptotic wave of germinal cells and for sperm quality control during spermatogenesis. *Biology of Reproduction*, 73(1), S.29-35.
- Labasi, J.M. et al., 2002. Absence of the P2X7 receptor alters leukocyte function and attenuates an inflammatory response. *Journal of Immunology (Baltimore, Md.: 1950)*, 168(12), S.6436-6445.
- Laeremans, Stortelers et al. 05.10.2011: European Patent EP2370465: GENETIC IMMUNIZATION FOR PRODUCING IMMUNOGLOBULINS AGAINST CELL-ASSOCIATED ANTIGENS SUCH AS P2X7, CXCR7 OR CXCR4
- Larsen, C.N., Krantz, B.A. & Wilkinson, K.D., 1998. Substrate specificity of deubiquitinating enzymes: ubiquitin C-terminal hydrolases. *Biochemistry*, 37(10), S.3358-3368.
- Leenen, P.J. u. a., 1994. Markers of mouse macrophage development detected by monoclonal antibodies. *Journal of immunological methods*, 174(1-2), S.5–19.
- Lewis, C.J., Gitterman, D.P., et al., 2000. Effects of diadenosine polyphosphates (Ap(n)As) and adenosine polyphospho guanosines (Ap(n)Gs) on rat mesenteric artery P2X receptor ion channels. *British Journal of Pharmacology*, 129(1), S.124-130.
- Li, C. et al., 2000. CD2AP is expressed with nephrin in developing podocytes and is found widely in mature kidney and elsewhere. *American Journal of Physiology. Renal Physiology*, 279(4), S.F785-792.
- Li, J. & Sinoway, L.I., 2002. ATP stimulates chemically sensitive and sensitizes mechanically sensitive afferents. *American Journal of Physiology. Heart and Circulatory Physiology*, 283(6), S.H2636-2643.

## List of references

---

- Liu, Yichin et al., 2002. The UCH-L1 gene encodes two opposing enzymatic activities that affect alpha-synuclein degradation and Parkinson's disease susceptibility. *Cell*, 111(2), S.209-218.
- Liu, Yichin et al., 2003. Discovery of inhibitors that elucidate the role of UCH-L1 activity in the H1299 lung cancer cell line. *Chemistry & Biology*, 10(9), S.837-846.
- Liu, Yuan, Wu, J., et al., 2009. UCH-L1 expression of podocytes in diseased glomeruli and in vitro. *The Journal of Pathology*, 217(5), S.642-653.
- Lowe, J. et al., 1990. Ubiquitin carboxyl-terminal hydrolase (PGP 9.5) is selectively present in ubiquitinated inclusion bodies characteristic of human neurodegenerative diseases. *The Journal of Pathology*, 161(2), S.153-160.
- Lucattelli, M. et al., 2011. P2X7 receptor signaling in the pathogenesis of smoke-induced lung inflammation and emphysema. *American Journal of Respiratory Cell and Molecular Biology*, 44(3), S.423-429.
- Lüllmann-Rauch, R. & Rauch, R.L.-, 2006. *Histologie. Verstehen - Lernen - Nachschlagen* 2. Aufl., Thieme, Stuttgart.
- Manago, Y. et al., 2005. Potentiation of ATP-induced currents due to the activation of P2X receptors by ubiquitin carboxy-terminal hydrolase L1. *Journal of Neurochemistry*, 92(5), S.1061-1072.
- Marshall, C.B. & Shankland, Stuart J, 2006. Cell cycle and glomerular disease: a minireview. *Nephron. Experimental Nephrology*, 102(2), S.e39-48.
- Marshall, C.B. & Shankland, S.J., 2007. Cell cycle regulatory proteins in podocyte health and disease. *Nephron. Experimental Nephrology*, 106(2), S.e51-59.
- Martínez-Navarro, E.M. et al., 2011. Epidermal growth factor receptor (EGFR) mutations in a series of non-small-cell lung cancer (NSCLC) patients and response rate to EGFR-specific tyrosine kinase inhibitors (TKIs). *Clinical & Translational Oncology: Official Publication of the Federation of Spanish Oncology Societies and of the National Cancer Institute of Mexico*, 13(11), S.812-818.
- McGaraughty, S. et al., 2007. P2X7-related modulation of pathological nociception in rats. *Neuroscience*, 146(4), S.1817-1828.
- Melenhorst, W.B. et al., 2009. ADAM17 upregulation in human renal disease: a role in modulating TGF-alpha availability? *American Journal of Physiology. Renal Physiology*, 297(3), S.F781-790.

## List of references

---

- Mehta, V.B., Hart, J. & Wewers, M.D., 2001. ATP-stimulated release of interleukin (IL)-1beta and IL-18 requires priming by lipopolysaccharide and is independent of caspase-1 cleavage. *The Journal of Biological Chemistry*, 276(6), S.3820-3826.
- Meyer-Schwesinger, C et al., 2009. A new role for the neuronal ubiquitin C-terminal hydrolase-L1 (UCH-L1) in podocyte process formation and podocyte injury in human glomerulopathies. *The Journal of Pathology*, 217(3), S.452-464.
- Meyer-Schwesinger, C. et al., 2011. Ubiquitin C-terminal hydrolase-L1 activity induces polyubiquitin accumulation in podocytes and increases proteinuria in rat membranous nephropathy. *The American Journal of Pathology*, 178(5), S.2044-2057.
- Meyer-Schwesinger, C., Dehde, S., Klug, P., Becker, J.U., Mathey, S., Arefi, K., Balabanov, S., Venz, S., Endlich, K.-H., Pekna, M., Gessner, J.E., Thaiss, F. & Meyer, T.N., 2011b. Nephrotic Syndrome and Subepithelial Deposits in a Mouse Model of Immune-Mediated Anti-Podocyte Glomerulonephritis. *Journal of Immunology*, Sep 15;187(6):3218-29.
- Miller, H.R., Avrameas, S. & Ternynck, T., 1973. Intracellular distribution of antibody in immunocytes responding to primary challenge with horseradish peroxidase. *The American journal of pathology*, 71(2), S.239–260.
- Moeller, M.J. et al., 2004. Podocytes populate cellular crescents in a murine model of inflammatory glomerulonephritis. *Journal of the American Society of Nephrology: JASN*, 15(1), S.61-67.
- Mullis, K.B., 1990. Target amplification for DNA analysis by the polymerase chain reaction. *Annales de biologie clinique*, 48(8), S.579–582.
- Mundel, P & Kriz, W, 1995. Structure and function of podocytes: an update. *Anatomy and Embryology*, 192(5), S.385-397.
- Mundel, Peter & Shankland, Stuart J, 2002. Podocyte biology and response to injury. *Journal of the American Society of Nephrology: JASN*, 13(12), S.3005-3015.
- Murea, M. et al., 2010. Expression of Notch pathway proteins correlates with albuminuria, glomerulosclerosis, and renal function. *Kidney International*, 78(5), S.514-522.
- Murphy, G., 2008. The ADAMs: signalling scissors in the tumour microenvironment. *Nature Reviews. Cancer*, 8(12), S.929-941.
- Muyldermans, S, 2001. Single domain camel antibodies: current status. *Journal of Biotechnology*, 74(4), S.277-302.

- Nangaku, M., Shankland, Stuart J & Couser, William G, 2005. Cellular response to injury in membranous nephropathy. *Journal of the American Society of Nephrology: JASN*, 16(5), S.1195-1204.
- Nicke, A., 2008. Homotrimeric complexes are the dominant assembly state of native P2X7 subunits. *Biochemical and Biophysical Research Communications*, 377(3), S.803–808.
- Niranjan, T. et al., 2008. The Notch pathway in podocytes plays a role in the development of glomerular disease. *Nature Medicine*, 14(3), S.290-298.
- North, R Alan, 2002. Molecular physiology of P2X receptors. *Physiological Reviews*, 82(4), S.1013-1067.
- O A, 2009. *Innere Medizin 2010* 2010. Aufl., Gerd Herold.
- Okada, A. et al., 2005. Development of gender differences in DBA/2Cr mouse kidney morphology during maturation. *The Journal of Veterinary Medical Science / the Japanese Society of Veterinary Science*, 67(9), S.877-882.
- Osaka, H. et al., 2003. Ubiquitin carboxy-terminal hydrolase L1 binds to and stabilizes monoubiquitin in neuron. *Human Molecular Genetics*, 12(16), S.1945-1958.
- Pavenstädt, Hermann, Kriz, Wilhelm & Kretzler, M., 2003. Cell biology of the glomerular podocyte. *Physiological Reviews*, 83(1), S.253-307.
- Peschon, J.J. et al., 1998. An essential role for ectodomain shedding in mammalian development. *Science (New York, N.Y.)*, 282(5392), S.1281-1284.
- Petermann, Arndt T et al., 2003. Mitotic cell cycle proteins increase in podocytes despite lack of proliferation. *Kidney International*, 63(1), S.113-122.
- Ramos-Vara, J.A., 2005. Technical Aspects of Immunohistochemistry. *Veterinary Pathology Online*, 42(4), S.405–426.
- Rauscher, F.J., 3rd u. a., 1998. Characterization of monoclonal antibodies directed to the amino-terminus of the WT1, Wilms' tumor suppressor protein. *Hybridoma*, 17(2), S.191–198.
- Rastaldi, M.P. et al., 2006. Glomerular podocytes contain neuron-like functional synaptic vesicles. *The FASEB Journal: Official Publication of the Federation of American Societies for Experimental Biology*, 20(7), S.976-978.
- Ronco, P., 2007. Proteinuria: is it all in the foot? *Journal of Clinical Investigation*, 117(8), S.2079-2082.

## List of references

---

- Ronco, P. & Debiec, H., 2010. Membranous glomerulopathy: the evolving story. *Current Opinion in Nephrology and Hypertension*, 19(3), S.254-259.
- Ronco, P. & Debiec, H., 2006. New insights into the pathogenesis of membranous glomerulonephritis. *Current Opinion in Nephrology and Hypertension*, 15(3), S.258-263.
- Saftig, P. & Reiss, K., 2011. The „A Disintegrin And Metalloproteases“ ADAM10 and ADAM17: novel drug targets with therapeutic potential? *European Journal of Cell Biology*, 90(6-7), S.527-535.
- Sakurai, M. et al., 2006. Ubiquitin C-terminal hydrolase L1 regulates the morphology of neural progenitor cells and modulates their differentiation. *Journal of Cell Science*, 119(Pt 1), S.162-171.
- la Sala, A. et al., 2003. Alerting and tuning the immune response by extracellular nucleotides. *Journal of Leukocyte Biology*, 73(3), S.339-343.
- Saleem, M.A. et al., 2002. A conditionally immortalized human podocyte cell line demonstrating nephrin and podocin expression. *Journal of the American Society of Nephrology: JASN*, 13(3), S.630-638.
- Satoh, J.I. & Kuroda, Y., 2001. Ubiquitin C-terminal hydrolase-L1 (PGP9.5) expression in human neural cell lines following induction of neuronal differentiation and exposure to cytokines, neurotrophic factors or heat stress. *Neuropathology and Applied Neurobiology*, 27(2), S.95-104.
- Scheller, J. et al., 2011. ADAM17: a molecular switch to control inflammation and tissue regeneration. *Trends in Immunology*, 32(8), S.380-387.
- Schiffer, M et al., 2001. Apoptosis in podocytes induced by TGF-beta and Smad7. *The Journal of Clinical Investigation*, 108(6), S.807-816.
- Schilling, W.P. et al., 1999. Maitotoxin and P2Z/P2X(7) purinergic receptor stimulation activate a common cytolitic pore. *The American Journal of Physiology*, 277(4 Pt 1), S.C766-776.
- Schwarz, N. et al., 2009. Activation of the P2X7 ion channel by soluble and covalently bound ligands. *Purinergic Signalling*, 5(2), S.139-149.
- Sekiguchi, S. et al., 2006. Localization of ubiquitin C-terminal hydrolase L1 in mouse ova and its function in the plasma membrane to block polyspermy. *The American Journal of Pathology*, 169(5), S.1722-1729.
- Seliger, B. et al., 2007. Ubiquitin COOH-terminal hydrolase 1: a biomarker of renal cell carcinoma associated with enhanced tumor cell proliferation and migration. *Clinical Cancer Research: An Official Journal of the American Association for Cancer Research*, 13(1), S.27-37.

## List of references

---

- Seman, M. et al., 2003. NAD-induced T cell death: ADP-ribosylation of cell surface proteins by ART2 activates the cytolytic P2X7 purinoceptor. *Immunity*, 19(4), S.571-582.
- Shah, B.H. & Catt, K.J., 2006. TACE-dependent EGF receptor activation in angiotensin-II-induced kidney disease. *Trends in Pharmacological Sciences*, 27(5), S.235-237.
- Shankland, S J, 2006. The podocyte's response to injury: role in proteinuria and glomerulosclerosis. *Kidney International*, 69(12), S.2131-2147.
- Shankland, S J et al., 2000. Differential expression of cyclin-dependent kinase inhibitors in human glomerular disease: role in podocyte proliferation and maturation. *Kidney International*, 58(2), S.674-683.
- Shirato, I., Asanuma, K., Takeda, Y., Hayashi, K. & Tomino, Y., 2000a. Protein gene product 9.5 is selectively localized in parietal epithelial cells of Bowman's capsule in the rat kidney. *Journal of the American Society of Nephrology: JASN*, 11(12), S.2381-2386.
- Shirato, I., Asanuma, K., Takeda, Y., Hayashi, K. & Tomino, Y., 2000b. Protein gene product 9.5 is selectively localized in parietal epithelial cells of Bowman's capsule in the rat kidney. *Journal of the American Society of Nephrology: JASN*, 11(12), S.2381-2386.
- Siebert, P.D. & Chenchik, A., 1993. Modified acid guanidinium thiocyanate-phenol-chloroform RNA extraction method which greatly reduces DNA contamination. *Nucleic acids research*, 21(8), S.2019–2020.
- Silbernagl, S. & Despopoulos, A., 2007. *Taschenatlas Physiologie*, Stuttgart [u.a.]: Thieme [u.a.].
- Solini, A. et al., 2005. Purinergic modulation of mesangial extracellular matrix production: role in diabetic and other glomerular diseases. *Kidney International*, 67(3), S.875-885.
- Somlo, S. & Mundel, P, 2000. Getting a foothold in nephrotic syndrome. *Nature Genetics*, 24(4), S.333-335.
- Sperlágh, B. et al., 2006. P2X7 receptors in the nervous system. *Progress in Neurobiology*, 78(6), S.327-346.
- Srivastava, T., Garola, R.E. & Singh, H.K., 2006. Cell-cycle regulatory proteins in the podocyte in collapsing glomerulopathy in children. *Kidney International*, 70(3), S.529-535.

## List of references

---

- Steinberg, T.H. et al., 1987. ATP4- permeabilizes the plasma membrane of mouse macrophages to fluorescent dyes. *The Journal of Biological Chemistry*, 262(18), S.8884-8888.
- Surprenant, A et al., 1996. The cytolytic P2Z receptor for extracellular ATP identified as a P2X receptor (P2X7). *Science (New York, N.Y.)*, 272(5262), S.735-738.
- Surprenant, Annmarie & North, R Alan, 2009. Signaling at purinergic P2X receptors. *Annual Review of Physiology*, 71, S.333-359.
- Susor, A. et al., 2007. Proteomic analysis of porcine oocytes during in vitro maturation reveals essential role for the ubiquitin C-terminal hydrolase-L1. *Reproduction (Cambridge, England)*, 134(4), S.559-568.
- Taylor, S.R.J. et al., 2009. P2X7 deficiency attenuates renal injury in experimental glomerulonephritis. *Journal of the American Society of Nephrology: JASN*, 20(6), S.1275-1281.
- Tesch, G.H. et al., 1997. Intrinsic renal cells are the major source of interleukin-1 beta synthesis in normal and diseased rat kidney. *Nephrology, Dialysis, Transplantation: Official Publication of the European Dialysis and Transplant Association - European Renal Association*, 12(6), S.1109-1115.
- Tossidou, I., Teng, B., et al., 2010. CIN85/RukL is a novel binding partner of nephrin and podocin and mediates slit diaphragm turnover in podocytes. *The Journal of Biological Chemistry*, 285(33), S.25285-25295.
- Trivedi, S., Zeier, M. & Reiser, J., 2009. Role of podocytes in lupus nephritis. *Nephrology, Dialysis, Transplantation: Official Publication of the European Dialysis and Transplant Association - European Renal Association*, 24(12), S.3607-3612.
- Tsukimoto, M. et al., 2006. P2X7 receptor-dependent cell death is modulated during murine T cell maturation and mediated by dual signaling pathways. *Journal of Immunology (Baltimore, Md.: 1950)*, 177(5), S.2842-2850.
- Turner, C M et al., 2004. Altered ATP-sensitive P2 receptor subtype expression in the Han:SPRD cy/+ rat, a model of autosomal dominant polycystic kidney disease. *Cells, Tissues, Organs*, 178(3), S.168-179.
- Turner, C M et al., 2003. The pattern of distribution of selected ATP-sensitive P2 receptor subtypes in normal rat kidney: an immunohistological study. *Cells, Tissues, Organs*, 175(2), S.105-117.
- Turner, Clare M, Elliott, J.I. & Tam, F.W.K., 2009. P2 receptors in renal pathophysiology. *Purinergic Signalling*, 5(4), S.513-520.

## List of references

---

- Turner, Clare M et al., 2007. Increased expression of the pro-apoptotic ATP-sensitive P2X7 receptor in experimental and human glomerulonephritis. *Nephrology, Dialysis, Transplantation: Official Publication of the European Dialysis and Transplant Association - European Renal Association*, 22(2), S.386-395.
- Verhoef, P.A. et al., 2003. P2X7 receptor-dependent blebbing and the activation of Rho-effector kinases, caspases, and IL-1 beta release. *Journal of Immunology (Baltimore, Md.: 1950)*, 170(11), S.5728-5738.
- Vial, C. & Evans, R.J., 2000. P2X receptor expression in mouse urinary bladder and the requirement of P2X(1) receptors for functional P2X receptor responses in the mouse urinary bladder smooth muscle. *British Journal of Pharmacology*, 131(7), S.1489-1495.
- Di Virgilio, F et al., 2001. Nucleotide receptors: an emerging family of regulatory molecules in blood cells. *Blood*, 97(3), S.587-600.
- Di Virgilio, F, Falzoni, S, et al., 1999. ATP receptors and giant cell formation. *Journal of Leukocyte Biology*, 66(5), S.723 -726.
- Di Virgilio, F et al., 1999. The P2Z/P2X7 receptor of microglial cells: a novel immunomodulatory receptor. *Progress in Brain Research*, 120, S.355-368.
- Virginio, C. et al., 1999. Kinetics of cell lysis, dye uptake and permeability changes in cells expressing the rat P2X7 receptor. *The Journal of Physiology*, 519 Pt 2, S.335-346.
- Vonend, Oliver et al., 2004. Glomerular expression of the ATP-sensitive P2X receptor in diabetic and hypertensive rat models. *Kidney International*, 66(1), S.157-166.
- Wesolowski, J., Alzogaray, V., et al., 2009. Single domain antibodies: promising experimental and therapeutic tools in infection and immunity. *Medical Microbiology and Immunology*, 198(3), S.157-174.
- Wilkinson, K.D., 1997. Regulation of ubiquitin-dependent processes by deubiquitinating enzymes. *The FASEB Journal: Official Publication of the Federation of American Societies for Experimental Biology*, 11(14), S.1245-1256.
- Wilkinson, K.D., 2000. Ubiquitination and deubiquitination: targeting of proteins for degradation by the proteasome. *Seminars in Cell & Developmental Biology*, 11(3), S.141-148.
- Wilkinson, K.D. et al., 1989. The neuron-specific protein PGP 9.5 is a ubiquitin carboxyl-terminal hydrolase. *Science (New York, N.Y.)*, 246(4930), S.670-673.

## List of references

---

- Wilson, H.L. et al., 2002. Epithelial membrane proteins induce membrane blebbing and interact with the P2X7 receptor C terminus. *The Journal of Biological Chemistry*, 277(37), S.34017-34023.
- Wirkner, K., Köfalvi, A., et al., 2005. Supersensitivity of P2X receptors in cerebrocortical cell cultures after in vitro ischemia. *Journal of Neurochemistry*, 95(5), S.1421-1437.
- Yamamoto, T. & Wilson, C.B., 1987. Quantitative and qualitative studies of antibody-induced mesangial cell damage in the rat. *Kidney International*, 32(4), S.514-525.
- Yu, D. et al., 2005. Urinary podocyte loss is a more specific marker of ongoing glomerular damage than proteinuria. *Journal of the American Society of Nephrology: JASN*, 16(6), S.1733-1741.
- Zhang, X.-F. et al., 2005. Functional expression of P2X7 receptors in non-neuronal cells of rat dorsal root ganglia. *Brain Research*, 1052(1), S.63-70.

## 9. Appendix

### Acknowledgements

Zunächst gilt mein besonderer Dank Frau Dr. Catherine Meyer-Schwesinger und Herrn Prof. Dr. Friedrich Koch-Nolte - für die Möglichkeit meine Arbeit in ihrer Abteilung bzw. Arbeitsgruppe zu absolvieren, für die sehr spontane Überlassung des spannenden Themas, die immer fürsorgliche und intensive Betreuung in allen Phasen der Arbeit sowie das große entgegengebrachte Vertrauen, welches mir freies und selbstständiges Experimentieren mit großer Freude am Thema ermöglichte. Auch bedanke ich mich herzlich für die tolle Gelegenheit der Teilnahme am ASN Renal Week Kongress in Denver, CO, USA.

Herrn Prof. Dr. Rolf A. K. Stahl danke ich dafür, dass ich meine experimentelle Arbeit in der Nephrologie absolvieren konnte.

Ebenso danke ich Herrn Prof. Dr. Bernhard Fleischer für die Möglichkeit, Doktorandin des Institutes für Immunologie sein zu können.

Weiterhin bedanke ich mich herzlich für die Möglichkeit im Rahmen meiner Arbeit Stipendiatin der IRTG des SFB 877 des Biochemischen Institutes der Christian-Albrechts-Universität zu Kiel gewesen zu sein. Bei Frau Dr. Christine Desel und Herrn Prof. Dr. Joachim Grötzinger bedanke ich mich in diesem Kontext für die Ermöglichung meiner IRTG-Teilnahme sowie die freundliche Betreuung.

Marlies Sachs danke ich herzlich für die geduldige Einarbeitung in die angewandten Techniken, das große Verständnis, die viele praktische Unterstützung und zahlreiche Hilfestellungen in Notlagen.

Frithjof Lohmann, Anne Wegner, Victoria Radon und Dr. Elion Hoxha danke ich für die gute Atmosphäre im Labor und den kritischen Austausch. Eva Klupp gilt mein spezieller Dank für die hilfsbereite Vermittlung der Doktorarbeit sowie die permanente Unterstützung in allen Lebenslagen.

Gudrun Dubberke und Marion Nissen danke ich sehr herzlich für das geduldige Bereitstellen von Antikörpern, Wissen und Kompetenz. Ebenso gilt mein Dank Mariola Reszka, Melanie Schaper und Stefan Gatzemeier für diverse Hilfestellungen und geduldiges Erklären.

Bei Welbeck Danquah und Björn Rissiek bedanke ich mich für die gute Zusammenarbeit an der Nanobody-Studie.

Herrn Prof. Dr. Friedrich Haag danke ich für die freundliche Unterstützung und Betreuung im Rahmen des Wahlfaches Immunologie.

Für ihre stete Ermutigung, die liebevolle Unterstützung, die nicht zu erschütternde Geduld mit mir und ihren Glauben an mich danke ich schließlich von ganzem Herzen meinen Eltern Ulrike und Dieter Hammel, meinen Großeltern Loni und Ludwig Hammel und Gisela und Hans Ludwig sowie meinem Bruder Johannes.

The experimental work on this thesis was supported by a scholarship of the IRTG of the CRC 877 'Proteolysis and Pathophysiology' of the Christian-Albrechts-University in Kiel.

Parts of this work were presented at the Renal Week Nephrology Meeting of the American Society of Nephrology in November 2010 in Denver, CO, USA.


 1Department of Internal Medicine, Nephrology, University Medical Center Hamburg-Eppendorf, Hamburg, Germany;  
 2University Cancer Center Hamburg-Eppendorf, Hamburg, Germany;  
 3Department of Experimental and Clinical Pharmacology and Toxicology, Cardiovascular Research Center, University Medical Center Hamburg-Eppendorf, Hamburg, Germany;  
 4Assenm 1974, Paris, France;  
 5Université Pierre et Marie Curie-Paris, UMR-S974, CNRS UMR7215, Institut de Myologie, IFR14, Paris, F-75013, France.  
 6 Department of Pathology, Nierenregister, University Medical Center Hamburg-Eppendorf, Hamburg, Germany

## Ubiquitin C-Terminal Hydrolase-L1 (UCH-L1) Activity Induces Polyubiquitin Accumulation in Podocytes and Increases Proteinuria in Rat Membranous Nephropathy

Catherine Meyer-Schwesinger<sup>1\*</sup>, Tobias N. Meyer<sup>1\*</sup>, Henning Sievert<sup>2</sup>, Frithjof Lohmann<sup>1</sup>, Anna Hammel<sup>1</sup>, Elion Hoxha<sup>1</sup>, Marlies Sachs<sup>1</sup>, Eva-Maria Klupp<sup>1</sup>, Silvia Münster<sup>1</sup>, Stefan Balabanov<sup>2</sup>, Lucie Carrier<sup>3,4,5</sup>, Udo Helmchen<sup>6</sup>, Friedrich Thaiss<sup>1</sup>, Rolf A.K. Stahl<sup>1</sup> \*Contributed equally

### Introduction:

UCH-L1 is a key protease in the ubiquitin-proteasome pathway that regulates the intracellular pool of monoubiquitin and is associated with neurodegenerative diseases and cancer. Recently, we described the de novo expression of UCH-L1 in podocytes of patients with membranous nephropathy where UCH-L1 expression correlated with increased ubiquitin content. Here, we investigated the role of UCH-L1 for the ubiquitin homeostasis and proteasomal degradation in a rat model of membranous nephropathy.

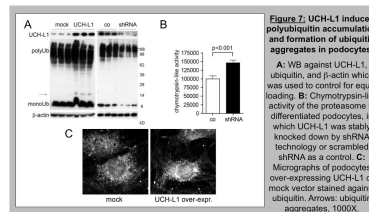
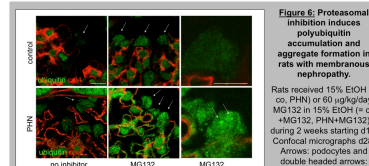
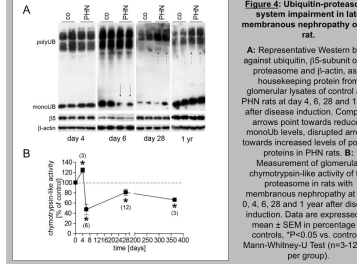
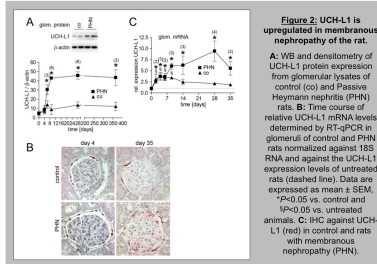
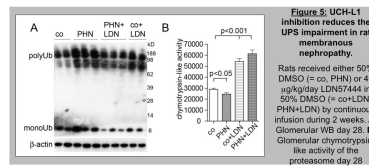
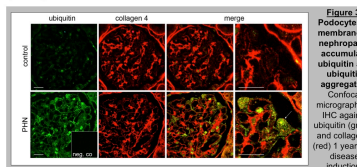
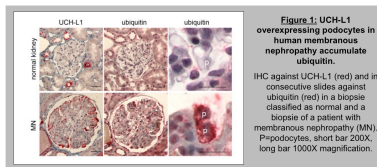
### Methods:

Passive Heymann nephritis was induced in 200-250 g Sprague Dawley rats by two consecutive i.v. injections of sheep FX1A antiserum (500 and 750 µl). Kidneys and Glomeruli were isolated at 0, 2, 4, 9, 14, 28, 35 and 365 days after disease induction and analyzed. Proteasomal activity was measured using fluorescent Suc-LLVY-AMC as a proteasomal substrate. UCH-L1 hydrolase function or the proteasome was inhibited in PHN versus control rats by continuous administration of LDN57444 (40 µg/KG/day, UCH-L1 inhibitor) or MG132 (60 mg/KG/day, proteasomal inhibition) over s.c. implanted osmotic minipumps for 14 days. UCH-L1 was stably overexpressed or knocked down by shRNA technology in cultured murine podocytes.

### Conclusion:

These data show that ubiquitin C-terminal hydrolase L1 activity results in polyubiquitin accumulation, proteasome inhibition and disease aggravation in experimental membranous nephropathy.

Contact: c.meyer-schwesinger@uke.uni-hamburg.de



## **Affidavit**

### **Eidesstattliche Versicherung**

Ich versichere ausdrücklich, dass ich die Arbeit selbständig und ohne fremde Hilfe verfasst, andere als die von mir angegebenen Quellen und Hilfsmittel nicht benutzt und die aus den benutzten Werken wörtlich oder inhaltlich entnommenen Stellen einzeln nach Ausgabe (Auflage und Jahr des Erscheinens), Band und Seite des benutzten Werkes kenntlich gemacht habe. Ferner versichere ich, dass ich die Dissertation bisher nicht einem Fachvertreter an einer anderen Hochschule zur Überprüfung vorgelegt oder mich anderweitig um Zulassung zur Promotion beworben habe.

Unterschrift: .....